JOURNAL OF THE Electrochemical Society

l. 104, No. 10 October 195

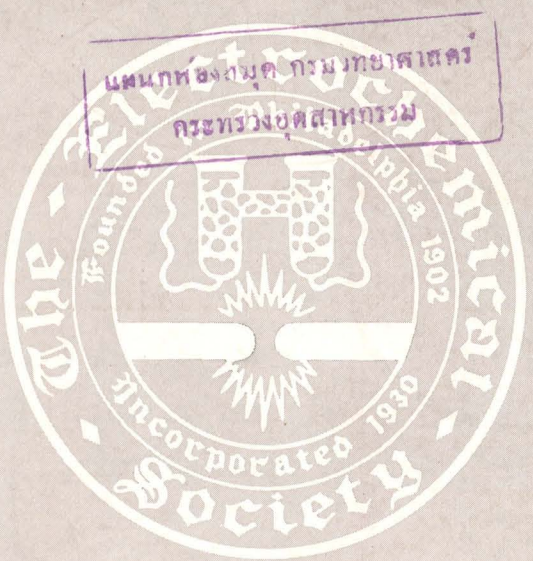

How can graphite be used in our new cell design?

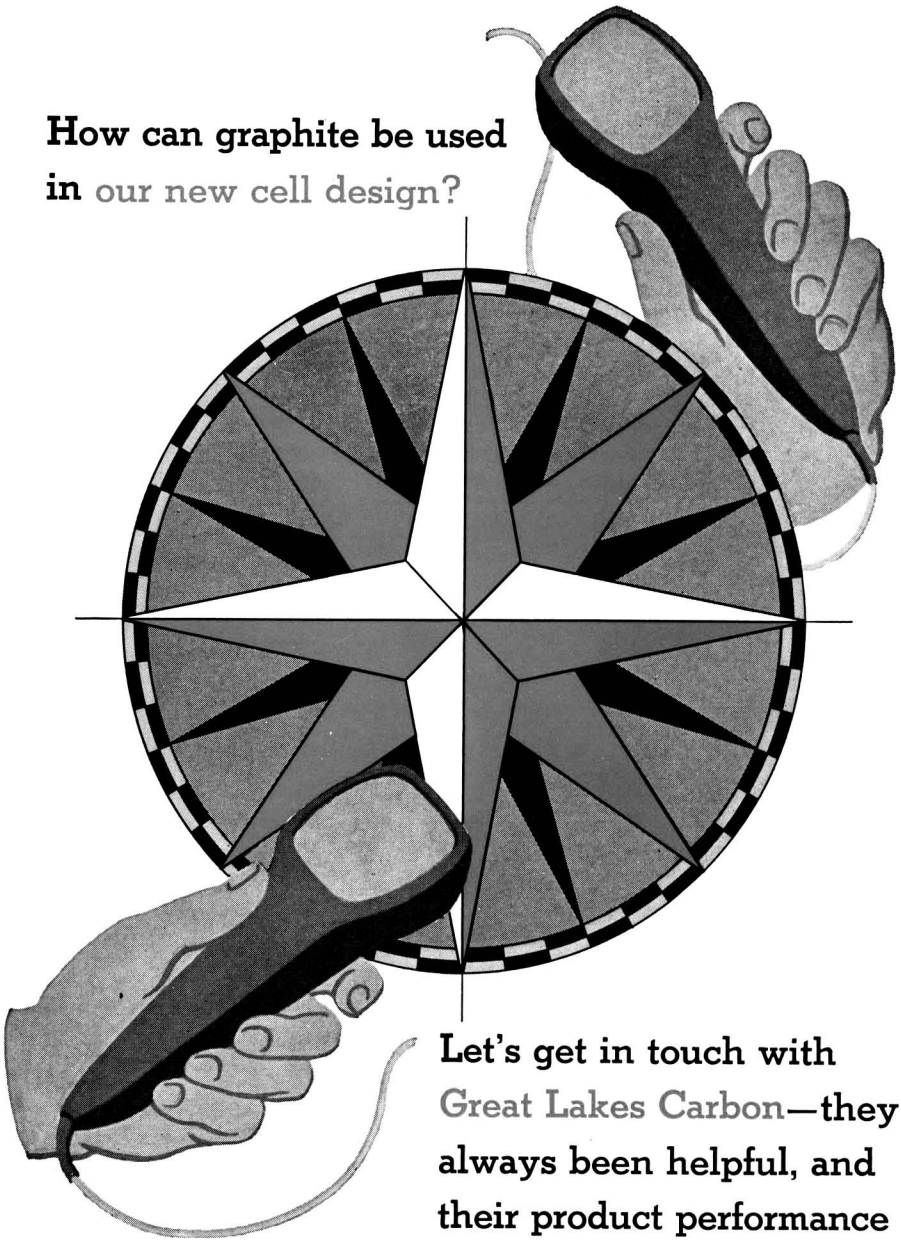

Let's get in touch with Great Lakes Carbon—they've always been helpful, and their product performance is outstanding!

ELECTRODE GLC® DIVISION

GREAT LAKES CARBON CORPORATION

18 EAST 48TH STREET, NEW YORK 17, N.Y. · OFFICES IN PRINCIPAL CITIES

Journal of the Electrochemical Society

OCTOBER 1957 **VOL. 104 • NO. 10**

CONTENTS

Published monthly by The Electrochemical Society, Inc., from Manchester, N. H., **Executive Offices, Editorial Office** and **Circulation Dept.** at 1860 Broadway, New York 23, N. Y., **Advertising Office** at 545 Fifth Ave., New York, N. Y., combining the JOURNAL and TRANSACTIONS OF THE ELECTROCHEMICAL SOCIETY. Statements and opinions given in articles and papers in the JOURNAL OF THE ELECTROCHEMICAL SOCIETY are those of the contributors, and The Electrochemical Society assumes no responsibility for them. Non-deductible subscription to members $5.00; subscription to nonmembers $18.00. Single copies $1.25 to members, $1.75 to nonmembers. Copyright 1957 by The Electrochemical Society, Inc. Entered as second-class matter at the Post Office at Manchester, N. H., under the act of August 24, 1912.

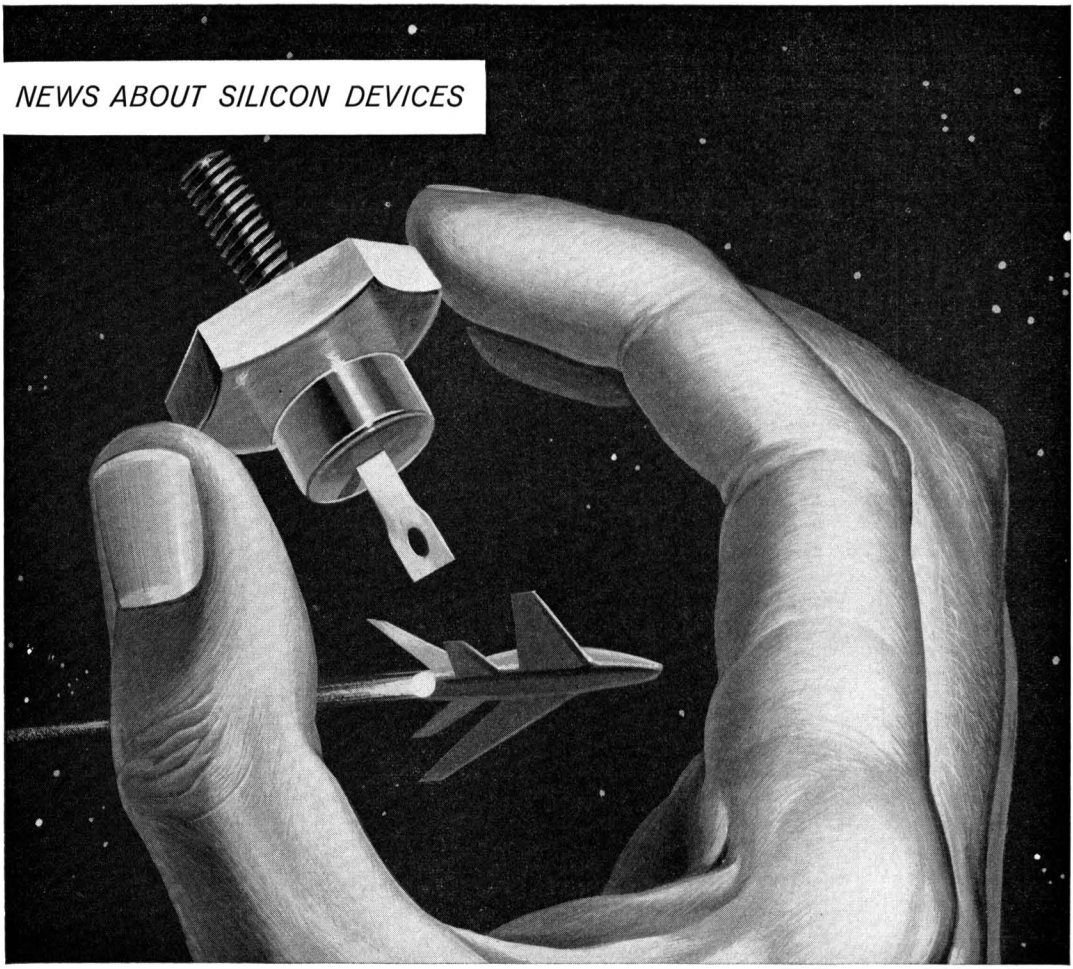

SILICON RECTIFIERS are finding increasing use at elevated temperatures in aircraft and missile applications by providing more power per pound.

Now...design improvements made possible with components of Du Pont Hyperpure Silicon

Today silicon rectifiers make possible a vast improvement in jet-age aircraft generators—the use of engine oil as a coolant instead of less-efficient ram air. Silicon rectifiers take the place of oil-sensitive brushes, commutator and slip rings . . . are completely unaffected by 150°C. engine oil. Result: a *brushless* generator of less weight and size than ordinary generators.

Silicon devices can similarly help you miniaturize—improve design and performance. Silicon rectifiers have excellent stability . . . can operate continuously at −65 to 200°C. They're up to 99% efficient—reverse leakages are only a fraction of those of other semiconductors. Both transistors and rectifiers of silicon can pack *more* capacity into *less* of your equipment space.

Note to device manufacturers: You can produce high-quality silicon transistors and rectifiers with Du Pont Hyperpure Silicon now available in three grades for maximum efficiency and ease of use... purity range of 3 to 11 atoms of boron per billion... available in 3 forms, needles, densified, cut-rod. Technical information is available on crystal growing from Du Pont... pioneer producer of semiconductor-grade silicon.

NEW BOOKLET ON DU PONT HYPERPURE SILICON

You'll find our new, illustrated booklet about Hyperpure Silicon helpful and interesting—it describes the manufacture, properties and uses of Du Pont Hyperpure Silicon. Just drop us a card for your copy. E. I. du Pont de Nemours & Co. (Inc.), Pigments Department, Silicon Development Group, Wilmington 98, Delaware.

PIGMENTS DEPARTMENT

DU PONT

REG. U. S. PAT. OFF.

BETTER THINGS FOR BETTER LIVING
...THROUGH CHEMISTRY

Editorial

Publication Plus Efficiente in Le Scientia

LE CIRCULATION prompte e efficiente de ideas e informationes es justo si importante pro le scientia como le circulation del sanguine in le corpore human. Infelicemente, iste circulation scientific es nunc grandemente impedite per le systema archaic de publication del materias scientific in si multe linguas. Es impossible que le scientista pote leger omne iste linguas.

Le progresso del scientia esserea tremendemente accrescite si un singule lingua esserea usate pro publicationes scientific. Preferibilemente, iste lingua deberea esser legibile practicamente a prime vista per le scientista e deberea haber un grammatica multo simple.

Si omne materias scientific esserea assi publicate, le scientista haberea un accesso immediate e personal al litteratura scientific del mundo e poterea colliger reimpressiones de omne articulos que pertine a su campo special de recerca. Isto eliminarea le costo in tempore e moneta de traductiones (si vermente istos es disponibile del toto) e in alicun casos de un repetition innecessari del recerca mesme.

Extra le costo, il ha le possibilitate de errores o misconceptiones si le traductor non es familiar con le campo special del articulo. Es multo desirabile que le scientista mesme pote leger le articulo original e facer su proprie evalutation del resultatos. Promptitude etiam es importante. Si le scientista debe passar un mense in le procuration del traduction, le articulo es frequentemente decrescite in valor. Quando un scientista ha le necessitate de un articulo, ille desira lo immediatemente, non un mense plus tarde.

Un lingua simile a illo mentionate supra deveniva disponibile in 1951, post 25 annos de recerca, con le publication del *Interlingua-English Dictionary* e le *Interlingua Grammar* (Storm Publishers, New York 3). Interlingua esseva obtenite per un regularisation e standardisation del elementos international del linguas europee, includente anglese.

Impressionate per le convenientia de iste lingua pro le communication scientific, le scriptor comenciava in maio 1952 le publication in interlingua de un parve periodico mensual, appellate *Spectroscopia Molecular,* in su campo proprie de recerca. Isto nunc va a 800 spectroscopistas e bibliothecas in 38 paises. Experientia demonstra que le recipientes pote leger lo sin difficultate e que illes senti que le periodico es un servicio importante al nivello international. Le publication se supporta completemente per contributiones financiari ab illes qui beneficia de su existentia. Le reception sympathic de iste periodico suggere que le tempore es plus matur que haberea essite expectate pro publication de resultatos scientific in un lingua international.

(Continued on next page)

Interlingua etiam es usate in 17 jornales medic pro le summarios de lor articulos e ha essite usate como le sol lingua secundari in le programmas de 7 congressos medic international. Un summario in interlingua de recente disveloppamentos scientific es date cata mense in *Science News Letter,* publicate per *Science Service, Inc.* (1719 N St., N. W., Washington 6, D. C.).

Pro assister scientistas e redactores de jornales scientific qui desira investigar le utilitate de iste lingua auxiliar in lor campos special, *Science Service, Inc.* ha establite un Division de Interlingua (80 E. 11th St., New York 3). Dr. Alexander Gode, un linguista competente, es le director de iste division.

In iste dies quando communication via le radio e television es practicamente instantanee e quando un aviator pote volar a transverso le Statos Unite a un velocitate plus grande que ille del sono, il pare improbabile que scientistas va tolerar pro longe le presente stato costose e inefficiente de publication in le scientia.

FORREST F. CLEVELAND
Professor de Physica
Instituto Technologic de Illinois
Chicago 16, Illinois
Le 7 de augusto 1957

SARGENT-SLOMIN ANALYZERS
are standard equipment in prominent laboratories

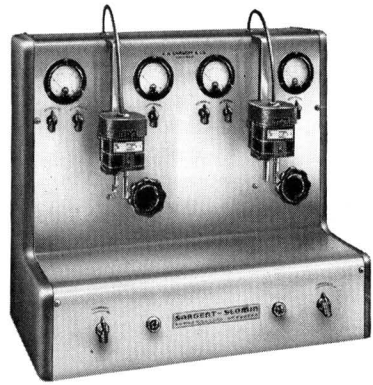

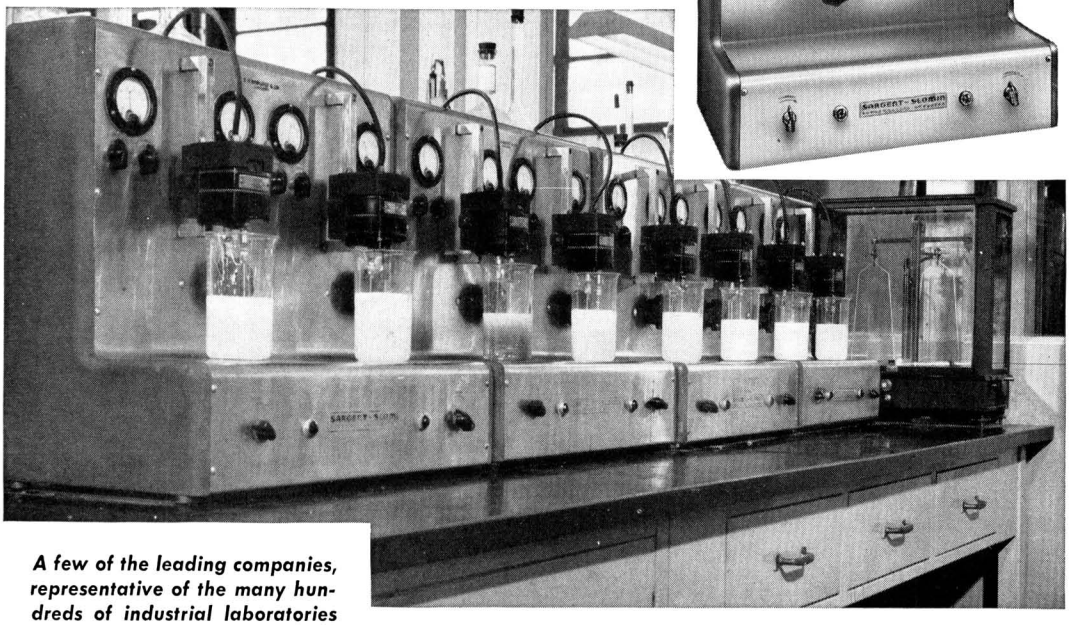

A few of the leading companies, representative of the many hundreds of industrial laboratories using the Sargent - Slomin and Heavy Duty Analyzers for control analyses . . .

AMPCO METAL, Inc.
ANDERSON LABORATORIES
CALERA MINING COMPANY
EUREKA WILLIAMS COMPANY
THE FEDERAL METAL CO.
FORD MOTOR COMPANY
THE GLIDDEN COMPANY—Chemical, Metal and Pigment Division
HOT POINT CO.
HOWARD FOUNDRY COMPANY
INTERNATIONAL HARVESTER COMPANY
KENNAMETAL Inc.
McQUAY - NORRIS MANUFACTURING CO.
NATIONAL LEAD COMPANY, Fredericktown, Missouri
PIASECKI HELICOPTER CORPORATION
REVERE COPPER & BRASS INCORPORATED
THE RIVER SMELTING & REFINING COMPANY
SILAS MASON COMPANY
THE STUDEBAKER CORPORATION
THOMPSON PRODUCTS, INC.

Photo Courtesy INTERNATIONAL HARVESTER COMPANY, Melrose Park, Illinois

Sargent-Slomin Electrolytic Analyzers are recommended for such electro analytical determinations as: Copper in—ores, brass, iron, aluminum and its alloys, magnesium and its alloys, bronze, white metals, silver solders, nickel and zinc die castings. Lead in—brass, aluminum and its alloys, bronze, zinc and zinc die castings. Assay of electrolytical copper, nickel and other metals.

Sargent analyzers are completely line operated, employing self-contained rectifying and filter circuits. Deposition voltage is adjusted by means of autotransformers, with meters indicating volts and amperes and controls on the panel. An easily replaceable fuse guards against circuit overload. Maximum D.C. current capacity is 5 to 15 amperes; maximum D.C. voltage available, 10 volts.

Sargent-Slomin Analyzers stir through a rotating chuck operated from a capacitor type induction motor, having a fixed speed of 550 r.p.m. with 60 cycle A.C. current or 460 r.p.m. with 50 cycle A.C. current. Motors are sealed against corrosive fumes and are mounted on cast metal brackets, sliding on ½" square stainless steel rods, permitting vertical adjustment of electrode position over a distance of 4". Pre-lubricated ball-bearings support the rotating shaft. All analyzers accommodate electrodes having shaft diameters no greater than 0.059 inch. Stainless steel spring tension chucks permit quick, easy insertion of electrodes and maintain proper electrical contact. Special Sargent high efficiency electrodes are available for these analyzers. Illustrated above is one model of the five types of Sargent-Slomin and Heavy Duty Analyzers.

S-29465 ELECTROLYTIC ANALYZER—Motor stirred, Two Position, 5 Ampere. With two adjustable heaters, pilot lights and control knobs. For operation from 115 volt, 50 or 60 cycle A.C. circuits.....**$530.00**

SARGENT

SCIENTIFIC LABORATORY INSTRUMENTS • APPARATUS • SUPPLIES • CHEMICALS

E. H. SARGENT & COMPANY, 4647 W. FOSTER AVE., CHICAGO 30, ILLINOIS
MICHIGAN DIVISION, 8560 WEST CHICAGO AVENUE, DETROIT 4, MICHIGAN
SOUTHWESTERN DIVISION, 5915 PEELER STREET, DALLAS 35, TEXAS
SOUTHEASTERN DIVISION, 3125 SEVENTH AVE., N., BIRMINGHAM 4, ALA.

For FLUORINE gas or liquid

HYDROFLUORIC ACID aqueous or anhydrous

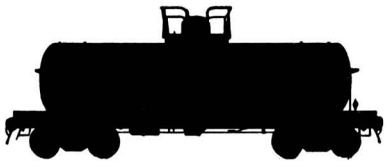

INORGANIC FLUORINE COMPOUNDS

see GENERAL CHEMICAL

General Chemical's leadership in fluorine chemistry is well established . . . widely recognized. The inorganic fluorine compounds listed here are available now—in commercial or research quantities. Many others are under investigation, or can be produced readily if required. Whenever you need fluorine chemicals of any type—call *General Chemical*, industry's primary source of supply for elemental fluorine, hydrofluoric acid and the fluorine compounds produced from them.

FLUORINE
Elemental Fluorine, Gaseous & Liquid

ACIDS
Fluoboric Acid
Fluosulfonic Acid
Hydrofluoric Acid, Anhydrous
Hydrofluoric Acid, Anhydrous High Purity
Hydrofluoric Acid, Aqueous
Hydrofluoric Acid, Aqueous, Purified & Reagent
Hydrofluoric Acid, Electronic

ACID FLUORIDES
Ammonium Bifluoride
Potassium Bifluoride
Sodium Bifluoride

ALKALI FLUOBORATES
Ammonium Fluoborate
Potassium Fluoborate
Sodium Fluoborate

ALKALI FLUORIDES
Ammoninum Fluoride
Potassium Fluoride, Crystal & Anhydrous
Sodium Fluoride, Technical
Sodium Fluoride, Reagent

BORON FLUORIDE COMPLEXES
Boron Fluoride Ether (Diethyl) Complex
Boron Fluoride Phenol Complex
Boron Fluoride Diacetic Acid Complex
Boron Fluoride Di-n-Butyl Ether Complex
Boron Fluoride Dihydrate
Boron Fluoride Piperidine Complex
Boron Fluoride Ethyl "Cellosolve" Complex
Boron Fluoride Hexamethylene-tetramine Complex
Boron Fluoride Monoethylamine Complex
Boron Fluoride Para-cresol Complex
Boron Fluoride Triethanolamine Complex
Boron Fluoride Urea Complex

DOUBLE FLUORIDES
Chromium Potassium Fluoride
Potassium Ferric Fluoride
Potassium Nickel Fluoride
Potassium Titanium Fluoride
Potassium Zinc Fluoride
Potassium Zirconium Fluoride
Sodium Zirconium Fluoride
Sodium Silico Fluoride
Potassium Aluminum Fluoride

HALOGEN FLUORIDES
Bromine Trifluoride
Bromine Pentafluoride
Chlorine Trifluoride
Iodine Pentafluoride

METAL FLUORIDES
Aluminum Fluoride
Aluminum Fluoride, Crystal
Antimony Trifluoride
Antimony Pentafluoride
Barium Fluoride
Bismuth Trifluoride
Cadmium Fluoride
Calcium Fluoride
Chromium Fluoride
Cupric Fluoride
Lead Tetrafluoride
Magnesium Fluoride (Not Optical Grade)
Mercuric Fluoride
Manganese Trifluoride
Molybdenum Hexafluoride
Nickelous Fluoride
Selenium Hexafluoride
Silicon Tetrafluoride
Silver Difluoride
Stannous Fluoride
Strontium Fluoride
Titanium Tetrafluoride
Tellurium Hexafluoride
Tungsten Hexafluoride
Zirconium Tetrafluoride

NON-METALLIC FLUORIDES
Boron Fluoride, Gas
Sulfur Hexafluoride

METAL FLUOBORATE SOLUTIONS
Cadmium Fluoborate
Chromium Fluoborate
Cobalt Fluoborate
Copper Fluoborate
Ferrous (Iron) Fluoborate
Indium Fluoborate
Lead Fluoborate
Nickel Fluoborate
Silver Fluoborate
Stannous (Tin) Fluoborate
Zinc Fluoborate

GC Allied Chemical

Basic Chemicals for American Industry

GENERAL CHEMICAL DIVISION
ALLIED CHEMICAL & DYE CORPORATION
40 Rector Street, New York 6, N. Y.

An Investigation of the Discharge Characteristics of Groups Ib-Vb Oxides in an Alkaline Electrolyte

R. Glicksman and C. K. Morehouse

RCA Laboratories, Radio Corporation of America, Princeton, New Jersey

ABSTRACT

Experimental half-cell discharge data are given for a number of Groups Ib-Vb oxides in strongly alkaline NaOH solution, along with comparisons between these data and their theoretical potentials. The effect of cathode solubility on the half-cell discharge potential of a few sparingly soluble silver salts is also discussed.

Many of the desirable features of a battery cathode material, such as a high reversible electrode potential and coulombic capacity, stability, and compatability with other cell components, are found among the metallic oxides. In practice, cathodes operate at potentials lower than their reversible values, due to polarization effects encountered under load conditions, while their electrode efficiencies also vary with current drain. Thus, evaluation of these materials is best made under conditions of discharge. In this paper experimental half-cell discharge data for a number of Group Ib-Vb oxides in an alkaline NaOH electrolyte are given, along with comparisons between these data and thermodynamically calculated values of the reversible electrode potentials.

Experimental

Discharge data on the various oxides were obtained using a technique described by the authors (1). This technique involves discharging at constant current in a large volume of electrolyte a 0.5-g sample of the cathode material mixed with 10% Shawinigan acetylene black. The change in the operating cathode potential with time is measured with a L&N Type K potentiometer using a saturated calomel reference electrode. The discharge data were corrected for the *IR* drop associated with the apparatus and electrolyte by means of an oscillographic technique (2).

The half-cell potentials are all referred to the normal hydrogen scale, and represent the average of two or three runs, the reproducibility being ±0.01-0.02 v when measured with a saturated calomel electrode (S.C.E.). The variation of the S.C.E. potential with temperature over the course of the measurements was less than 0.01 v, usually lower than 0.005 v, and no correction was made for this factor, i.e., all measured results were calculated using a value of 0.246 v for the S.C.E. potential.

In this study a zinc anode was employed with an alkaline electrolyte of 30% NaOH solution by weight which was saturated with ZnO, the solution being 10.7*M* prior to the addition of ZnO. The addition of ZnO decreases the molality of the solution in accordance with the following equation

$$ZnO + 2NaOH = Na_2ZnO_2 + H_2O \qquad (I)$$

the purpose of the ZnO being to reduce the corrosion of the Zn anode in the strongly alkaline electrolyte. During the course of the discharge, hydroxide ions are formed, but as the solution is strongly alkaline initially, the change in hydroxide ion activity of the solution is negligible.

Potential measurements of the HgO electrode in this electrolyte vs. a S.C.E. give a value of +0.043 v for the HgO half-cell referred to the normal hydrogen scale. The deviation from the standard potential of the HgO electrode ($E^\circ - E = +0.055$ v) is due to the greater hydroxide ion activity of the electrolyte, as well as to the existence of a liquid junction potential at the alkaline-saturated KCl interface. As these factors are constant for all measurements of the half-cell potentials, one can add +0.055 v to the experimentally determined discharge potentials of the various oxides in order to compare these values with their standard electrode potentials.

Group Ib Oxides

Presented in Table I are the standard potentials of the group Ib-Vb oxides in basic solution, the potentials being computed from the free energy data given by Latimer (3).

These potentials are referred to the normal hydrogen electrode, but in alkaline solutions this couple has the form

$$H_2 + 2OH^- = 2H_2O + 2e^- \qquad E^\circ = 0.828 \qquad (II)$$

so the E° values of the half reactions in alkaline solution will be designated as E°_B to indicate that this basic potential of the hydrogen couple must be used to obtain the completed reaction potential against hydrogen.

Early studies of the anodic oxidation of Ag in alkaline solution by Luther and Pokorny (4) and Zimmerman (5) show Ag to be oxidized quantitatively first to Ag_2O and then to AgO; when the AgO was made cathodic, the reverse reactions took place. This type of stepwise reduction would be expected from the standard potentials presented in Table I.

Typical discharge curves of commercial Zn-AgO cells (6) indicate a two-step reduction only at low

Table I. Standard potentials of the group Ib-Vb oxides in basic solution

Group		E°_B
Ib	AgO-Ag	+0.458
	AgO-Ag_2O	+0.570
	Ag_2O-Ag	+0.345
	CuO-Cu	−0.258
	CuO-Cu_2O	−0.159
	Cu_2O-Cu	−0.357
IIb	HgO-Hg	+0.098
IIIb	$Tl(OH)_3$-Tl	−0.148
	$Tl(OH)_3$-TlOH	−0.050
	TlOH-Tl	−0.343
	Tl_2O-Tl	−0.304
	$In(OH)_3$-In	−1.00
	$H_2GaO_3^-$-Ga	−1.22
IVb	PbO_2-Pb	−0.166
	PbO_2-PbO	+0.247
	PbO-Pb	−0.580
	$HPbO_2^-$-Pb	−0.540
	$Sn(OH)_6^=$-$HSnO_2^-$	−0.93
	SnO-Sn	−0.93
	$HSnO_2^-$-Sn	−0.91
	$HGeO_3^-$-Ge	−1.0
Vb	Bi_2O_3-Bi	−0.457
	SbO_2^--Sb	−0.658
	AsO_2^--As	−0.675

current drains; at the higher current drains AgO discharge takes place in one step at a potential corresponding to Ag_2O. The latter finding is in agreement with the data shown in Fig. 1, where it is seen that both AgO [1] and Ag_2O [1] are discharged in one step, in 30% NaOH electrolyte, at a rate of 0.005 amp/g, at a potential of +0.25 v on the normal hydrogen scale, a value 0.04 v lower than the thermodynamically calculated value of the reversible potential of the Ag_2O electrode. The observed capacities of the AgO and Ag_2O cathodes to a −0.40 v cut off are 21.5 and 13.5 amp-min/g, respectively, which correspond to efficiencies of 83 and 97%, indicative of a 2 and 1 electron change per gram atom of silver, for the respective oxides.

According to the thermodynamic data, electrochemical reduction of CuO in basic solution also should take place in two steps.

$$2CuO + H_2O + 2e^- = Cu_2O + 2OH^- \quad (III)$$

$$Cu_2O + H_2O + 2e^- = 2Cu + 2OH^- \quad (IV)$$

Evidence to support this view is found in the work of Johnson (7) who studied the charge and discharge characteristics of CuO plates in alkaline solution. Johnson noted a two-step reduction of the CuO plates in 4.2*N* KOH solution, the first step, which was thought to be the reduction of CuO to Cu_2O, consisted of approximately 20% of the total discharge time, while the remaining 80% was attributed to the reduction of Cu_2O.

On the other hand, discharge curves of present day alkaline CuO cells show no breaks that would

[1] Chemically prepared by Merck & Company, Inc., Rahway, New Jersey.

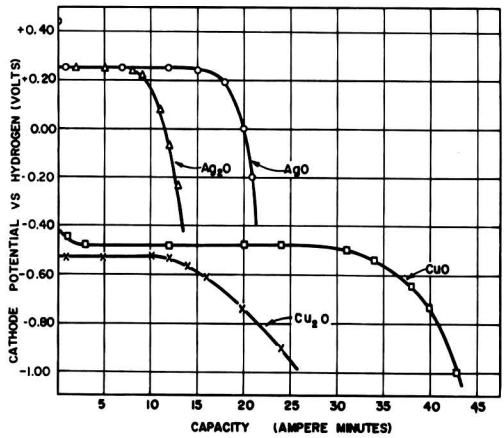

Fig. 1. Cathode potential of various group Ib oxides discharged in 30% NaOH −70% H_2O, sat'd with ZnO, electrolyte at a rate of 0.005 amp/g.

indicate a change in the reaction mechanisms. Schumacher and Heise (8) attribute this to the fact that CuO can react with Cu in accordance with the following equation:

$$CuO + Cu \rightarrow Cu_2O \quad (V)$$

and after the initial stages of discharge, Eq. (IV) is assumed to be the principal cathodic reaction.

The discharge data presented in Fig. 1 show CuO [2] to be reduced in one step at a potential of −0.48, while the discharge potential of Cu_2O [2] is −0.53 v. The fact that CuO operates at a higher potential level than Cu_2O indicates the reaction is not simply one of reduction of Cu_2O, but rather represents a more complex reduction.

Allmand and Ellingham (9) suggest that initially CuO is reduced to Cu_2O, but polarization lowers the potential to a point at which Cu_2O is reduced to Cu, this latter reaction being the chief process, although the further reduction of CuO to Cu_2O occurs simultaneously. This being the case, one would expect the discharge potential of CuO to be close to that of Cu_2O, but slightly higher; in addition, CuO should give about twice the ampere minute per gram capacity of Cu_2O on comparable tests. This is in agreement with the data presented here.

Group IIb and IIIb Oxides

Mercuric oxide, which has found use as a reference electrode in strongly alkaline solutions and for the measurement of hydroxyl ion concentration (10), constitutes the cathode of the alkaline HgO dry cell (11, 12).

Because of the instability of Hg_2O in aqueous solutions, HgO is reduced directly to Hg (3). This type of mechanism is evident from the flat voltage discharge curves of commercial HgO/KOH/Zn dry cells, as well as from the half-cell discharge data presented in Fig. 2. Under the latter conditions of discharge, the HgO cathode operated at 80% efficiency (assuming −0.40 v end point), and at a potential of +0.03 v which approximates the reversi-

[2] Fisher Scientific Company certified grades.

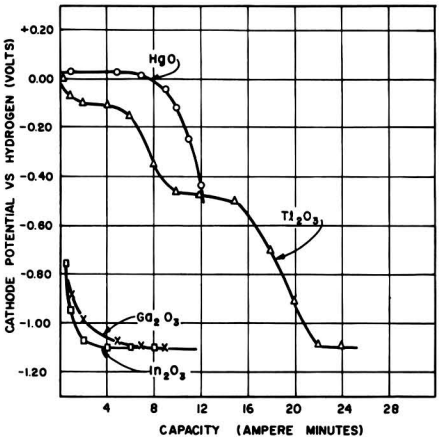

Fig. 2. Cathode potential of various group IIb and IIIb oxides discharged in 30% NaOH —70% H_2O, sat'd with ZnO, electrolyte at a rate of 0.005 amp/g.

ble electrode potential value given in Table I, after a correction of 0.055 v is made for the increased hydroxide ion activity of the electrolyte and the liquid junction potential.

Also shown in Table I and Fig. 2 are standard potentials and discharge curves for a few of the Group IIIb oxides. The reduction of Tl_2O_3 in alkaline solution takes place in two well-defined steps as expected from the chemical properties of this compound and its lower oxide, while Ga_2O_3 and In_2O_3 appear to have discharge potentials of —1.10 v or lower. However the —1.10 value is the potential characteristic of the discharge of hydrogen on the carbon electrode in this alkaline solution. This value was obtained by placing a 0.5-g sample of Shawinigan acetylene black in the cathode chamber in the absence of any other cathode material and discharging the experimental cell in the usual manner at a 0.0025 amp rate, the measured cathode potential of —1.10 v being due to the discharge of hydrogen on the carbon black.

The discharge data for Tl_2O_3 show an efficiency of 67% for the first step of reduction, and 94% for the complete reduction to the metal, assuming end points of —0.45 and —0.90 v, respectively.

Thallic oxide, because of its relatively high oxidation potential, has been considered as a cathode material for a storage cell, and in a primary fuel cell, but neither of these applications has met with any appreciable success (13).

Group IVb Oxides

It follows from the oxidation-reduction potentials for Pb that this metal is a fair reducing agent in acid solutions and a strong reducing agent in alkaline solutions, and that the dioxide is an extremely powerful oxidizing agent in acid solutions, but much weaker in alkaline solutions.

A Pb anode in an alkali hydroxide solution dissolves at first in the plumbous state, to form plumbite, but, when the solution in the vicinity of the anode becomes saturated, the dioxide is deposited. It has also been found that the oxidation of plumbite at a Pt anode yields lead dioxide (14).

Grube (15), who used both these methods to prepare alkali plumbates, made systematic measurements of the oxidation potentials of the processes. He found, at a temperature of 18°C, in 8.4*N* KOH, that the potential on the normal hydrogen scale of Pb against K_2PbO_2 was —0.613 v, while that of the plumbite-plumbate couple was +0.208. This latter potential appears to correspond to an E°_B of about +0.28 v (16), i.e., for a hydroxide ion activity of unity.

According to Glasstone (17), the reversible potential of the PbO-PbO_2 couple cannot be measured directly in alkaline solution because of the formation of the intermediate oxide, Pb_3O_4, and probably also Pb_2O_3. He estimates an E°_B value of +0.27 v on the basis of his experimental results, which is approximately the same as the E°_B value obtained from Grube's measurements. Reversible potential measurements of the Pb-PbO couple in alkaline solution have been made by Smith and Woods (18) who report a value of $E^\circ_B = -0.5785$ v for this system.

In Table I and Fig. 3 are presented the standard potentials and discharge curves for both the monoxide and dioxide of Pb, along with those of the other group IVb oxides. It is seen that PbO_2 is reduced in two steps in accordance with theory, and at potentials close to the thermodynamically calculated values of the reversible electrode potentials. The discharge potential of PbO corresponds almost exactly to the second step of the PbO_2 discharge, leaving no doubt as to the nature of the discharge.

The cathodic discharge curves of SnO, SnO_2, and GeO_2 in alkaline solution are also presented in Fig. 3, and it is seen that the SnO_2 and GeO_2 cathodes operate at too low a potential to be measured under the experimental conditions. The SnO cathode, however, operates at a potential close to its reversible value after corrections are made for the hydroxide ion activity and liquid junction potential, and is reduced with a 63% efficiency. This low cathode efficiency is probably due to the high solu-

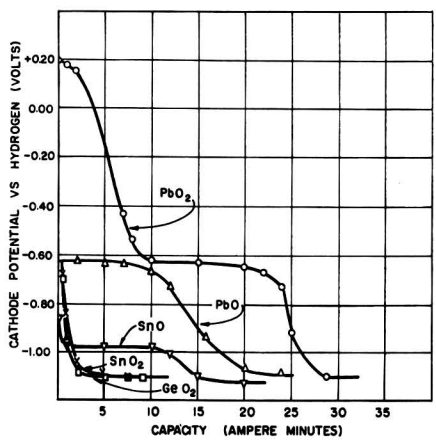

Fig. 3. Cathode potential of various group IVb oxides discharged in 30% NaOH —70% H_2O, sat'd with ZnO, electrolyte at a rate of 0.005 amp/g.

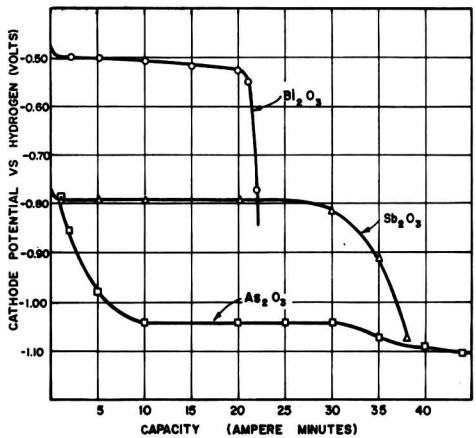

Fig. 4. Cathode potential of various group Vb oxides discharged in 30% NaOH —70% H_2O, sat'd with ZnO, electrolyte at a rate of 0.005 amp/g.

bility of the SnO with subsequent local discharge at the anode.

Group Vb Oxides

Presented in Fig. 4 are discharge curves of the +3 oxides of As, Sb, and Bi, the more metallic of the group Vb elements, when discharged in a 30% NaOH solution saturated with ZnO, at a current drain of 0.005 amp/g. It is seen from these curves and the standard potentials listed in Table I that the oxidizing power of the +3 oxides increases with increasing atomic weight of the metal.

Both the Bi_2O_3 and Sb_2O_3 cathodes display flat voltage discharge curves, corresponding to a 3-electron reduction step. This is in agreement with the work of Grube and Schweigardt (19) who found that both Bi and Sb dissolve anodically in alkaline solution in the form of tervalent ions, with the formation of alkali bismuthites and antimonites. The Bi_2O_3 electrode operates at a value close to the thermodynamically calculated value of its reversible potential, while the Sb_2O_3 cathode is seen to show a 0.07-v deviation from its reversible electrode potential. The reduction efficiencies of these materials are approximately 100%, giving the best efficiencies of all the cathodes studied.

Although the reversible electrode potential of As_2O_3 is close to that of Sb_2O_3, this electrode polarizes slowly to a potential of —1.04 v after 10 amp-min of discharge at the 0.005 amp/g rate, and remains at that potential for the remainder of its discharge.

Effect of Cathode Solubility on Discharge Potential

In the present study, only the oxides of the group I-Vb elements have been considered as cathode materials. However, compounds containing anions, such as the halides and sulfides, can also function as cathode materials. The oxides, because of their high theoretical capacity, stability, and availability are preferred as cathodes, and are used extensively in both dry and storage cells. However, there are some applications in which compounds containing other anions are used; for example in standard cells Hg_2SO_4 and Hg_2Cl_2 are used, while in reserve-type batteries, AgCl finds use as a cathode material.

The reduction of Hg_2Cl_2 is typical of these materials and is represented by the following equation

$$Hg_2Cl_2 + 2e^- \rightleftarrows 2Hg + 2Cl^- \qquad (VI)$$

Electrodes in which reactions such as the above occur and which involve a metal, M, a sparingly soluble salt of the metal, MX, and a solution of a soluble salt containing X, are termed "electrodes of the second kind". The potential of such sparingly soluble salts depends on the reversible electrode potential of the metal as well as its own solubility product (20).

Latimer (21) has listed $E°$ values and solubility products for a number of Ag compounds; the data for a few of these materials are presented in Table II along with their coulombic capacities. It is evident that the capacity of the Ag salts increases with increasing anion valency and decreasing anion weight. It is also seen that the oxidizing potential of the Ag salt increases with increasing solubility of the salt.

In Fig. 5 discharge data are presented for these Ag salts, discharged at a rate of 0.030 amp/g in the 30% NaOH solution. It is seen that the AgI and Ag_2S cathodes operate at values close to their reversible electrode potentials, as does the Ag_2O electrode when its reversible potential is corrected for the activity of the hydroxide ion. The cathodes are reduced with an efficiency of 85-95% under these conditions of discharge. The reversible electrode potential and solubility data for Ag_2Se were not available, but from the discharge curves one would predict a lower solubility for this compound than for Ag_2S.

The use of this method in making approximate measurements of salt solubilities should apply to any couple containing a precipitate or a complex ion which is only a variation of the simple couple involving the free ions; then its potential may be

Table II. Half-cell reactions, capacity, and solubility products of various Ag Compounds

Cathode	Half-cell reaction	$E°$	Solubility product	Cathode capacity (amp-min/g)
Ag^+	$Ag^+ + e^- = Ag$	+0.7991	—	—
Ag_2O	$Ag_2O + H_2O + 2e^- = 2Ag + 2OH^-$	+0.344	2.0×10^{-8}	13.9
AgI	$AgI + e^- = Ag + I^-$	—0.151	8.5×10^{-17}	6.8
Ag_2S	$Ag_2S + 2e^- = 2Ag + S^=$	—0.69	5.5×10^{-51}	13.0
Ag_2Se	$Ag_2Se + 2e^- = 2Ag + Se^=$	—	—	10.9

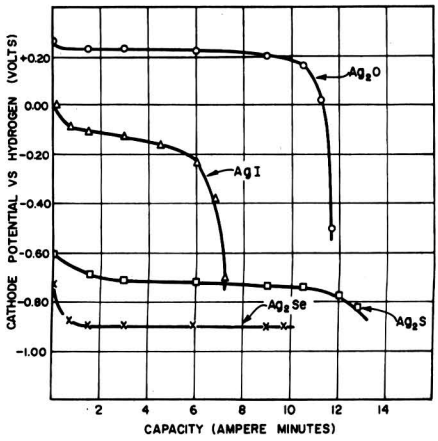

Fig. 5. Cathode potential of various Ag salts discharged in 30% NaOH —70% H_2O, sat'd with ZnO, electrolyte at a rate of 0.030 amp/g.

regarded as a corrected value based on the standard potential of the simple reaction.

Summary

1. The reduction of AgO and CuO in concentrated NaOH electrolyte takes place in one step (in disagreement with predictions based on available thermodynamic data). When cells with these cathodes undergo reduction, the AgO is reduced to Ag at the same potential as that found for the discharge of Ag_2O to Ag under similar conditions, while the reduction of CuO to Cu takes place at a potential 0.05 v higher than the corresponding reduction of Cu_2O to Cu.

2. Among the Group IIb and IIIb oxides, HgO is reduced directly to Hg in concentrated NaOH electrolyte, while Tl_2O_3 shows two well-defined reduction steps corresponding to the +3 and +1 oxidation states of Tl.

3. PbO_2 also shows a two-step reduction at potentials corresponding to the theoretical values of the PbO_2-PbO, and PbO-Pb couples, while SnO_2 and GeO_2 polarize under load to low potential levels.

4. Among the Group Vb oxides, Bi_2O_3 and Sb_2O_3 display flat voltage discharge curves corresponding to a 3-electron reduction step, the former operating close to its reversible potential level, while the latter shows a small deviation from its theoretical potential.

5. The electrode potential, under current drain, of a few sparingly soluble Ag salts has been found to be dependent on its solubility product, the oxidizing power of the Ag salt increasing with increasing solubility of the salt.

Manuscript received Nov. 1, 1956. This paper was prepared for delivery before the Cleveland Meeting, Sept. 30-Oct. 4, 1956.

Any discussion of this paper will appear in a Discussion Section to be published in the June 1958 JOURNAL.

REFERENCES

1. C. K. Morehouse and R. Glicksman, *This Journal*, **103**, 94 (1956).
2. R. Glicksman and C. K. Morehouse, *ibid.*, **102**, 273 (1955).
3. W. M. Latimer, "Oxidation Potentials," 2nd ed., Prentice Hall, Inc., New York (1952).
4. R. Luther and F. Pokorny, *Z. Anorg. Chem.*, **57**, 290 (1908).
5. J. G. Zimmerman, *Trans. Electrochem. Soc.*, **68**, 231 (1935).
6. G. W. Vinal, "Storage Batteries," 4th ed., p. 101, John Wiley & Sons, Inc., New York (1955).
7. W. M. Johnson, *Trans. Amer. Electrochem. Soc.*, **1**, 187 (1902).
8. E. A. Schumacher and G. W. Heise, *This Journal*, **99**, 191C (1952).
9. A. J. Allmand and H. J. T. Ellingham, "The Principles of Applied Electrochemistry," 2nd ed., p. 212, Edward Arnold & Co., London (1924).
10. D. A. MacInnes, "The Principles of Electrochemistry," p. 253, Rheinhold Publishing Corp., New York (1939).
11. S. Ruben, *Trans. Electrochem. Soc.*, **92**, 183 (1947).
12. M. Friedman and C. E. McCauley, *ibid.*, **92**, 195 (1947).
13. S. Glasstone and A. Hickling, "Electrolytic Oxidation and Reduction," p. 105, D. Van Nostrand Co., Inc., New York (1936).
14. Ref. (13), p. 111.
15. G. Grube, *Z. Elektrochem.*, **28**, 273 (1922).
16. Ref. (3), p. 156.
17. S. Glasstone, *J. Chem. Soc.*, **121**, 1469 (1922).
18. D. F. Smith and H. K. Woods, *J. Am. Chem. Soc.*, **45**, 2632 (1923).
19. G. Grube and F. Schweigardt, *Z. Elektrochem.*, **29**, 257 (1923).
20. Ref. (10), p. 255.
21. Ref. (3), p. 191.

Potential-*p*H Diagram of the Antimony-Water System

Its Applications to Properties of the Metal, Its Compounds, Its Corrosion, and Antimony Electrodes

Arthur L. Pitman

Naval Research Laboratory, Washington, D. C.

Marcel Pourbaix

University of Brussels, Brussels, Belgium, Belgian Center for Corrosion Study (CEBELCOR)

and

Nina de Zoubov

Belgian Center for Corrosion Study (CEBELCOR), Brussels, Belgium

ABSTRACT

Using methods and conventions described previously together with the available thermodynamic and electrochemical data, equations have been formulated and represented as a potential-*p*H equilibrium diagram of the antimony-water system for 25°C. Other diagrams are presented for the domains of solubility, predominance of ions, and for corrosion. The reason for the observed resistance of antimony coatings to hydrochloric and hydrofluoric acids is made clear. Applications are made to the antimony electrodes. The free energies of formation of the antimonate, $Sb(OH)_6^-$, and the SbO_2^+ ion have been calculated and are given.

The usefulness of potential-*p*H diagrams in research has been shown previously by one of the authors (1), by Delahay and Van Rysselberghe (2), and others too numerous to mention. If a reaction is thermodynamically impossible under given conditions, one can dismiss that reaction from further consideration, directing his attention instead to other closely related reactions. Consider the case of the resistance of Sb coatings on Fe to nonoxidizing acids such as HCl or HF (3). The electrode potential[1] of an isolated Sb-coated electrode in such acids and in an oxygen-free atmosphere will lie a little above the potential of the hydrogen electrode. This is to be assumed at present, but will be demonstrated later. It will be shown by thermodynamical data and methods that a perfect coating of Sb cannot be attacked under the stipulated conditions. Therefore if attack occurs, it must be due to an oxidizing agent such as air which elevates the potential into a zone where attack occurs, or from pinholes in the coating of Sb.

A further field of use for diagrams such as are in this paper is that of simplifying and explaining the study of metals and their compounds in aqueous solutions (1).

The previously unknown free energies of formation for antimonate, $Sb(OH)_6^-$, and SbO_2^+ ions have been computed and are used in the preparation of the potential-*p*H diagram.

The free energies of formation of compounds and ions given in Table I are those recommended by Latimer (7) unless otherwise mentioned.

There are two known polymorphs of antimony trioxide. The cubic form, Sb_2O_3(c), existing in nature as the mineral senarmontite, and the orthorhombic form, existing as the mineral valentinite (8). As Table I shows, the free energy of formation of the cubic form is the more negative of the two at 25°C so that it is the inherently more stable of the two at this temperature. For this reason, it is the form which Latimer (7) tabulates, taking −149,000 cal as the value of free energy of formation from Table 21-2 of the U. S. Bureau of Standards' Tables

Table I. Free energies of formation used in calculating equilibrium equations

Solvent and dissolved substances	$\Delta Ff°$ (cal)	Solid substances	$\Delta Ff°$ (cal)
H_2O	−56,690	Sb_2O_3 (cubic)	−149,000
H^+	0	Sb_2O_3 (ortho) *	−147,000
OH^-	−37,595	Sb_2O_4	−165,900
SbO^+	−42,000	Sb_2O_5	−200,500
SbO_2^-	−82,500		
$HSbO_2$(aq)	−97,500	Gaseous substances	$\Delta Ff°$ (cal)
$Sb(OH)_4^-$*	−195,880		
SbO_2^+*	−65,500	SbH_3	35,300
$Sb(OH)_6^-$*	−293,000		

* $\Delta Ff°_{Sb(OH)_4^-} = \Delta Ff°_{SbO_2^-} + 2\Delta Ff°_{H_2O} = -195{,}880$ cal. The free energies of the other marked ions are derived by methods which are described later.

[1] The term "electrode potential" is the same as that recommended at the meeting of the International Union of Pure and Applied Chemistry at Stockholm, 1953, (4, 5); at the equilibrium it is equal to the emf of half-cells where electrons appear as reactants on the left side of the equations. When the algebraic sum of free energies in the reaction is positive, the sign of the electrode potential $E°$ is positive. Thus, the manner of writing the equations and the signs for electrode potential are the same as in reference (6). The electrode potential is thus positive for oxidizing systems (F_2, F^-) and negative for reducing systems (Zn, Zn^{++}).

(9). The basis for the National Bureau of Standards' value was the work of Roberts and Fenwick (10) who found $\Delta Ff^\circ_{Sb_2O_3(c)}$ equal to $-149{,}690 \pm 200$ cal. Roberts and Fenwick determined the potentials of the cells: Pt,H_2 solution, Sb_2O_3(c) Sb and Pt,H_2 solution, Sb_2O_3(o) Sb, both with air excluded. From these measurements they computed the free energy for Sb_2O_3(ortho) → Sb_2O_3(cubic) as $\Delta F^\circ = -1{,}800$ cal. From the free energy of formation of Sb_2O_3(c) in Table I, the free energy of formation of Sb_2O_3(o) becomes $-147{,}000$ cal in round numbers.

A review of the researches cited herein shows that only in two of them have single allotropic forms of Sb_2O_3 been used (8, 10). The results of these two researches have been used to compute $\Delta Ff^\circ_{HSbO_2(aq)} = -96{,}510$ cal from the use of Sb_2O_3(c) and $-96{,}440$ cal from the use of Sb_2O_3(o). Latimer's value (7) of $-97{,}500$ cal was derived from Schulze's solubility data at 15°C on mixed crystal forms combined with $\Delta Ff^\circ Sb_2O_3$(c) $= -149{,}000$ cal.

The value of $\Delta Ff^\circ_{Sb_2O_3(s)}$ equals $-148{,}640$ cal was determined by Schuhmann (11). His method of precipitating and purifying Sb_2O_3 was followed by Roberts and Fenwick (10) who found that it resulted in a mixture which was chiefly in the orthorhombic form. Tourky and Mousa (12) used practically the same method of preparation. Bloom (8) could precipitate the orthorhombic form with HCl, or the cubic form with $HClO_4$, both at $pH = 2.2$. Thus most experiments behind free energy values for Sb use a mixture of Sb_2O_3 crystals possibly high in the orthorhombic form. Furthermore, the free energy of formation of this Sb_2O_3(s) mixture as found by Schuhmann was 400 cal lower than $-149{,}000$ cal which is the value selected for the (c) form by the Bureau of Standards and by Latimer (7) which the authors have placed in Table I for use when Sb_2O_3(s) participates in a reaction.

Furthermore the solubility at measured pH values is of use in determining the form of ion or molecule in which the solute exists. The most useful relation to present (1) is used in Fig. 1 for Sb_2O_3, namely, the log solubility plotted against the pH. Such curves normally consist of straight-line branches. The slope of each branch is directly related to the formulas for the principal reaction occurring upon solution in the corresponding range of pH. In the pH range from 0 to 1+ taken from Schuhmann (11), the slope is −1. This corresponds to the presence of the SbO^+ ion, as previously established (8). Two circles at pH about 2 represent Bloom's (8) results for valentinite and senarmontite at approximately 25°C. Tourky and Mousa's (12) data at 35°C for the range of pH from 9 to 10.4 are essentially constant and nearly equal to Bloom's (8) data for senarmontite. Tourky and Mousa found some evidence for the Sb^{+++} ion just below $pH = 9.5$. The slope of log solubility with pH is zero from below $pH = 2$ to 10.4 indicating a nonionic solute. This solute has been regarded by Latimer (7) as meta-antimonious acid, $HSbO_2$, and is so treated in this paper. Finally the log solubility in the pH range of 11 to about 13.7 (12) forms a branch with a slope of 1. Latimer has regarded the corresponding ion to be SbO_2^-. His selected value for the free energy of formation are given in Table I, as is that for the $Sb(OH)_4^-$ ion. The latter form was identified by Brintzinger (13) in 2.5*N* KOH through dialysis experiments. The authors prefer the latter form of Brintzinger for the negative ion.

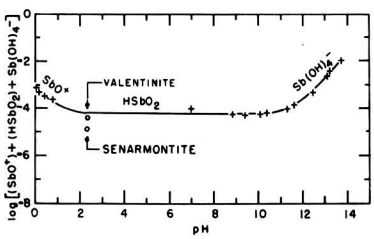

Fig. 1. Solubility of antimony trioxide (5, 8, 9)

The antimonate ion was shown by Brintzinger (13) to be $Sb(OH)_6^-$ in 2.5*N* KOH. It is now possible to compute the previously unknown energy of formation for this ion both by the use of oxidation-reduction potentials and from measurements of the solubilities of Sb_2O_5. The oxidation-reduction potentials of the anions of trivalent and pentavalent Sb were measured in 1923 by Grube and Schweigardt (14) in 3*N*-10*N* KOH. They assumed that the couple was SbO_2^--SbO_3^- corresponding to a two hydroxyl, two electron reaction, but could not prove it so far as the hydroxyl relation was concerned because data was then lacking on the activity coefficients of the electrolyte in the solutions of KOH employed. Since then these coefficients have been published by Akerlof and Bender (15). Haight (16) studied the oxidation-reduction potentials by polarographic methods. He measured the half-wave potential, $E_{1/2}$, of trivalent Sb anodically polarized in 1*M*-10*M* KOH and found that the 0.060 slope of $E_{1/2}$ to pH corresponded to a reversible reaction of the two hydroxyl, two electron form just as Grube and Schweigardt had conjectured. Haight proposed tentatively that the reaction might be

$$2OH^- + Sb(OH)_4^- \rightleftarrows Sb(OH)_6^- + 2e^- \qquad (I)$$

The evidence of Brintzinger cited already by the authors confirms this equation of Haight.

The formula corresponding to the equilibrium of reaction (I) is

$$E_A = E^\circ_A - 0.0591 \log (a_{OH^-}) + 0.0295 \log \frac{[Sb(OH)_6^-]}{[Sb(OH)_4^-]}$$

where E_A is the equilibrium electrode potential of reaction (I) with reference to the standard hydrogen electrode; E°_A is the standard electrode potential (for $pH = 14.0$), coresponding to value 1 for the activity a_{OH^-} of the OH^- ion and for the ratio $[Sb(OH)_6^-]/[Sb(OH)_4^-]$ of the concentrations of the $Sb(OH)_4^-$ and $Sb(OH)_6^-$. If reaction (I) is written as follows:

$$Sb(OH)_6^- + 2H^+ + 2e^- = Sb(OH)_4^- + 2H_2O \qquad (II)$$

its equilibrium electrode potential may be written as follows:

$$E_B = E^\circ_B - 0.0591\ pH + 0.0295 \log [Sb(OH)_6^-]/[Sb(OH)_4^-]$$

Table II. Thermodynamic data on antimonite-antimonate potentials

N KOH	E	log (a_{OH^-})	E°_B	E°_A
1	2	3	4	5
9	−0.577	1.9097	−0.464	+0.364
8	−0.567	1.6589	−0.469	0.359
7.5	−0.561	1.5755	−0.469	0.359
7	−0.555	1.4478	−0.469	0.359
6	−0.540	1.2269	−0.467	0.361
5	−0.516	1.0390	−0.455	0.373
4	−0.484	0.8108	−0.436	0.393
3	−0.428	0.4952	−0.399	0.429

where E°_B is the standard electrode potential (for pH = 0.0) corresponding to value 1 for the activity a_{H^+} of the H^+ ion and for the ratio $[Sb(OH)_6^-]/[Sb(OH)_4^-]$. As is well known, $E^\circ_B = E^\circ_A + E^\circ_A + 0.828$ volt. Thermodynamic data on the antimonite-antimonate potentials are given in Table II. The normality of KOH used by Grube and Schweigardt (14) and the values of the electrode potential, found when the Sb^V to Sb^{III} ratio is unity, are in columns 1 and 2. Columns 3, 4, and 5 give the calculated values for log a_{OH^-} (15) (which is assumed to be equal to log $a\pm$) E°_B and E°_A.

The values of the mean activity coefficient, γ, are from Akerlof and Bender (15). The $a\pm = \gamma m\pm$, where $m\pm$, the mean concentration of K^+ and OH^- ions, is assumed equal to m_{KOH} in the solution. A representative value for E°_B is +0.363 volt, the average of the top six values in column 5. This leads to the following formula for the equilibrium potential of the reaction:

$$E = 0.363 - 0.0591\ pH + 0.0295 \log \frac{[Sb(OH)_6^-]}{[Sb(OH)_4^-]}$$

From $E^\circ_B = 0.363$ volt, $\Delta Ff^\circ_{H_2O} = -56{,}690$ cal, $\Delta Ff^\circ_{Sb(OH)_4^-} = -195{,}880$ cal, the calculations are $\Delta Ff^\circ_{Sb(OH)_6^-} = -292{,}500$ cal ±2000 cal.

The free energy of formation of $Sb(OH)_6^-$ may be derived with somewhat greater accuracy from the solubility of Sb_2O_5 as measured by Tourky and Mousa (12) in HCl of various concentrations. From their data and published data on the activity coefficients of HCl, a graph has been prepared which shows log Sb^V (gram atoms per 1000 g H_2O) vs. pH (Fig. 2). The two branches of the curve meet at pH = −0.27, the isoelectric point. The branch above this point is linear and, from Brintzinger's results already noted, the ion must be $Sb(OH)_6^-$ (13). The equation for one branch of the curve, then, is

$$2Sb(OH)_6^- + 2H^+ = Sb_2O_5 + 7H_2O \quad (III)^2$$
$$2 \log [Sb(OH)_6^-] = \log K_c + 2pH$$

It follows from formula (III) and the data of Fig. 2 that at pH = 0 log K_c = 2 log $[Sb(OH)_6^-]$ or −8.31. Applying the conditions log K_c = −8.31, $\Delta Ff^\circ_{Sb_2O_5} = -200{,}500$ cal, and $\Delta Ff^\circ_{H_2O} = -56{,}690$ cal to the equilibrium formula for log K in terms of the free energies of formation, $\Delta Ff^\circ_{Sb(OH)_6^-} = -293{,}000$ cal. This value is within 500 cal of the value derived by the authors from Grube and Schweigardt's data (14). This value is used in Table I since it is the more accurate of the two computed.

[2] The theoretical slope of formula (III) is +1 pH but the experimental slope shown in Fig. 2 is +0.25 pH. No likely equation known to the writers has a slope of +0.25 pH. The cause of this difference is not known.

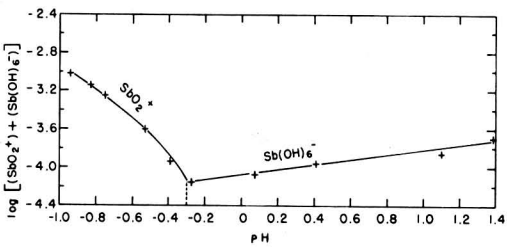

Fig. 2. Solubility of antimony pentoxide (9)

The pentavalent Sb cation, according to Tourky and Mousa (12) was probably SbO^{+3} but might be monovalent SbO_2^+ below the isoelectric point. The author's choice of SbO_2^+ is based on the theoretical slope of −1 for its formations in solutions saturated with Sb_2O_5 below the isoelectric point as indicated by Eq. [15] in the table of equations and formulas. Although the experimental slope shown in Fig. 2 varies from −1.2 to −2, one can hardly expect a constant slope in such acid solutions and the lowest theoretical slope is −1. On the other hand, the theoretical slope for the formation of SbO^{+++} is only −0.33. Of the two ions, therefore, SbO_2^+ is to be preferred since its theoretical slope is much nearer to the experimental one.

For the SbO_2^+ ion

$$SbO_2^+ + 4H_2O = Sb(OH)_6^- + 2H^+ \quad (IV)$$
$$\log \frac{[Sb(OH)_6^-]}{(SbO_2^+)} = \log K_d + 2\ pH$$

In Fig. 2 at the isoelectric point of pH = −0.27, the left-hand member of the formula equals zero and log K_d = −2 pH or 0.54. Substituting this value and the free energies of formation for water and for $Sb(OH)_6^-$, −56,690 and −293,000 cal, respectively, in the equilibrium formula for log K_d the authors calculate that $\Delta Ff^\circ_{SbO_2^+}$ equals −65,500 cal.

Equilibrium Equations

The equilibrium equations which follow have been calculated by the use of the usual thermodynamic formulas which are given by Pourbaix (1) and others (2).

For Water

$$2H^+ + 2e^- = H_2 \quad (a)$$
$$E = -0.0591\ pH - 0.0295 \log P_{H_2}$$

$$O_2 + 4H^+ + 4e^- = 2H_2O \quad (b)$$
$$E = 1.229 - 0.0591\ pH + 0.0148 \log P_{O_2}$$

For Antimony and Its Compounds

A. *Homogeneous Reactions Without Oxidation*

$$HSbO_2 + H^+ = SbO^+ + H_2O \quad [1]$$
$$\log \frac{(HSbO_2)}{(SbO^+)} = -0.87 + pH$$

$$Sb(OH)_4^- + H^+ = HSbO_2 + 2H_2O \quad [2]$$
$$\log \frac{[Sb(OH)_4^-]}{(HSbO_2)} = -11.00 + pH$$

$$Sb(OH)_6^- + 2H^+ = SbO_2^+ + 4H_2O \quad [3]$$
$$\log \frac{[Sb(OH)_6^-]}{(SbO_2^+)} = 0.54 + 2\,pH$$

With Oxidation

$$SbO_2^+ + 2H^+ + 2e^- = SbO^+ + H_2O \quad [4]$$
$$E = 0.720 - 0.0591\,pH + 0.0295 \log \frac{(SbO_2^+)}{(SbO^+)}$$

$$Sb(OH)_6^- + 4H^+ + 2e^- = SbO^+ + 5H_2O \quad [5]$$
$$E = 0.704 - 0.1182\,pH + 0.0295 \log \frac{[Sb(OH)_6^-]}{(SbO^+)}$$

$$Sb(OH)_6^- + 3H^+ + 2e^- = HSbO_2 + 4H_2O \quad [6]$$
$$E = 0.678 - 0.0886\,pH + 0.0295 \log \frac{[Sb(OH)_6^-]}{(HSbO_2)}$$

$$Sb(OH)_{6^-} + 2H^+ + 2e^- = Sb(OH)_4^- + 2H_2O \quad [7]$$
$$E = 0.353 - 0.0591\,pH + 0.0295 \log \frac{[Sb(OH)_6^-]}{[Sb(OH)_4^-]}$$

B. *Heterogeneous Reactions Involving Two Sides With Oxidation*

$$Sb_2O_3 + 6H^+ + 6e^- = 2Sb + 3H_2O \quad [8]$$
(cubic) $E = 0.152 - 0.0591\,pH$
(ortho) $= 0.167 - 0.0591\,pH$

$$Sb_2O_4 + 2H^+ + 2e^- = Sb_2O_3 + H_2O \quad [9]$$
(cubic) $E = 0.863 - 0.0591\,pH$
(ortho) $= 0.819 - 0.0591\,pH$

$$Sb_2O_5 + 2H^+ + 2e^- = Sb_2O_4 + H_2O \quad [10]$$
$$E = 0.479 - 0.0591\,pH$$

$$Sb_2O_5 + 4H^+ + 4e^- = Sb_2O_3 + 2H_2O \quad [11]$$
(cubic) $E = 0.671 - 0.0591\,pH$
(ortho) $= 0.649 - 0.0591\,pH$

C. *Heterogeneous Reactions Involving One Solid Without Oxidation*

$$Sb_2O_3 + 2H^+ = 2SbO^+ + H_2O \quad [12]$$
(cubic) $\log (SbO^+) = -3.05 - pH$
(ortho) $= -2.32 - pH$

$$Sb_2O_3 + H_2O = 2HSbO_2 \quad [13]$$
(cubic) $\log (HSbO_2) = -3.92$
(ortho) $= -3.19$

$$2\,Sb(OH)_4^- + 2H^+ = Sb_2O_3 + 5H_2O \quad [14]$$
(cubic) $\log [Sb(OH)_4^-] = -14.91 + pH$
(ortho) $= -14.18 + pH$

$$Sb_2O_5 + 2H^+ = 2SbO_2^+ + H_2O \quad [15]$$
$$\log (SbO_2^+) = -4.70 - pH$$

$$2Sb(OH)_6^- + 2H^+ = Sb_2O_5 + 7H_2O \quad [16]$$
$$\log [Sb(OH)_6^-] = -4.16 + pH$$

With Oxidation

$$Sb + 3H^+ + 3e^- = SbH_{3\,gas} \quad [17]$$
$$E = -0.510 - 0.0591\,pH - 0.0197 \log P_{SbH_3}$$

$$SbO^+ + 2H^+ + 3e^- = Sb + H_2O \quad [18]$$
$$E = 0.212 - 0.0394\,pH + 0.0197 \log (SbO^+)$$

$$HSbO_2 + 3H^+ + 3e^- = Sb + 2H_2O \quad [19]$$
$$E = 0.230 - 0.0591\,pH + 0.0197 \log (HSbO_2)$$

$$Sb(OH)_4^- + 4H^+ + 3e^- = Sb + 4H_2O \quad [20]$$
$$E = 0.446 - 0.0788\,pH + 0.0197 \log [Sb(OH)_4^-]$$

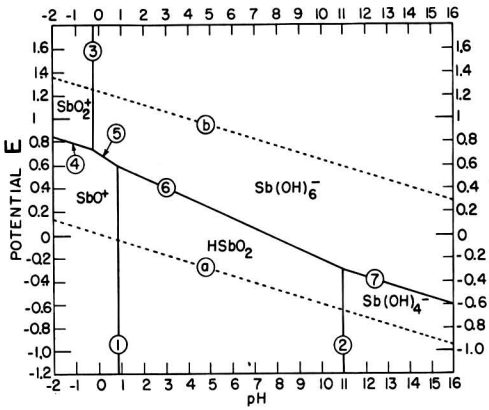

Fig. 3. Zones of predominance for ions containing Sb

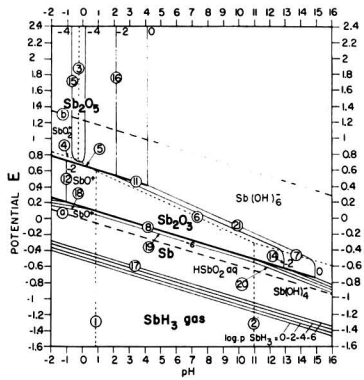

Fig. 4. Equilibria of antimony-water

$$2Sb(OH)_6^- + 6H^+ + 4e^- = Sb_2O_3 + 9H_2O \quad [21]$$
(cubic) $E = 0.794 - 0.0886\,pH + 0.0295 \log [Sb(OH)_6^-]$
(ortho) $= 0.722 - 0.0886\,pH + 0.0295 \log [Sb(OH)_6^-]$

$$Sb_2O_5 + 6H^+ + 4e^- = 2SbO^+ + 3H_2O \quad [22]$$
$$E = 0.581 - 0.0886\,pH - 0.0295 \log (SbO^+)$$

Stability of Antimony, Its Oxides, and Its Solutions

The zones of predominance of the solutes are shown in Fig. 3. The lines show the loci of points for which the activities (or the concentrations in ideal solutions) of two Sb ions, simultaneously present in the solution, are equal to one another.

SbO_2^+	:	Limited by lines 3 and 4.
$Sb(OH)_6^-$	:	Limited by lines 3, 5, 6, and 7.
SbO^+	:	Limited by lines 4, 5, and 1.
$HSbO_2$	:	Limited by lines 1, 6, and 2.
$Sb(OH)_4^-$	:	Limited by lines 2 and 7.

Figure 4 is a diagram for the thermodynamic equilibria of the system Sb-H_2O at 25°C as developed from Eq. (I), (II), and [2] through [22]. When one ion takes part in a reaction, the equilibrium is shown for values of concentration in dissolved Sb equal to 1, 10^{-2}, 10^{-4}, and 10^{-6} g at./l. For the reaction [17] of reduction of solid Sb to gaseous SbH_3, the equilibrium is shown for partial pressures of SbH_3 equal to 1, 10^{-2}, 10^{-4}, and 10^{-6}, the metal or

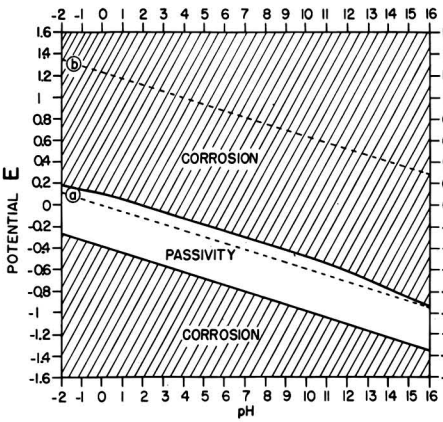

Fig. 5. Corrosion and passivity of Sb

oxide in contact with the solution is considered to be stable (1, 2).

Domains of stability of solid compounds shown in Fig. 4 are:

- Sb : Below line 8, and within the families of lines 18, 19, 20, and 17.
- Sb_2O_3 : Between lines 8 and 11, and between the families of lines 12 and 21.
- Sb_2O_5 : Possibly in a narrow zone above line 11 and between the families of lines 15 and 16.
- Sb_2O_4 : This oxide is never thermodynamically stable at 25°C in the presence of water.

Gaseous SbH_3 is stable below the family of line 17.

The great area of stability of the $Sb(OH)_6^-$ ion is responsible for a strong tendency of Sb_2O_3 to dissolve at potentials more positive than those of line 21. In this, the Sb diagram resembles that of Cr (1).

Antimony tetroxide Sb_2O_4 in the dry state is well defined and shows a distinctive x-ray diffraction pattern (17). Konopik and Zwiauer (18) found that when the dry oxide is dissolved in water, however, it behaved like a compound of trivalent and pentavalent oxides, giving rise to a mixture of Sb^{III} and Sb^{V} in solution. This is in accordance with the above-mentioned fact that Sb_2O_4 is thermodynamically unstable in the presence of aqueous solutions.

Figure 4 shows that SbH_3 may be prepared, together with hydrogen, by a sufficiently strong reductive action on Sb salt solutions or on metallic Sb in the presence of water, but that it is thermodynamically unstable and tends to decompose into Sb and H_2.

In fact, SbH_3 may be prepared by electrolysis of acid or alkaline solutions with a cathode of metallic Sb (19); yields of SbH_3 as high as 15% by volume in the gas evolved at the cathode have been reported. SbH_3 is usually prepared by acid treatment of an alloy of Sb with a reactive metal such as Zn or Mg.

SbH_3 is unstable in the presence of aqueous solutions, and tends then to decompose with formation of Sb and of H_2; but Salzberg and Andreatch (20) found that the velocity of this decomposition is negligible between the limits set by 0.1*N* acid and 0.1*N* alkali, i.e., approximately between a *p*H of 1 and 13.7. The decomposition is rapid in solutions which are strongly alkaline (20, 21) or strongly acid (21).

Applications of the Diagrams

A few applications are made here of the equilibrium diagrams to the study of electrochemical systems. Because the diagrams represent equilibrium conditions they can be used only to set limits within which practical, nonequilibrium systems operate.

Reduction of Corrosion by Antimony Coatings or by Its Compounds

Figure 5, which is derived from the equilibrium diagram (Fig. 4), represents the theoretical conditions of corrosion and of immunity (noncorrosion) of Sb, according to assumptions which have been made previously (1). Passivation is not considered in Fig. 5 because of the great solubility of the antimony oxides.

According to Burns and Bradley (3), nonporous coatings of Sb on steel resist attack by HCl and HF but are attacked by HNO_3. A study of the diagram as simplified in Fig. 5 would have led to the same general conclusions. From this diagram one would expect that *p*H = 0 in HCl or HF, Sb would be passive since the potential of the metal-metal ion couple would be about 0.1 volt more positive than the hydrogen potential at the same *p*H. Under such a condition hydrogen ions will not be displaced from solution by the metal ions. The above acids are nonoxidizing. On the other hand, when Burns and Bradley tested an Sb-coating against strong HNO_3 which is a powerful oxidizing agent, the metal was attacked. This is because the HNO_3 would cause the potential of the metal in it to be higher than 0.1 volt above line (a). Such a potential would be in the upper corrosion zone of Fig. 5.

Piontelli and Fagnani (22) have reviewed the theory of pickling inhibitors and have experimented with Sb_2O_3 in 3*M* to 10*M* HCl to restrain the corrosion of mild steel under treatment. It was concluded that metallic Sb displaces Fe in the stronger solutions and this action is in accordance with predictions which may be made from the thermodynamic emf of the process, a statement which is readily verified. They pointed out that because the overvoltage of hydrogen is higher on Sb than on Fe, corrosion is lessened as the deposited Sb film spreads. As discussed in the previous paragraph, Fig. 5 shows that, as the surface is covered progressively, with Sb, the potential of the isolated metallic surface will approach that of Sb. Such a potential is more positive than the hydrogen potential. Attack of the metal will lessen and can cease for this reason.

Figure 5 also shows that there is a possibility of cathodic corrosion of Sb under very reducing conditions, with formation of gaseous SbH_3. Salzberg and Andreatch (20) have formed gaseous SbH_3 in this manner.

Antimony Electrodes

The prevalent theory of the Sb electrodes (10) is not entirely accurate since the Sb^{+++} ion, assumed to take part in an intermediate electrode reaction, is now shown by the authors to be unproven in aqueous solutions. In the following, a mechanism is suggested which is consistent with the facts about the two general types of Sb electrode in use: the Sb-Sb_2O_3 electrode and the Sb rod electrode.

The Sb-Sb_2O_3 electrode contains a mixture of powdered Sb and of Sb_2O_3 in an electrode vessel with a side arm. Electrolyte moves slowly through the vessel and is saturated with respect to Sb_2O_3 before entering the side arm at the tip of which the liquid junction occurs. The cell is kept saturated with nitrogen. Under such conditions, Roberts and Fenwick (10) determined $\Delta F^\circ_{Sb_2O_3(c)}$ and $\Delta F^\circ_{Sb_2O_3(o)}$, and Schuhmann (11) determined ΔF_{SbO^+}.

At present, the accepted theory for the Sb-Sb_2O_3 electrode is that of Roberts and Fenwick (10). They proposed these intermediate reactions for the Sb-Sb_2O_3 couple:

$$2\,Sb \rightleftarrows 2\,Sb^{+++} + 6e^- \qquad (V)$$

$$2Sb^{+++} + 6\,OH^- \rightleftarrows Sb_2O_3 + 3H_2O \qquad (VI)$$

Conceivably, the Sb^{+++} ion could possibly be derived from orthoantimonious acid, $Sb(OH)_3$, solid salts of which are known. The above mechanism is considered to be unlikely since the Sb^{+++} ion has not been found to be present in any part of the pH range from 0 to 14. However, the SbO^+ ion has been shown to exist in solutions of low pH (11), *see* Eq. [12], and the $Sb(OH)_4^-$ ion has been shown to exist in solutions of high pH (Eq. [14]); for intermediate values of the pH, the dissolved Sb exists as undissociated $HSbO_2$ molecules.

According to Schuhmann (11) and Roberts and Fenwick (10), the value of the potential of Sb-$Sb_2O_{3\ cubic}$ electrodes is given by Eq. [8].

$$E = 0.152 - 0.0591\ pH\ (at\ 25°C)$$

It may be seen on Fig. 4 and 1 that for pH approximately from 2 to 10, the Sb-Sb_2O_3 electrode can be represented by the Sb-$Sb_2O_{3\ cubic}$ couple, in the presence of a constant concentration in dissolved Sb $10^{-3.9}$ mole $HSbO_2$/l, or 10 mg Sb/l; for pH lower than 1-2, or higher than 10-11, the electrode potentials may correspond to the theoretical value given by Eq. [8] only if the solution has a higher content in dissolved Sb, respectively as SbO^+ or as $Sb(OH)_4^-$ ions.

The Sb rod electrode may be used under controlled conditions, preferably with mechanical agitation and in the absence of dissolved oxygen. Potential values given by Kolthoff and Hartong (23) for the temperature of 14°C are shown in Fig. 6. The two following equations are given for these values:

For pH 1-5

$E = -0.0415 - 0.0485\ pH$ (14°C) shown as line A

For pH 9-12

$E = -0.009 - 0.0536\ pH$ (14°C) shown as line B

Grube and Schweigardt (14) have reported that potential values may be appreciably lower for pH higher than 12.

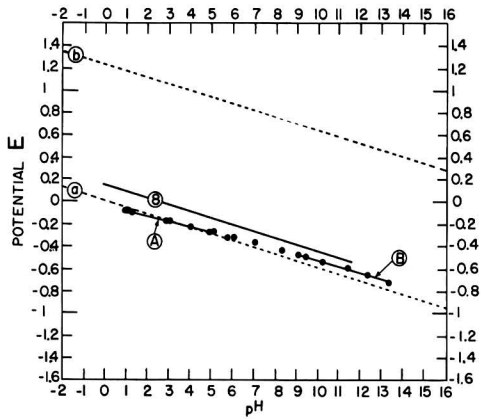

Fig. 6. Antimony electrodes. Line 8—powdered Sb-$Sb_2O_{3(cubic)}$ electrode data from reference (10). Dots and Lines A and B—results obtained by Kolthoff and Hartong (23) with cast electrodes of Sb-Sb_2O_3.

It may be seen on Fig. 6 that, if the values for 25°C are approximately the same as the values given by Kolthoff (23) for 14°, they do not correspond to a Sb-Sb_2O_3 equilibrium shown as line 8; they correspond approximately to a H_2-H^+ equilibrium under 0.01 to 1 atm hydrogen pressure.Thus, it seems that the Sb rod electrode behaves approximately as a hydrogen electrode, this hydrogen being formed at the surface of the Sb as a result of a very minute corrosion of the metal. As the equilibrium concentration of dissolved Sb at these potentials is extremely low (approximately 10^{-10}), the amount of dissolved Sb is usually not noticeable; care should be taken to avoid the formation of Sb_2O_3, which could increase the potential. Some more experimental investigations on this subject might be welcome.

Acknowledgment

Two of the authors, M. Pourbaix and N. de Zoubov, wish to thank the l'Union Minière du Haut Katanga and l'Institut pour l'Encouragement de la Recherche Scientifique dans l'Industrie et dans l'Agriculture, IRSIA (Brussels, Belgium) for their support in this work.

Manuscript received Sept. 24, 1956. This paper was prepared for delivery before the Cleveland Meeting, Sept. 30-Oct. 4, 1956.

Any discussion of this paper will appear in a Discussion Section to be published in the June 1958 JOURNAL.

REFERENCES

1. M. J. N. Pourbaix, "Thermodynamics of Dilute Aqueous Solutions," Edward Arnold and Co., London (1949).
2. P. Delahay, M. Pourbaix, and P. Van Rysselberghe, *This Journal*, **98**, 57 (1951); *J. Chem. Educ.*, **27**, 683 (1950).
3. R. M. Burns and W. W. Bradley, "Protective Coatings for Metals," 2nd Ed., p. 274, Reinhold Publishing Co., New York (1955).
4. J. A. Christiansen and M. Pourbaix, *Compt. rend. XVII Conf. inter. union pure and appl. chem.*,

Stockholm, (1953) p. 82-84, Maison de la Chimie, Paris (1954).
5. A. J. de Bethune, *This Journal*, **102**, 288C (1955).
6. Paul Delahay, Marcel Pourbaix, and Pierre Van Rysselberghe, *ibid.*, **98**, 57, 65 (1951).
7. W. M. Latimer, "The Oxidation States of the Elements and their Potentials in Aqueous Solutions," 2nd Ed., pp. 117-18, Prentice-Hall, Inc., New York (1952).
8. M. C. Bloom, *Am. Mineralogist*, **24**, 281 (1939).
9. F. D. Rossini, U. S. Bureau of Standards, "Selected Values of Chemical Thermodynamic Properties," (1949), Table 21-2, p. 90; Part IV, p. 823 ff.
10. E. J. Roberts and F. Fenwick, *J. Am. Chem. Soc.*, **50**, 2125 (1928).
11. R. Schuhmann, *ibid.*, **46**, 52 (1924).
12. A. R. Tourky and A. A. Mousa, *J. Chem. Soc. (London)*, **1948**, Part I, 759.
13. H. Brintzinger, *Z. Anorg. Chem.*, **256**, 98 (1948).
14. G. Grube and F. Schweigardt, *Z. Elektrochem.*, **29**, 257 (1923).
15. G. C. Akerlof and Paul Bender, *J. Am. Chem. Soc.*, **70**, 2366 (1948).
16. G. P. Haight, Jr., *ibid.*, **75**, 3848 (1953).
17. Alphabetical Index of X-Ray Diffraction Patterns, A.S.T.M., Philadelphia, Pa., June, August, 1945.
18. A. N. Konopik and J. Zwiauer, *Monatsheft*, **83**, 189 (1952).
19. D. T. Hurd, "Chemistry of the Hydrides," John Wiley & Sons, Inc., New York (1952).
20. H. W. Salzberg and A. J. Andreatch, *This Journal*, **101**, 528 (1954).
21. H. J. S. Sands, E. J. Weeks, and S. W. Worrell, *J. Chem. Soc. (London) TRANS.*, Part I, **123**, 456 (1923).
22. R. Piontelli and L. Fagnani, *Korr. und Metallsch.*, **19**, 259 (1943).
23. I. M. Kolthoff and B. D. Hartong, *Rec. Trav. Chim.*, **44**, 113 (1925).

The Relation between Pitting Corrosion and the Ferrous-Ferric Oxidation-Reduction Kinetics on Passive Surfaces

Milton Stern

Metals Research Laboratories, Electro Metallurgical Company,

A Division of Union Carbide Corporation, Niagara Falls, New York

ABSTRACT

Ferrous-ferric electrode kinetics have been studied on a variety of passive alloys. Activation polarization parameters are not markedly different for all the surfaces studied except for titanium where the exchange current is an order of magnitude smaller. The local anodic polarization curve for solution of metal under passive conditions was found to be extremely steep. This is suggested as typical behavior for the passive condition.

Pitting of a metal may be divided into two separate aspects, pit initiation and pit propagation.

Streicher (1) has developed an accelerated pit initiation test and has described several of the factors which are important in initiation of pitting on stainless steels. His discussion contains an excellent review of the literature in the field; this need not be repeated here.

Uhlig (2) and Liebhafsky (3) have contributed significantly to an understanding of the basic processes which occur during pit growth. At the base of the pit, which is the anode in a passive-active cell, metal goes into solution. A reduction reaction occurs on the cathode regions of the surface which correspond to the unattacked areas. In $FeCl_3$ solution, the primary cathodic reaction is reduction of ferric ions to form ferrous ions. It has also been shown that the pitting process is essentially under cathodic control. The anodic areas do not appear to polarize significantly, while the cathodic areas polarize markedly. Thus, the pitting rate is a direct function of the exposed cathode area.

The discussion presented here is limited to a consideration of the electrochemical factors entailed in the pit propagation process. Since the system is primarily under cathodic control, the overvoltage behavior for ferric ion reduction on the cathode surface should influence the rate of pit growth.

Ferric-ferrous activation overvoltage behavior was determined on a series of alloys with different inherent pitting resistance to evaluate the importance of this aspect of the corrosion process in determining the differences in resistance to pit propagation of the various compositions.

When a metal pits in $FeCl_3$, the corrosion potential is active to the equilibrium potential of the ferrous-ferric oxidation-reduction potential of the system. The cathodic overvoltage during corrosion may amount to more than 1 v. In addition, the corrosion current is often extremely high. Since currents greater than the corrosion current must be applied in order to polarize a pitting electrode (4), experimental difficulties arise in the determination of activation overvoltage due to interference from concentration polarization and resistance drop effects. It was found that this interference could be eliminated without significantly changing ferric-ferrous activation polarization parameters by inhibiting the pitting process with $NaNO_3$ additions to $FeCl_3$. Uhlig (2) and Gilman (5) have demonstrated the effec-

tiveness with which nitrate inhibits pitting. Addition of $NaNO_3$ to a ferrous-ferric solution does not affect the equilibrium ferrous-ferric potential measured with a Pt electrode. Nitrate additions also produce a steady-state potential for stainless steel which is very close to the potential of Pt in the same solution. That nitrate does not significantly affect activation overvoltage parameters (6) was demonstrated with overvoltage measurements on stainless steel in ferric sulfate solutions[1] with and without nitrate additions. Similar measurements on a Ti surface in $FeCl_3$ where pitting does not occur even in the presence of chloride also showed no significant effect of nitrate on ferric-ferrous activation overvoltage behavior.

Thus, activation polarization measurements on a variety of surfaces in $FeCl_3$ containing nitrate as a pitting inhibitor may be considered representative of that activation polarization behavior which exists during pitting without nitrate.

Procedure

The procedure and equipment used for potential and overvoltage measurements have been described previously (6). The analysis of the alloys used is presented in Table I. The Ti was vacuum arc-melted and contained 0.05% C, 0.12% O, and 0.004% H. Ferric-ferrous chloride solutions were prepared by the addition of 100 g of $FeCl_3 \cdot 6H_2O$ and 0.9 g of $FeCl_2 \cdot 4H_2O$ to 1000 g of distilled water.[2]

Results

Type 310 Stainless Steel

Type 310 stainless steel was placed in a ferric-ferrous chloride solution containing approximately 0.4*N* $NaNO_3$. The equilibrium ferric-ferrous potential of the solution measured with platinized Pt was 0.858 v on the standard hydrogen scale. After the sample had reached a steady-state potential of −13 mv vs. Pt in the same solution, polarization measurements were conducted. Fig. 1 shows the cathodic polarization data obtained. The curve shows the normal expected shape for activation polarization (4) and represents the reduction rate of ferric ions on a Type 310 surface as a function of overvoltage. The exchange current is 0.021 μa/cm^2, and the measured Tafel slope, β_c, is 0.121 v. Fig. 2 illustrates the anodic polarization behavior. Two distinct Tafel lines are obtained. As illustrated previously (6), during anodic polarization, a potential region is reached where another oxidation proceeds at a rate comparable to the rate of oxidation of ferrous ions. This reaction is most likely oxygen-evolution produced by oxidation of water. Thus, at any potential, the experimental curve represents the sum of the rate of oxidation of ferrous ions, $\overleftarrow{i}_{Fe^{++}}$, and the rate of oxidation of water, $\overleftarrow{i}_w$. The low current Tafel region provides the quantitative expression for activation polarization for ferrous ion oxidation.

$$\eta = \beta_A \log \overleftarrow{i}_{Fe^{++}}/i_o \qquad (I)$$

where $\beta_A = 0.141$ and $i_o = 0.021$ μa/cm^2. Thus, in the region where the experimental curve bends from a slope of 0.141 to a lower value, $\overleftarrow{i}_w$ may be calculated at any potential by subtracting $\overleftarrow{i}_{Fe^{++}}$ from the applied anodic current, $\overleftarrow{i}_x$. At any potential in this region

$$\overleftarrow{i}_w = \overleftarrow{i}_x - \overleftarrow{i}_{Fe^{++}} \qquad (II)$$

The Tafel slope for oxygen evolution, β_w, is thus determined as 0.038 v. The exchange current for

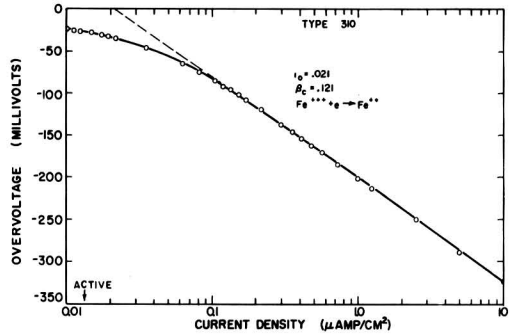

Fig. 1. Cathodic polarization of a nitrate-inhibited ferric-ferrous chloride solution with an equilibrium potential of 0.858 v on Type 310 stainless steel.

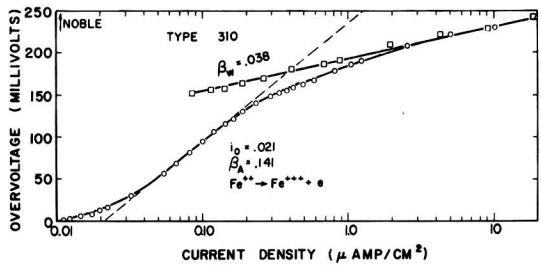

Fig. 2. Anodic polarization of a nitrate-inhibited ferric-ferrous chloride solution with an equilibrium potential of 0.858 v on Type 310 stainless steel.

[1] Pitting of stainless steel does not occur in ferric sulfate solutions without nitrate, whereas pitting in chloride solutions is extremely rapid.

[2] The equilibrium potential of a solution prepared in this manner and measured with a platinized Pt electrode is approximately 0.83 v on the standard hydrogen scale. The potential is not exactly reproducible from batch to batch because the ferrous salt contains varying amounts of ferric contamination. When a more active ferric-ferrous potential was required, ferrous chloride was added to the above solution until the desired potential was reached. The actual ferrous ion concentration was not determined.

Table I. Analysis of alloys

	% Cr	% Ni	% Mn	% Mo	% C	% Others
Type 304 stainless	18.36	9.06	0.94	—	0.05	bal. Fe
Type 316 stainless	17.25	13.02	1.66	2.54	0.04	bal. Fe
Type 310 stainless	24.66	19.68	1.27	—	0.05	bal. Fe
Hastelloy* alloy F	21.73	46.35	1.70	6.89	0.08	19.50 Fe
Hastelloy* alloy C	16.03	55.85	0.53	15.85	0.06	5.60 Fe 4.04 W

* A trade mark of the Haynes Stellite Company, Division of Union Carbide Corporation.

this reaction cannot be calculated since the equilibrium potential is not known.

It has been shown previously (6) that, if the steady-state potential of an electrode is equal to the equilibrium ferrous-ferric potential, then the reverse current which exists during polarization may be calculated. That is, $\overleftarrow{i}_{Fe^{++}}$ as a function of overvoltage on the active side of the reversible potential may be calculated from a measurement of overvoltage as a function of applied cathodic current. Also, the current equivalent to the rate of reduction of ferric ions during anodic polarization may be calculated. The method used is explained briefly in the following discussion. When an electrode at equilibrium is polarized cathodically, the total rate of reduction of ferric ions is equal to the sum of the applied current, $\overrightarrow{i}_x$, and the rate of oxidation of ferrous ions (the reverse current).

$$\overrightarrow{i}_{Fe^{+++}} = \overrightarrow{i}_x + \overleftarrow{i}_{Fe^{++}} \qquad \text{(III)}$$

The Tafel equation describes $\overrightarrow{i}_{Fe^{+++}}$ as a function of overvoltage.

$$\eta = -\beta_c \log \overrightarrow{i}_{Fe^{+++}}/i_o \qquad \text{(IV)}$$

Thus, with a measurement of β_c and i_o, Eqs. (III) and (IV) permit calculation of $\overleftarrow{i}_{Fe^{++}}$ at overvoltage values more active than the equilibrium potential. The method is similar for anodic polarization.

The steady-state potential of 310 stainless steel is more active by 13 mv than the equilibrium potential of the ferrous-ferric solution. This is best explained by considering that the sample is corroding so that, at the corrosion potential, the rate of reduction of ferric ions is equal to the sum of the rate of oxidation of ferrous ions and the rate of solution (oxidation) of metal. Thus,

$$\overrightarrow{i}_{Fe^{+++}} = \overleftarrow{i}_{Fe^{++}} + \overleftarrow{i}_m \qquad \text{(V)}$$

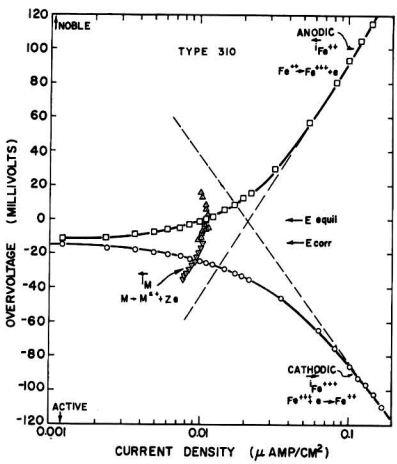

Fig. 3. Low current-density polarization data for Type 310 stainless steel showing corrosion current as a function of potential.

where $\overleftarrow{i}_m$ is that current which is equivalent to the rate of oxidation of metal. If the electrode is polarized cathodically with an external current, the total reduction rate of ferric ions is equal to that which is reduced by the applied current plus that amount of reduction which is equivalent to the rate of oxidation of both metal and ferrous ions. Thus, for cathodic polarization,

$$\overleftarrow{i}_m = \overrightarrow{i}_{Fe^{+++}} - \overleftarrow{i}_{Fe^{++}} - \overrightarrow{i}_x \qquad \text{(VI)}$$

The analogous equation for anodic polarization is

$$\overleftarrow{i}_m = \overrightarrow{i}_{Fe^{+++}} - \overleftarrow{i}_{Fe^{++}} + \overleftarrow{i}_x \qquad \text{(VII)}$$

Fig. 3 shows the low current data on Fig. 1 and 2 extended to lower currents and plotted on an expanded potential scale. The calculated values of $\overleftarrow{i}_m$ as a function of overvoltage are included. This is essentially a plot of the local anodic polarization curve of the metal. It is important to note the steep slope of $\overleftarrow{i}_m$ plotted as a function of overvoltage.

Type 316 Stainless Steel

Measurements were conducted on Type 316 stainless steel surfaces in two inhibited solutions with different ferrous-ferric potentials. The steady-state potential of Type 316 in a solution with an oxidation-reduction potential of 0.757 v on the standard hydrogen scale was the same as Pt to within 0.1 mv. This means that the ferrous-ferric system is at equilibrium on the stainless steel surface and that corrosion, $\overleftarrow{i}_m$, is negligible. The polarization curves are similar to those already illustrated for Type 310 and may be represented in terms of the Tafel constants. The exchange current is 0.49 μa/cm^2, $\beta_A = 0.185$ v, and $\beta_C = 0.095$ v. A value for β_w could not be obtained since the equilibrium ferric-ferrous potential of this solution is relatively active, and *IR* drop errors were introduced during anodic measurements in the potential region where oxygen is evolved.

In a solution with a ferrous-ferric potential of 0.832, the steady-state potential of Type 316 stain-

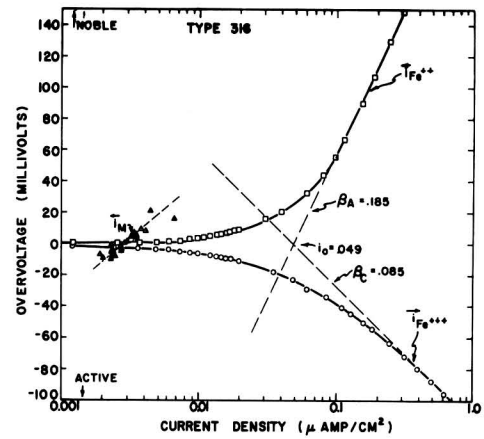

Fig. 4. Low current-density polarization data for Type 316 stainless steel, $E_{Fe^{+++}-Fe^{++}} = 0.832$ v.

less steel is 1 mv more active than Pt in the same solution. In this case, a slight corrosion current must exist which, though small in comparison to i_o, is sufficient to polarize the electrode by 1 mv. Fig. 4 shows the polarization curves only in the low current region to illustrate how $\overleftarrow{i_m}$ varies with potential. In this case, the corrosion current is of the order of 0.003 μa/cm^2, and $\overleftarrow{i_m}$ plotted as a function of overvoltage is not so steep as is found for Type 310 stainless steel. The Tafel constants obtained for this system are $i_o = 0.049$ μa/cm^2, $\beta_c = 0.085$ v, $\beta_A = 0.185$ v, $\beta_w = 0.032$ v.

In many discussions of the shape of electrochemical polarization curves, the question continually arises as to whether polarization should be a linear or logarithmic (Tafel) function of applied current. For example, Straumanis, Shih, and Schlechten (7,8) have observed Tafel behavior for hydrogen overvoltage on Ti in HCl, HBr, and H_2SO_4, but report a linear dependence of overvoltage on applied current in HF. In addition, these authors show that the linear relation is maintained if the Ti corrodes, while the Tafel relation holds if the Ti ceases to dissolve because of fluoride additions. Results of this type have been explained in terms of theory (4) which shows that an electrode whose potential is determined by two intersecting Tafel functions (whether corroding or at equilibrium) exhibits a linear dependence of overvoltage as a function of applied current values less than the exchange current or corrosion current. For an electrode at equilibrium, the slope of the linear polarization curve is given by Eq. (VIII).

$$\left(\frac{d\eta}{di_x}\right)_{\eta\to 0} = \frac{\beta_A \beta_C}{(2.3)\,(i_o)\,(\beta_A+\beta_C)} \qquad \text{(VIII)}$$

For a corroding electrode, the expression becomes

$$\left(\frac{d\epsilon}{di_x}\right)_{\epsilon\to 0} = \frac{\beta_A \beta_C}{(2.3)\,(i_{corr})\,(\beta_A+\beta_C)} \qquad \text{(IX)}$$

where ϵ is the difference in potential between the corrosion potential, E_{corr}, and the polarized potential.

Tafel behavior is not observed until applied current values become significantly larger than the exchange current or the corrosion current. The linear relation reported by Straumanis and coworkers is consistent with this picture since their applied currents were smaller than the very large corrosion current of Ti in HF. Thus, the extent of the linear dependence is determined by the magnitude of the exchange current or corrosion current, and the slope of the linear function is inversely proportional to i_o or i_{corr}.

This behavior can be illustrated quantitatively with the low current data obtained for the Type 316 electrode described above where two markedly different exchange currents were observed for the two ferric-ferrous solutions investigated. Fig. 5 shows the low current data plotted on a linear scale for Type 316 stainless steel in solutions with ferric-ferrous equilibrium potentials of 0.757 and 0.832 v. The slopes obtained are inversely proportional to the

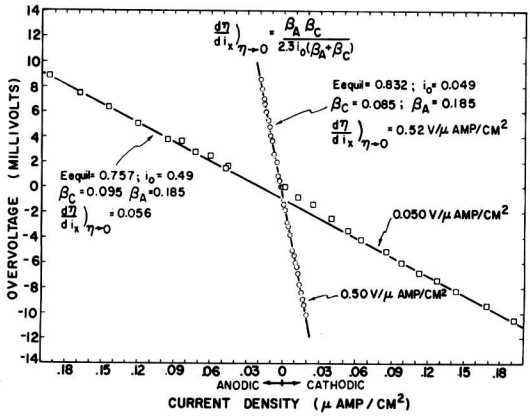

Fig. 5. Linear relationship between overvoltage and applied current density for two different ferric-ferrous solutions on Type 316 stainless steel.

exchange current, and the calculated value of $d\eta/di_x$ using Eq. (VIII) checks the experimental determination within experimental error.

Type 304 Stainless Steel

The polarization curves for Type 304 stainless steel are similar to those already illustrated and may be summarized in terms of the experimental electrochemical constants. In an inhibited ferric-ferrous chloride solution with a reversible potential of 0.824 v vs. the standard hydrogen electrode, the values obtained are: $\eta_{corr} = -0.006$ v, $\beta_c = 0.146$ v, $\beta_A = 0.165$ v, $i_o = 0.0634$ μa/cm^2, and $\left(\frac{d\eta}{di_x}\right)_{\eta\to 0} = 0.48$ v/μa/cm^2.

If sufficient ferrous chloride is added to the solution to bring the equilibrium ferrous-ferric potential down to a value of 0.744 v, then the measured constants become: $\eta_{corr} = -0.002$ v, $\beta_c = 0.139$ v, $\beta_A = 0.161$ v, $i_o = 0.172$ μa/cm^2, and $\left(\frac{d\eta}{di_x}\right)_{\eta\to 0} = 0.188$ v/μa/cm^2. Insufficient data were obtained in the low current region to calculate $\overleftarrow{i_m}$ as a function of potential. At the corrosion potential, however, the corrosion current was calculated as 0.013 μa/cm^2 in the former case and 0.014 μa/cm^2 in the latter experiment.

Hastelloy F

Hastelloy F is an alloy with good pit and corrosion resistance in oxidizing environments. Anodic and cathodic polarization measurements in a ferric-ferrous chloride solution with an equilibrium potential of 0.830 v are illustrated in Fig. 6. It is interesting to note in this case that $\beta_A = \beta_c = 0.148$ v. The exchange current is 0.063 μa/cm^2 while $\beta_w = 0.035$ v. Fig. 7 shows part of the same data plotted on an expanded potential scale and extended to lower values of applied current than that shown in Fig. 6. During these experiments, the steady-state potential of the alloy prior to anodic measurements was

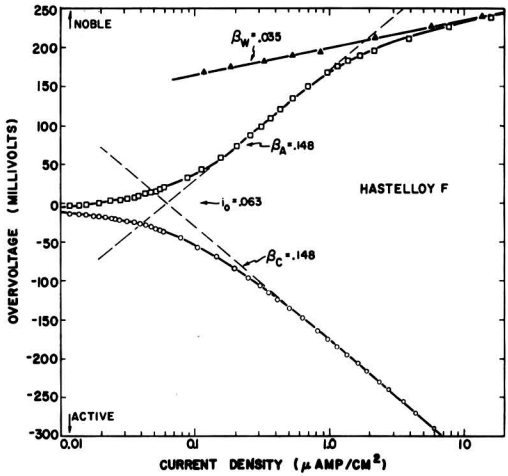

Fig. 6. Anodic and cathodic polarization of nitrate-inhibited ferric-ferrous chloride with an equilibrium potential of 0.830 v on Hastelloy alloy F.

9.5 mv more active than Pt in the same solution. However, prior to cathodic polarization, the potential had changed to 8.0 mv. This change is reflected in an abrupt change in $\overleftarrow{i}_m$ calculated from anodic data as compared to that calculated from cathodic measurements. The values of $\overleftarrow{i}_m$ as a function of potential are plotted on Fig. 7. The data calculated from both anodic and cathodic polarization show a remarkably steep slope. Thus, $\overleftarrow{i}_m$ is essentially independent of overvoltage. When the steady-state potential is −9.5 mv, $\overleftarrow{i}_m$ is 0.020 μa/cm², whereas $\overleftarrow{i}_m$ is 0.016 μa/cm² when the corrosion potential is −8.0 mv.

Further evidence that $\overleftarrow{i}_m$ is independent of potential may be found in application of Eq. (VIII) to the low current data. Eq. (VIII) is based on the assumption that the steady-state potential is determined by only two interesting Tafel functions. If the electrode is in a region where three potential-current

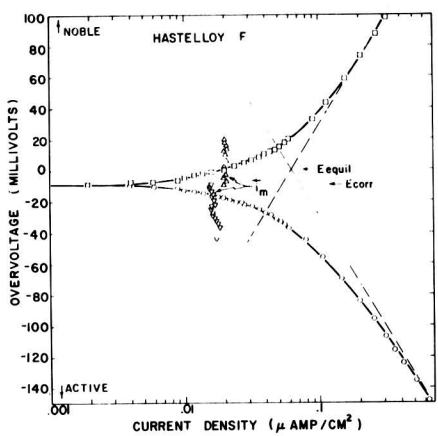

Fig. 7. Low current-density polarization data for Hastelloy alloy F showing corrosion current as a function of potential.

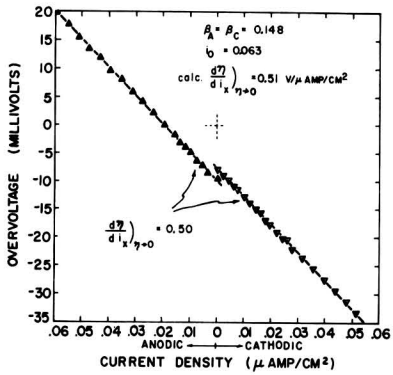

Fig. 8. Linear relationship between overvoltage and applied current density for Hastelloy alloy F.

functions are operative, Eq. (VIII) becomes more complex and cannot be expected to apply in its present form. This would be the case for an electrode 9 mv removed from the reversible ferric-ferrous potential. However, if one of the three polarization curves which determine the potential of the electrode shows an independence of current on potential, then it can be shown that Eq. (VIII) is still applicable.

Fig. 8 illustrates the low current data for Hastelloy F. Both the anodic and cathodic data are linear and yield the same value of $d\eta/di_x$, 0.50 v/μa/cm². The value of $d\eta/di_x$ calculated from Eq. (VIII) is 0.51 v/μa/cm². As stated above, this is further evidence that the local anodic polarization curve for Hastelloy F is practically vertical. This behavior undoubtedly explains, in part, the excellent corrosion resistance of this alloy.

Hastelloy C

Hastelloy alloy C is a Ni-Mo-Cr alloy with excellent corrosion resistance in a wide variety of oxidizing and reducing media. It shows no weight loss or pitting after a ten-year immersion in sea water, nor does it pit in the annealed condition in boiling 10% $FeCl_3$ (9).

The behavior of this alloy is similar to that already illustrated for Hastelloy alloy F. Thus, the results may be summarized in terms of the Tafel constants. In a ferric-ferrous system with an equilibrium potential of 0.758 v, the alloy exhibits a steady-state potential which is 27 mv more active than Pt in the same solution. The exchange current is 0.10 μa/cm² with $\beta_c = 0.190$ v and $\beta_A = 0.167$ v. As was the case with Hastelloy alloy F, calculated values of $\overleftarrow{i}_m$ for Hastelloy alloy C were relatively independent of potential, the average value in this solution being 0.07 μa/cm².

Results for a ferric-ferrous system with a reversible potential of 0.825 v are shown in Table II. The local action current in this case was 0.3 μa/cm².

Titanium

Titanium metal shows no pitting tendency in chloride solutions. Measurements were conducted

Table II. Summary of electrochemical constants for various alloys

Alloy	$Fe^{+++}-Fe^{++}$* potential, v	η_{corr}† v	β_C v	β_A v	β_w v	i_o‡
Type 304 stainless	0.824	−0.006	0.146	0.165	0.039	0.063
Type 304 stainless	0.744	−0.002	0.139	0.161	—	0.172
Type 316 stainless	0.832	−0.001	0.085	0.185	0.032	0.049
Type 316 stainless	0.757	0.000	0.095	0.185	—	0.49
Type 310 stainless	0.858	−0.013	0.121	0.141	0.038	0.021
Hastelloy alloy F	0.830	−0.009	0.148	0.148	0.035	0.063
Hastelloy alloy C	0.825	−0.070	0.228	0.222	0.030	0.20
Hastelloy alloy C	0.758	−0.027	0.190	0.167	0.039	0.10
Titanium	0.830	−0.016	0.104	—	—	0.0052
Titanium	0.789	−0.003	0.102	0.358	—	0.0110
Titanium	0.736	0.000	0.091	0.352	—	0.024

* Standard hydrogen scale.
† Potential alloy vs. Pt in same solution.
‡ Microampere/cm².

on the same sample in three different ferric-ferrous chloride solutions containing $NaNO_3$ with equilibrium potentials of 0.830 v (solution A), 0.789 v (solution B), and 0.736 v (solution C). Solutions B and C were prepared by addition of ferrous chloride to solution A. Subsequent experiments showed that the nitrate addition had no significant effect on the polarization characteristics. It was included here in order to compare the results with those obtained with alloys which require nitrate to inhibit pitting.

Fig. 9 illustrates the anodic and cathodic measurements obtained in the three environments. The results are quite different from those shown previously in that the anodic exchange current (determined by extrapolation from the Tafel region) is greater than the cathodic exchange current in solutions A and B. The electrochemical constants obtained for solution A are: $\beta_C = 0.104$ v, $\beta_A = 0.286$ v, $i_{oa} = 0.0085$ μa/cm², and $i_{oc} = 0.0052$ μa/cm². Also the intersection of the anodic and cathodic Tafel curves occurs at a potential 15 mv more active than Pt in the same solution, while the steady-state potential was 16 mv more active than Pt.

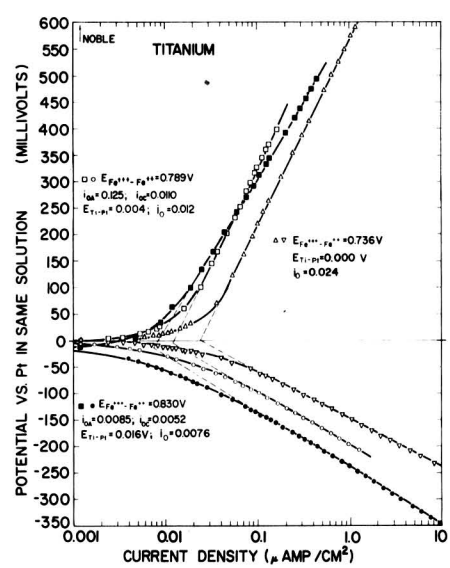

Fig. 9. Anodic and cathodic polarization of three different ferric-ferrous solutions on Ti.

These observations are best explained by considering that Ti is reacting in this environment and that during anodic polarization measurements the rate of oxidation of Ti metal is the same order of magnitude as the rate of oxidation of ferrous ions. Thus, the observed anodic data represent the summation of $\overleftarrow{i_m}$ and $\overleftarrow{i_{Fe^{++}}}$ at any potential. The sum of two Tafel lines can result in data which are Tafel-like in appearance. Thus, the value of β_A given above cannot be considered as representative of the oxidation of ferrous ions. The exchange current for the ferric-ferrous system, however, can be considered as equal to the value determined from the cathodic data, since the cathodic Tafel slope would not be influenced significantly by Ti solution. It is interesting to note that the corrosion current necessary to polarize the ferric-ferrous system to the steady-state electrode potential of 16 mv is only about 0.003 μa/cm². This corrosion rate is too low to measure by direct weight-loss techniques since a 1 cm² sample would lose only about 1 mg in 60 years. This extremely small corrosion rate affects the potential significantly because the exchange current in this environment is very small.

A situation similar to that described above exists for solution B where the electrochemical constants were found to be: $\beta_C = 0.102$ v, $\beta_A = 0.358$ v, $i_{oa} = 0.0125$ μa/cm², and $i_{oc} = 0.0110$ μa/cm².

The intersection of anodic and cathodic curves in this case occurs at a potential 4 mv more active than Pt in the same solution whereas the steady-state potential was 3 mv more active than Pt. In this case, β_A is probably not markedly affected by $\overleftarrow{i_m}$.

The potential of Ti in solution C is the same as Pt to within 0.1 mv. In this case, the anodic and cathodic exchange currents were equal. The electrochemical constants determined from the polarization curves are $\beta_C = 0.091$ v, $\beta_A = 0.352$ v, $i_o = 0.024$ μa/cm². Also, the cathodic polarization curve for reduction of ferric ions can be calculated from anodic data, and the anodic polarization curve for oxidation of ferrous ions can be calculated from cathodic measurements in the manner described previously (6).

It is interesting to note that no indication of oxygen evolution was observed in the anodic data of Fig. 9 even though potentials more noble than 1.2 v vs. the standard hydrogen electrode were reached. This must mean that the Tafel parameters for oxygen evolution are such that polarization is quite pronounced. The exchange current must be very small, and the β_w value may be higher than the values reported for the Fe- and Ni-base alloys investigated.

Discussion

One of the factors which affects the rate of propagation of pitting of an alloy in $FeCl_3$ is the degree of cathode polarization. This may be measured by the activation overvoltage parameters for the reduction of ferric ions. Polarization is more pronounced if β_C is greater or if i_o is smaller. The exchange cur-

rent is actually a function of the ferric and ferrous ion activity (10) and, thus, different alloys should be compared in solutions of similar composition. Table II gives a summary of electrochemical data for all the alloys investigated.

Exchange currents at similar ferric-ferrous potentials for all the materials except Ti are of similar magnitude. The exchange current on a Ti surface is consistently an order of magnitude smaller. The cathodic Tafel slope, β_c, does not vary in any uniform manner with regard to the general pitting resistance of the alloys. However, the largest values were obtained with Hastelloy alloy C.

Thus, only small differences in pit propagation rates among the various materials can be explained in terms of differences in local cathodic polarization. The major difference must, therefore, reside in variations in local anodic polarization during pitting and differences in pit initiation.

The calculated anodic polarization curve for solution of metal (potential vs. $\overleftarrow{i_m}$) should not be considered that which exists during pitting. Uhlig (2) has shown that a pit in stainless steel contains metallic ions in amounts proportional to the original alloy composition in their lower valent state. Thus, active Fe goes into solution as ferrous ions. However, when Fe is passive, the element apparently goes into solution directly as ferric ions (11).

O'Connor (12) has also shown that chromate is formed during anodic passivation of an Fe-Cr alloy in sodium sulfate and in nitric acid. Chromate was also detected during the corrosion of this material in concentrated nitric acid where the alloy is passive.

Thus, the data shown for the local anodic polarization of the alloys used here are best considered as solution of metal to directly form ions in a higher state of oxidation. Little is known about the kinetics of such processes, and, therefore, it is difficult to provide a reason for the very steep slope of the anodic polarization curve. However, this may well be a characteristic feature of passive surfaces. For example, Vetter (13) has shown that the corrosion rate of Fe passivated in nitric acid can be determined electrochemically by polarizing the surface anodically to the potential of Pt in the same solution. The current required to polarize to the Pt potential is equivalent to the corrosion rate. This can be true only if the local anodic polarization curve for passive Fe is practically vertical.

Since nitrate does not affect ferric-ferrous electrode kinetics significantly, it must be concluded that this pitting inhibitor affects either the local anodic polarization behavior of the metal or the pit initiation process. It is possible that nitrate competes with the chloride ion for adsorption surface sites, thus eliminating the tendency for local breakdown of passivity which chloride normally would create.

Acknowledgments

The author would like to acknowledge the skillful assistance of E. A. Tomes who carried out the extensive calculations and conducted many of the polarization measurements. R. C. Wilson conducted the measurements with Type 304 stainless steel, while R. M. Roth determined the effect of nitrate additions upon the polarization behavior of Ti.

Manuscript received Nov. 29, 1956. This paper was prepared for delivery before the Washington Meeting, May 12-16, 1957.

Any discussion of this paper will appear in a Discussion Section to be published in the June 1958 JOURNAL.

REFERENCES

1. M. A. Streicher, *This Journal*, **103**, 375 (1956).
2. H. H. Uhlig, *Trans. Am. Inst. Mining Met. Engrs.*, **140**, 442 (1940).
3. H. A. Liebhafsky and A. E. Newkirk, *Corrosion*, **9**, 432 (1953); *ibid.*, **12**, 48 (1956).
4. M. Stern and A. L. Geary, *This Journal*, **104**, 56 (1957).
5. J. R. Gilman, B. S. Thesis, Chemical Engrg. Dept., Massachusetts Institute of Technology (1940).
6. M. Stern, *This Journal*, **104**, 559 (1957).
7. M. E. Straumanis, S. T. Shih, and A. W. Schlechten, *ibid.*, **102**, 573 (1955).
8. M. E. Straumanis, S. T. Shih, and A. W. Schlechten, *J. Phys. Chem.*, **59**, 317 (1955).
9. E. D. Weisert, Submitted to *Corrosion*, June 1956.
10. J. E. B. Randles, *Trans. Faraday Soc.*, **48**, 828 (1952).
11. H. H. Uhlig and G. E. Woodside, *J. Phys. Chem.*, **57**, 280 (1953).
12. T. L. O'Connor and H. H. Uhlig, *This Journal*, **102**, 562 (1955).
13. K. J. Vetter, *Z. Elektrochem.*, **55**, 274 (1951).

Filamentary Growths on Copper Cathodes

T. C. J. Ovenston, C. A. Parker, and A. E. Robinson

Admiralty Materials Laboratory, Holton Heath, Poole, Dorset, England

ABSTRACT

An investigation has been made of the filamentary growths which are produced under certain conditions during copper plating at low current density. The conditions under which these growths occur have now been defined more clearly and the effect of various types of surface active agent in enhancing or preventing their occurrence has been demonstrated. Possible mechanisms for the formation of the filaments have been discussed.

The formation of polycrystalline filamentary growths of Cu during Cu plating at low current density was first reported from this laboratory by Gollop (1). At that time considerable data had already been accumulated about the conditions under which such growths would take place. The investigation was continued and it is now possible to define these conditions more clearly and to put forward a tentative theory to account for this phenomenon.

This investigation arose through the occurrence, during operation, of filamentary growths in electrolytic cells, made of Bakelite, and coated internally with a water-proof varnish, which were in extensive use. To elucidate the possible effect of the varnish coating, a large number of experiments were also carried out in glass cells. This paper reports the results of both series of experiments.

Since the original publication from this laboratory, and after the further work had been completed, van der Meulen and Lindstrom (2) reported the results of a similar investigation of filamentary growth in which the size of cell, composition of electrolyte, and current density used were all similar to those used in the present investigation. Some of the observations and certain details of procedure differed, however, and, in particular, the work of van der Meulen and Lindstrom also covered the effect of addition of chloride to the electrolyte (a study not covered at all by the present authors). To avoid confusion, therefore, references to and comparisons with this work have been made where appropriate.

Experimental

Electrolysis was carried out in sealed cylindrical cells having an internal diameter of 3.5 cm and a volume of about 30 ml. The electrodes were disks of pure Cu, the cathode having a diameter of about 2 cm. Separation between the electrode faces was 1.5 cm. In all experiments the main constituents of the electrolyte were $CuSO_4 \cdot 5H_2O$, 105; H_2SO_4, 65.5; hydroxylamine sulfate, 5.0 g/l. During electrolysis the current density on the cathode was kept constant (generally at 1 ma/cm^2) by means of a rheostat in series with the cell and 6 v storage battery. Throughout electrolysis the cells were kept entirely undisturbed with either the anode or the cathode face downward. Electrolysis was allowed to proceed for at least two weeks, but the first sign of filaments, when they were generated, usually appeared within one or two days.

Two types of plating cell were employed. The first was of Bakelite, coated internally with a bituminous varnish. The second was of glass, with polythene ends in which the electrodes were fixed. In certain experiments the glass sides of the cells were fitted with flat windows for visual and photographic observation. No attempt was made to deaerate the solutions before sealing the cells. A small air bubble (approx. 3 ml) was present in the sealed cells. In this respect, the procedure differed from that of van der Meulen and Lindstrom who flushed the electrolyte with N before electrolysis.

Some cells were fitted with an internal reference electrode of Cu through the side of the cell in a position approximately midway between the anode and cathode. Potential measurements between anode and cathode and between anode or cathode and the reference electrode were made with a d-c valve voltmeter.

The resistance of the electrolyte between anode and cathode was less than 5 ohms, giving rise to a potential drop of less than 5 mv. All potential values include the ohmic potential drop which, however, was negligible compared with the cathode overvoltages associated with filament formation.

Observations from trials in varnished cells suggested that filamentary growths were associated with some surface-active substance arising from the varnish coating, and in some experiments, therefore, commercial surface-active agents (1 g/l) were added to the electrolyte to determine their effect. The agents used were:

Anionic—Belloid: sodium salt of dinaphthylmethane disulfonic acid; Teepol: sodium salt of sulfonated secondary alcohol; Effesay L: sodium lauryl sulfate.

Nonionic—Lubrol: ethylene oxide condensed with alcohols.

Cationic—Fixanol C: cetyl pyridinium bromide.

It is understood that these are commercial products and the chemical description given is only a representation of their general character. They probably consist of a complex mixture of reacted or partly reacted substances and are likely to be

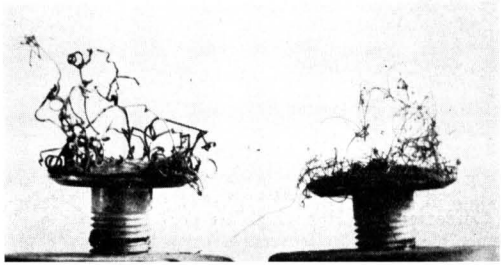

Fig. 1. Typical filamentary growth on Cu cathode

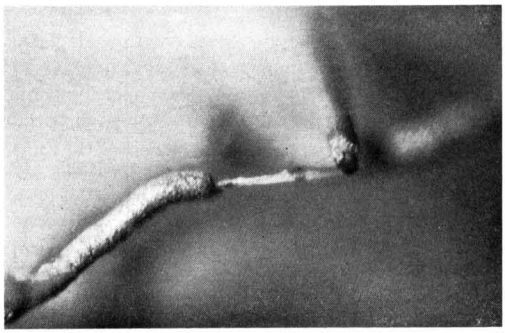

Fig. 2. Cotton fiber partly Cu plated

polymerized in varying degrees. Of the anionic agents, Effesay L was found most effective and was the one used after the first preliminary experiments.

Nature of the Filaments

The filaments were first observed in the varnished cells after plating for about two weeks. Fig. 1 shows two cathodes, selected from a large number of similar ones, which exhibit typical filamentary growths. The proportion of Cu deposited as filaments varied considerably and, in many cases such as these, it was found that an appreciable fraction of the total deposition on the cathode had occurred in the form of these filaments which were frequently several centimeters in length and of fairly uniform thickness up to 0.3 mm, depending on the duration of plating. A small proportion of the filaments were found to have a core of organic material, usually a cotton fiber. The fibers were adventitious impurity which had become electroplated. In certain cases the sheath of Cu had not extended along the whole length of the fiber. For example, Fig. 2 shows part of one such fiber, the two ends of which had been in contact with the cathode; plating had extended along the fiber from each end except for the short length in the center. It was clear, from a comparison of the thickness of Cu on the fiber with that deposited on the cathode proper, that in many cases plating had occurred on the fiber from an early stage in the electrolysis.

Although the occurrence of plating on an apparently nonconducting fiber was in itself remarkable, the nature of the majority of the filaments was even more so. Microscopic examination of sections through the latter failed to reveal any discrete core. Fig. 3 shows a section through the root of a typical filament at the point where it joins the main cathode. The core consists of fine-grain Cu similar to

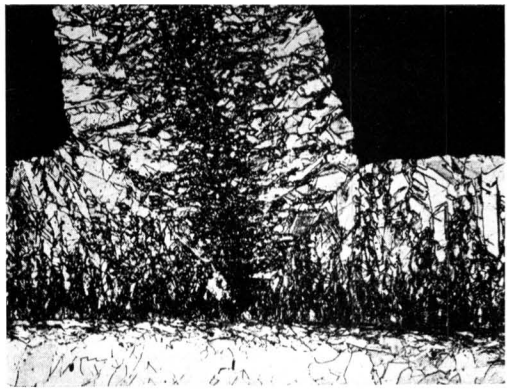

Fig. 3. Section through root of a typical filament

that which was first deposited on the cathode. Subsequent plating consists of much larger oriented crystals, again similar to those subsequently deposited on the cathode. After examination of many such sections one is bound to postulate the existence of invisibly fine conducting paths leading from the cathode at an early stage in the plating process, notwithstanding the fact that such growths appeared even after filtration of the electrolyte through sintered glass filters and prewashing of the cells with distilled water.

Correlation of Filamentary Growths with Cathode Potential

When a number of varnished plating baths were run simultaneously under apparently identical conditions, filamentary growths did not necessarily appear in all cells. Over a period of time, a large number of apparently identical tests were run in which measurements of interelectrode potential were made. As might be expected it was found that the occurrence of the abnormal growths was associated with very high interelectrode potentials. Thus, in 155 such tests in varnished cells, 82 gave anode-cathode voltages between 100 and 250 mv, even after plating had proceeded for several days. Of these 82 cells, 59 produced filaments and the plating in the remainder was abnormal, being of nodular form. All cells showing an interelectrode potential greater than 150 mv produced filaments, while none which showed potentials less than 100 mv produced them. It was also observed that those cells which had stood for one or two weeks with the electrolyte in contact with the varnish before electrolysis gave higher potentials and showed a greater tendency to filamentary growth than those in which electrolysis had been started almost immediately after filling.

That the high potentials and growths were due to impurities leached from the varnish was demonstrated by experiments with the glass cells. With unadulterated electrolyte, low cell potentials were invariably obtained (30-50 mv) and no filamentary growths were formed. Electrolyte which had been in contact with the varnish produced high potentials and, frequently, filamentary growths. In the latter experiments it was demonstrated, by measurements

Table I. Some typical electrode potentials

Time	Cell (a) (plain electrolyte) Cathode	Cell (a) (plain electrolyte) Cathode − anode	Cell (b) (electrolyte adulterated with varnish) Cathode	Cell (b) (electrolyte adulterated with varnish) Cathode − anode	Cell (c) (electrolyte containing 0.1% "Fixanol C") Cathode	Cell (c) (electrolyte containing 0.1% "Fixanol C") Cathode − anode
Start of electrolysis	20-30	40-50	160	240	300	420
After 10 min	20-30	40-50	175	220	300	360
After 2 weeks	20-30	40-50	150	170	290	350

against the third reference electrode, that the persistently high potentials originated at the cathode, the anodic potential always remaining low (20-30 mv) except during the very early stages of the electrolysis.

Experiments with Surface Active Agents

From the experiments just described it was clear that the cause of the abnormal growths was some impurity leached from the varnish by the action of the electrolyte. This impurity apparently became adsorbed on the cathode to produce the high overvoltages observed. Experiments were therefore carried out with various surface active agents in attempts either to produce filaments in the absence of varnish extract or to suppress their formation in its presence.

The following effects were observed using commercial products (*see* experimental section) as compared with control experiments without additions: (*a*) in the presence of varnish, anionic agents gave fair or good plating with no Cu filaments; nonionic and cationic agents led to greatly increased crops of filaments; (*b*) in the absence of varnish, anionic and nonionic additions gave normal plating, but cationic additions led to numerous growths.

This was the first occasion on which the effect of cationic agents in promoting these filamentary growths had been demonstrated unambiguously, and was described by one of the authors (A.E.R.) in a report from this laboratory in February 1954, and which was communicated to van der Meulen and Lindstrom, who have recently reported similar experiments with surface-active agents (2). The latter authors have acknowledged this source of information in an unpublished report from their laboratory.

Table I records some typical electrode potentials observed in the presence of a cationic agent ("Fixanol C") as compared with those obtained with unadulterated electrolyte and with electrolyte adulterated by the varnish.

There was a marked similarity between the potentials obtained when the cationic agent was added to the electrolyte in glass cells, those from varnish-adulterated electrolyte in glass cells, and those from the varnished Bakelite cells. This strongly suggested that the substance responsible for the filamentary growths in varnished cells was cationic in character. Experiments with anionic agents, on the other hand, showed that these were able to neutralize the effect of the cationic ones. The increase in growths in the presence together of varnish and nonionic surface active agent was probably due to more effective wetting of the varnish surface and leaching of the active impurity. The results in columns 6 and 7 of Table I suggest that the cationic agent adsorbed on the anode is capable of producing a high overvoltage here also at the start of the electrolysis but, as might be expected, this is largely destroyed after electrolysis proceeded for a short while.

Because the substances responsible for filamentary growth in the varnished cells were shown to be cationic in character, it would be expected that the addition of an anionic agent would neutralize their effect. To test this possibility, trials were carried out with the anionic agent Effesay L, in concentrations 0.02-0.5 g/l, in 20 varnished cells. No cell gave filaments and in all cases the final potential difference was less than 100 mv.

After the present investigation had been completed, van der Meulen and Lindstrom (2) reported that the addition of 0.03 g/l of Dupont Safranine T "125%" to the electrolyte prevented filament formation caused by the presence of Polysoap G.147. To determine the effect of this addition in the varnished cells, trials were carried out by the present authors using cells drawn from the same group as the twenty referred to in the previous paragraph, and which were known to be prone to filament formation. Eight cells containing Dupont Safranine T "125%" (at the recommended concentration) and four cells containing Safranine T from another source all produced filaments. The cell potentials in these tests were all in the range 140-150 mv and remained high throughout the 14-day trial. Therefore, it seems that, although the Safranine T in the experiments of van der Meulen and Lindstrom was able to reduce cathodic overvoltage and prevent filament formation arising from the presence of Polysoap G.147, it was unable to prevent the formation of filaments caused by the agent in the varnish, and is not therefore of general application for the inhibition of filamentary growth.

Direct Observation of Filamentary Growth

Some experiments were carried out in sealed glass cells with plane windows so that successive stages in the development of the filaments could be closely watched and photographed. In these experiments the end caps of these cells were varnished, and the electrolyte was allowed to stand in contact with the varnish for a week before electrolysis. Thus, the observed behavior is as would have been expected for varnished cells. Successive stages in the filamentary growth are shown in Fig. 4 *a*, *b*, and *c*. Within a few hours after the start of electrolysis some very fine short tendrils of Cu were observed (Fig. 4*a*). With the passage of time these thickened and lengthened as shown in Fig. 4*b* and *c*. In a similar manner the growth of Cu along textile fibers was observed in

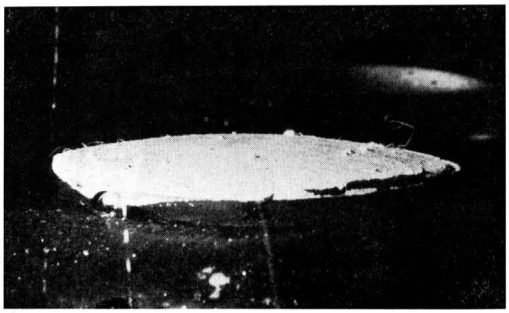

Fig. 4a. Stages in the growth of Cu filaments: after electrolysis for 7 hr.

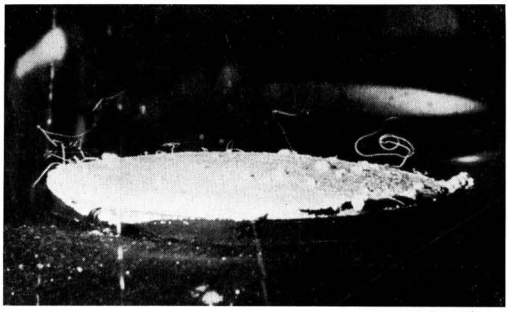

Fig. 4b. Stages in the growth of Cu filaments: after electrolysis for 27 hr.

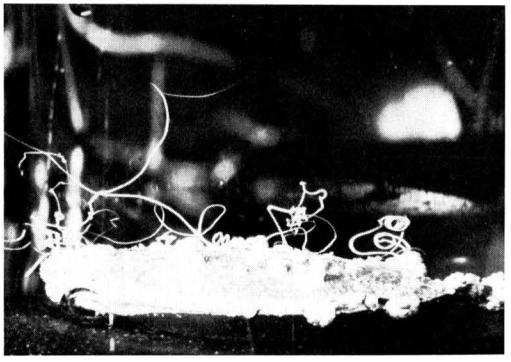

Fig. 4c. Stages in the growth of Cu filaments: after electrolysis for 6 days.

cells containing contaminated electrolyte (and showing a high cathodic overvoltage). For example, with a small bunch of untreated cotton wool in contact with the cathode, Cu plating was observed to extend along the fibers and ultimately thicken to produce filaments of the type already found in small numbers in the original experiments. Some cotton wool which has become partly Cu-plated by this process is shown in Fig. 5.

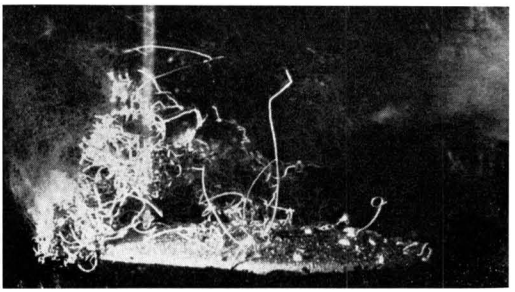

Fig. 5. Cotton wool plated by contact with cathode showing high overvoltage.

Mechanism of Filamentary Growth

From the results already described, it is evident that two types of filament have been observed in the present investigation. Both are of similar outward appearance but they differ in the fact that one contains an observable core of organic fibrous material on which the growth has taken place, while the other contains no such discrete core. It is possible, however, that the difference is only one of degree and before considering mechanisms for the formation of the second type of filament it is worth considering the first in more detail.

These two types of filaments should not be confused with the two types referred to by van der Meulen and Lindstrom (2), who have not reported the phenomenon of the plating of cotton fibers and other organic material, which plays a prominent part in the theory of filament formation discussed here. Van der Meulen and Lindstrom observed the convoluted type of filament associated with high cathodic overvoltage which corresponds to the second type described herein, and they also observed an unusual type of growth arising in the presence of chloride in the electrolyte. The chloride-produced filaments, which are apparently associated with lower cathodic overvoltages and have an entirely different structure, were not studied by the present authors, whose experiments were conducted throughout with chloride-free electrolyte (except in the later experiment in which Safranine T, which itself contained chloride, was used).

The observed requirement for the plating of certain organic material is, simply, contact with a cathode showing high and persistent overvoltage. In the absence of this high overvoltage, plating of such organic material never occurs, although all other conditions may be the same. It is suggested therefore that the cellulose fiber (for example) has the property of destroying locally the overvoltage at its point of contact with the cathode so that Cu is deposited rapidly at this point. Assuming that the newly deposited Cu itself rapidly adsorbs surface active agent (and thus effectively becomes a part of the main cathode), the only point at which plating can occur readily is at the newly formed interface between the deposited Cu and the fiber. It is postulated therefore that deposition continues to take place rapidly and preferentially at this point and that an exceedingly thin coating of Cu thus grows rapidly along the fiber from the cathode. In the early stages this coating might well be invisible and of comparatively high resistance per unit length of fiber. Forming part of the cathode, however, it subsequently plates in the normal manner but more rapidly at points close to the cathode than at more distant points owing to its very high resistance. Ultimately

the plating becomes thick enough to be visible, first near to the cathode and then at more distant points, as has actually been observed. The formation of Cu-coated fibers seems to be explained satisfactorily on this basis.

At first sight, the formation of filaments of the second type by a similar process seems likely. For example, the initial growth of Cu, i.e., to the point where the filament first becomes visible, certainly takes place from the main cathode outward (*see* Fig. 4). There is also evidence of the presence of a very fine conducting path on which the initial (fine grain) deposition of Cu takes place (*see* Fig. 3). However it is very difficult to account for the source of this conducting path in terms of a discrete thread of material on which the deposition could have taken place. Such threads would have to be up to an inch or more long and would surely have been removed by filtration. Therefore, if the filaments of the second type have indeed been formed in this way, the fine threads must have been built up in the solution from smaller units capable of passing the filter, e.g., the molecules of surface active agent. Unfortunately, no direct evidence of the formation of such long "polymer chains" in the solution is available.

Although the experimental evidence is at present insufficient to provide the basis for a complete explanation of the mechanism of the growth of the Cu filaments, it is worth mentioning one or two incidental observations which were made during the course of the experiments, and which have led to conjectures about the mechanism of their formation. In particular it was observed that soon after the start of electrolysis in the presence of the added cationic surface-active agent, a visible film of the coagulated surface-active agent was observed on the anode. This material subsequently broke away from the anode and fragments coming into contact with the cathode rapidly became Cu plated. It would seem, therefore, that the surface-active agent, which when adsorbed from solution causes a high overvoltage on the cathode, is capable, when coagulated, of breaking down this overvoltage locally. If a mechanism could be envisaged whereby the coagulated material formed long and extremely fine threads, then the formation of Cu filaments could be readily explained. One hypothesis which has been considered is that the organic thread is produced continuously at the tip of the growing filament (in the very early stages when the Cu coating is invisibly thin) by coagulation resulting from the rapid deposition of Cu occurring at an adjacent point on the tip. However, no theoretical basis for this mechanism can be produced.

Another unusual and possibly significant phenomenon was observed in solutions containing added cationic surface-active agent. After electrolysis had started and the film of coagulated surface-active agent on the anode was disrupted, fine particles were observed in the liquid; these occasionally appeared to form into fairly well defined streams between the anode and the cathode. It is perhaps tempting to connect these streams of particles with the filament formation, but again no reasonable mechanism has been formulated.

All these tentative theories for filamentary growth differ fundamentally from the theory advanced by van der Meulen and Lindstrom (2). Although these authors recognize the importance of the adsorbed layer on the cathode, they assume, apparently without experimental evidence, that the birth of a filament depends on the coincidence of a suspended particle meeting a break in this layer and, also, the propagation of the filament by the continuous displacement of this particle by the depositing Cu. The present authors prefer the mechanism in which the contact of the foreign matter itself causes the local breakdown of the high overvoltage and becomes Cu-plated, although whether the organic core of the resultant Cu filament is "pre-formed' in the solution or is built up simultaneously with the plating process has not been decided. This theory is strongly supported by the experimental evidence that (*a*) foreign matter in the form of filaments, e.g., cotton wool, does, in fact, become plated on contact with a cathode showing the high overvoltage, and (*b*) coagulated surface-active agent also becomes plated on contact with such a cathode.

Although the suggested mechanism of formation of filaments of the first type (having a discrete fibrous core) is a reasonable one, it has not yet been possible to show how this mechanism can be extended to explain in detail the formation of the second type of filament having no discrete organic core, and it must be admitted that this still remains largely a matter for conjecture and further experimental work.

Acknowledgment

This communication is published by permission of the Admiralty.

Manuscript received October 1, 1956. This paper was prepared for delivery before the Buffalo Meeting, Oct. 6-10, 1957.

Any discussion of this paper will appear in a Discussion Section to be published in the June 1958 JOURNAL.

REFERENCES

1. H. Gollop, *Bull. Inst. Metals*, **2** (1), 7 (1953).
2. P. A. van der Meulen and H. V. Lindstrom, *This Journal*, **103**, 390 (1956).

Cerium-Activated Halophosphate Phosphors

S. T. Henderson and P. W. Ranby

Thorn Electrical Industries Ltd., London, England

ABSTRACT

This paper describes the characteristics of a new group of alkaline earth halophosphate phosphors activated by cerium and manganese, and contrasts their behavior with that of halophosphates containing other primary activators. In their preparation these cerium-activated materials show marked differences from other previously known halophosphates, but the luminescent properties are similar to those of the tin-activated system. The behavior and possible uses of these phosphors in fluorescent lamps are described.

The use in fluorescent lamps of Sb-activated alkaline earth halophosphate phosphors of an apatite-like structure was first proposed in 1942; almost immediately it was found that the primary activator Sb could be replaced by other elements, As, Bi, Sn, or Pb (1). About eight years later a method of activating the matrix by Ag was developed (2). It has now been found that these materials can be activated by Ce; Mn can be incorporated as a secondary activator to modify the fluorescent emission in much the same way as with other primary activators (3). The discovery of new primary activators of this system has resulted from advances in the techniques of phosphor research, and also from a changing appreciation of the wide variations in formulation which can result in the formation of an apatite structure.

Preparation of Cerium-Activated Halophosphates

Essentially, these materials are prepared by the usual methods adopted for phosphate phosphors. For example, an intimate mixture of the matrix forming components and suitable compounds of the activators is heated to 1100°-1200°C in a mildly reducing atmosphere such as a mixture of H_2 and N_2.

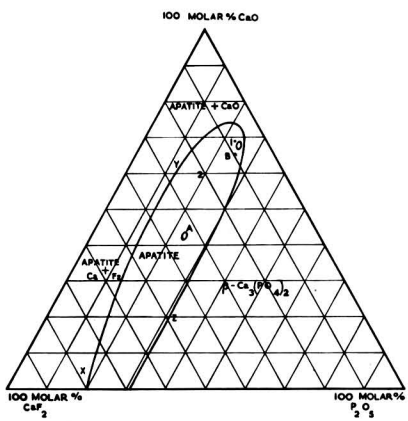

Fig. 1. XYZ: initial formulations (in molar percentages) of unfired mixtures which give products with the apatite crystal structure after firing. Points 1 and 2: theoretical apatite and wagnerite compositions, respectively. A, compositions for Ce-activated halophosphates; B, compositions for Sb-, As-, Sn-, Pb-, or Ag-activated halophosphates.

Formulation

The ratio of the matrix forming components in the initial mixture differs widely from that which would be expected to yield an apatite structure. However, x-ray analysis confirms the crystal structure of these Ce-activated phosphors to be essentially that of apatite. This wide divergence in initial formulation is shown in Fig. 1.

In Fig. 1 the ranges of formulations of starting components which will yield the apatite structure by heating to temperatures of the order of 1100°-1200°C are those within the continuous line XYZ. The formulations are expressed in terms of molar percentages of CaO added as $CaCO_3$, P_2O_5 added as diammonium hydrogen phosphate, and CaF_2 used in the initial mixtures. These were heated in silica crucibles, and reactions such as the following could account for the formation of apatite-like products from any mixtures initially free from $CaCO_3$, i.e., oxide.

$$25CaF_2 + 6P_2O_5 \rightarrow 5Ca_5(PO_4)_3F + 9PF_5$$
$$20CaF_2 + 6P_2O_5 + 9SiO_2 \rightarrow 4Ca_5(PO_4)_3F + 9SiF_4$$

Irrespective of the mechanism by which apatite results from initial mixtures widely differing from those which would be expected to yield apatite, it is found that the mixtures used to prepare bright Ce- or Ce- and Mn-activated phosphors lie within area A, whereas those for the preparation of Ag-, Sb-, Sn-, Pb-, and As-activated halophosphates (with or without Mn) lie within the area B. Area B is adjacent to point 1, which is the theoretical formulation of apatite $Ca_5(PO_4)_3F$; point 2 is theoretical wagnerite $Ca_2(PO_4)F$.

Analysis of Ce-activated fluorophosphate phosphors shows that, despite the high proportion of fluoride used in the preparation, they are readily soluble in acid without leaving any insoluble residue; the proportion of fluoride in the product is about 10% greater than in a normal fluoroapatite.

The formulations defining the areas A and B are empirical mixtures arrived at solely for the purpose of producing the optimum brightness of fluorescence,

using the normal type of phosphor preparation in silica ware. For the purposes of calculation all chloride in the initial mixtures, even when present as NH_4Cl, has been calculated as its equivalent in terms of CaF_2, all Mn and Sr compounds have been calculated as their equivalent of Ca compounds. Also, in practically all cases the formulations defining areas A and B utilized a precipitated phosphate such as $CaHPO_4$ as the source of phosphorus, and this has been calculated in terms of metal oxide and P_2O_5. In every case the primary activator has been ignored in the calculation. The outstanding feature shown by these calculations is that for calcium or calcium strontium fluoro- or fluorochloro-phosphates of an apatite structure, the initial compositions for the preparation of phosphors of the brightest luminescence are essentially the same irrespective of the primary activator, except when this is Ce.

Position of Activator

This effect, when the primary activator is Ce, is not explained by differences in the concentrations of the primary activators in the initial mixtures for the brightest luminescence (Table I), nor is it explained by differences in the volatility of the halides of the primary activators.

In view of the relatively low concentrations of activators present in a phosphor and the many assumptions which have to be made, it is felt that normal analytical methods give meaningless results for the valency of activators unless the system is a particularly simple one. It is therefore necessary to deduce the valency of Ce from the preparative conditions, which in this case indicate that the Ce is trivalent. The most likely position for the Ce in the apatite lattice is at alkaline earth metal sites especially as the ionic radius of the cerous ion is intermediate between those of Ca and Sr. This position for the trivalent Ce requires charge compensation satisfied by the incorporation of additional fluoride ions in the lattice. To achieve this increase in fluoride concentration in the matrix a relatively large excess of fluoride is required during the preparation.

Evidence in support of this explanation is provided by F estimations on calcium strontium fluorophosphate (Ce, Mn) phosphors. For a sample with a Ca to Sr ratio of 4:1 and containing known amounts of Ce and Mn, the calculated concentration of F would be 3.43% if present in only normal apatite proportions, and 3.95% if in addition 1 F atom/Ce atom is required for charge compensation. The amount of F actually found was 3.76%. In a similar fluoro-chloro-phosphor the total halogen was found to be equivalent to 3.70% F. These analyses would indicate that only about 60% of the Ce is charge-compensated by F if all the Ce is present in the trivalent form. It is interesting that in a study of the Ce- and Mn-activated calcium orthophosphates Froelich and Margolis (4) found that sufficient charge compensation of the (cerous) cerium activator was effected by 1 Na ion/2 cerous ions. It may be noted that in the present halophosphate materials there is some benefit from the incorporation during the preparation of an alkali metal (Li or Na) (3) which may complement the F as charge compensator.

Table I. Atoms of primary activator/atom of phosphorus used in initial mixtures for optimum fluorescence

Sb	4×10^{-2}
As	6×10^{-2}
Sn	6×10^{-2}
Pb	8×10^{-2}
Ag	6×10^{-3}
Ce	6×10^{-2}

In contrast to the behavior of these Ce-activated halophosphates, the Sb-activated materials generally contain less than the calculated concentration of halogen. For example, a Cool White type of halophosphate was found to contain 2.98% F and 0.61% Cl, giving a total equivalent of 3.30% of F compared with a theoretical value of 3.75% for apatite.

Except with Ag, the primary activators of the halophosphate matrix are all used in similar proportions (Table I). Some of these (Sn^{2+}, Pb^{2+}) are present in the matrix in the divalent form and require no excess of halide. The others (As, Sb) can occupy lattice sites other than those of the alkaline earth metals, for example the phosphorus positions, or they may be incorporated so that two alkaline earth atoms are replaced by two trivalent antimony atoms and one oxygen to maintain neutrality (5). The position of Ag is more difficult to explain unless pairs of ions replace a single alkaline earth metal, but the role of Ag is obviously different from that of any of the other primary activators as its smaller concentration shows.

Luminescence of Cerium-Activated Halophosphates

Like other halophosphate systems, these Ce-activated materials are strongly excited by short wavelength ultraviolet; long wave-length ultraviolet only excites a feeble luminescence associated with the secondary activator Mn. In general luminescent characteristics, these materials resemble those with Sn and Pb more closely than those with Sb.

In the absence of Mn, the Ce-activated phosphors emit strongly in the ultraviolet when excited by 2537Å radiation. For example, the relative values of the ultraviolet emission peaks, in energy per unit wave length, for calcium strontium halophosphate (Ce), calcium halophosphate (Sn), calcium halophosphate (Pb), and calcium silicate (Pb), are 75, 5, 2, and 20, respectively, whereas for barium disilicate (Pb), a system not capable of transforming its ultraviolet energy into the emission of another activator, the value is 100. Incorporation of Mn produces a strong emission in the visible and the posision of this band depends on the ratio of combined F to Cl in the matrix. Consequently a range of phosphors varying in color of fluorescence from yellow to orange-red can be obtained by variations in the concentration of Mn and ratio of F to Cl.

Replacement of Ca by Sr causes a slight shift of the emission to longer wave lengths and in addition products containing both Ca and Sr are brighter than the corresponding Ca material. An atomic ratio of Ca to Sr of 4:1 is desirable for maximum intensity of luminescence, and except where otherwise indi-

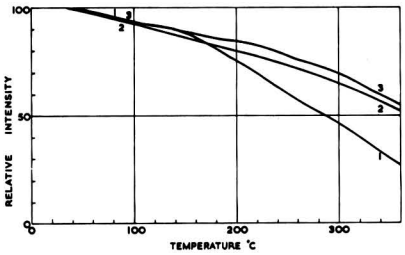

Fig. 2. Brightness vs. temperature curves of [1] calcium strontium fluorochlorophosphate (Ce, Mn); [2] calcium fluorochlorophosphate (Sn, Mn); [3] calcium fluorochlorophosphate (Sb, Mn).

cated this ratio has been used in all the materials described.

The fluorescence excited by 2537Å is slowly reduced in intensity as the temperature of the phosphor is raised (Fig. 2). The decline in intensity is of about the same order as that shown by other halophosphates and, as with these other materials, the color of the fluorescence is seen to become more green as the temperature is raised.

Use in lamps.—These materials can be used in conventional fluorescent discharge lamps but, as usual with phosphors whose preparation requires a reducing or partially reducing atmosphere, baking of coated tubes needs special care in order to minimize oxidation of the phosphor which would cause loss of brightness.

Although the initial intrinsic brightness of Ce-activated halophosphates is at least as high as that of similar Sb-activated materials, owing to the difficulties of lamp processing the brightest 48T12 40W lamps prepared by conventional suspension coating and baking techniques are only of the order of 55 lpw initially, with a maintenance of about 96% and 93% at 100 and 500 hr, respectively. However, binderless coating techniques may overcome the loss in brightness incurred by binder-removing processes; since these Ce-activated materials are not so susceptible to grinding as Sb-activated halophosphates they may prove very suitable for electrostatic coating.

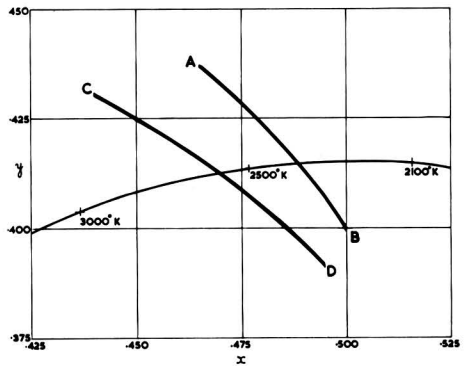

Fig. 3. Chromaticity plots of 48T12 40W lamps containing: (A-B) Ce- and Mn-activated halophosphates and (C-D) Sn- and Mn-activated halophosphates.

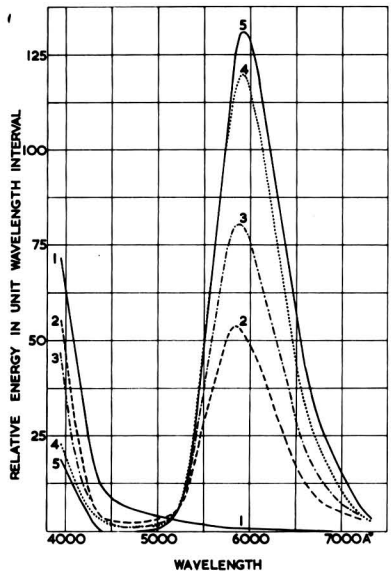

Fig. 4. Spectral energy distribution curves of calcium strontium fluorochlorophosphates activated by Ce and [1] 0, [2] 0.006, [3] 0.012, [4] 0.024, and [5] 0.036 atoms of Mn/atom of P, excited by 2537Å at room temperature. Phosphor composition: (Ca + Sr + Mn):Ce:P = 4.8:0.16:3. Ca:Sr = 4:1. F:Cl = 0.85:0.15. Fired at 1150°C for ½ hr in a closed crucible followed by ½ hr at 1150°C in N_2 + H_2.

Color measurements on 48T12 40W lamps show that the color changes obtained by variations in composition follow a narrow band about the line AB (Fig. 3) which cuts the black body locus at 2360°K. A similar series of lamps prepared using the Sn- and Mn-activated materials gives colors following a narrow band about the line CD which cuts the black body locus at 2580°K.

Cerium emission.—The fluorescent emission due to activation by Ce alone is a fairly broad band centered at about 3400Å when the phosphor is excited by 2537Å radiation. Activation of the halophosphate matrix by Sn or Pb produces similar emission bands in the ultraviolet centered at about 3900 and 4400Å, respectively.

Manganese emission.—Incorporation of Mn as a secondary activator produces emission in the visible of an intensity depending on the concentration of Mn. These changes are shown by the curves in Fig. 4. These materials differ only in concentration of Mn. As this concentration increases, the Mn emission increases in intensity to a maximum at about 0.036 atoms Mn/atom of P; the ultraviolet band due to Ce, of which only part is shown, decreases. This is obviously a case of sensitized luminescence similar to that of calcium orthophosphate (4), or calcium fluoride (6), similarly activated.

If these emission curves, converted to a frequency basis, are analyzed by the usual methods (7), it is found that the Mn emission consists of at least two bands, a major band in the yellow and a minor one in the red, and that both of these increase with Mn concentration. These results are tabulated in Table II.

Table II. Emission bands of Ce-activated halophosphates

Matrix	Mn content atoms Mn/ atom P	Relative intensity of maximum of Yellow band	Red band	Position of yellow band maximum Å
Fluoro-phosphate	0	0	0	—
	0.006	33	3.5	5750
	0.012	51	5.5	5760
	0.024	87	16	5815
	0.036	100	14.5	5840
Fluoro-chloro-phosphate	0	0	0	—
	0.006	33	3.5	5840
	0.012	51	8	5870
	0.024	76	11	5915
	0.036	84	13	5930

In all cases the main yellow band is very close to a Gaussian distribution, but the red emission may consist of more than one band. This red emission extends from 6000 to 7000Å in the fluorophosphates and even further, to 7300Å, in fluorochlorophosphates of high Mn content.

As indicated earlier, the intensity of the Mn emission is at a maximum when the atomic ratio of Ca to Sr in the matrix is about 4:1, but the effect on the position of the emission band of partially replacing Ca of the matrix by Sr is relatively slight. For example, the peak of the Mn yellow band is displaced to shorter wave lengths by only about 40Å when the alkaline earth metal is all Ca instead of the 4:1 ratio more generally used.

Conclusion

In a previous paper (8) on magnesium fluorosilicate it was suggested that the efficiency of emission in sensitized phosphors was increased by proximity of the sensitizer and activator bands. The optimum relation of these bands appeared to occur in Sb-sensitized halophosphates, but the present Ce-sensitized materials have a luminous efficiency at least as high as the Sb phosphors, in spite of the location of the sensitizing band in the ultraviolet. The original hypothesis assumed that all sensitizing bands were excited with equal efficiency by 2537Å radiation. It is clear that this is not the case, for the Ce-activated halophosphates, in the absence of Mn, show an exceptionally high ultraviolet emission compared with other systems having sensitizer emission bands in this region. This high efficiency would clearly have a favorable effect on the amount of emission in the Mn band and might offset the energy loss due to the production of one activator quantum from one much larger sensitizer quantum. A continued study of the efficiency of excitation of these sensitizer bands and their conversion to visible emission bands by secondary activators is in progress.

Acknowledgment

The authors thank the Directors of Thorn Electrical Industries Ltd. for permission to publish.

Manuscript received March 22, 1957. This paper was prepared for delivery before the Washington Meeting, May 12-16, 1957.

Any discussion of this paper will appear in a Discussion Section to be published in the June 1958 JOURNAL.

REFERENCES

1. H. G. Jenkins, A. H. McKeag, and P. W. Ranby, *J. (and Trans.) Electrochem. Soc.*, **96**, 1 (1949).
2. P. W. Ranby, *This Journal*, **98**, 299 (1951).
3. P. W. Ranby, British Pat. 21348/55, July 22, 1955; 8893/56, Mar. 21, 1956.
4. H. C. Froelich and J. M. Margolis, *This Journal*, **98**, 400 (1951).
5. K. H. Butler and C. W. Jerome, *ibid.*, **97**, 265 (1950).
6. R. J. Ginther, *ibid.*, **101**, 248 (1954).
7. P. W. Ranby, D. H. Mash, and S. T. Henderson, *Brit. J. Appl. Phys.*, Suppl. 4, S18 (1955).
8. P. W. Ranby and S. T. Henderson, *This Journal*, **102**, 631 (1955).

The System Cadmium Oxide-Boric Oxide

II. Fluorescence

F. A. Hummel and E. C. Subbarao

Department of Ceramic Technology, College of Mineral Industries,
The Pennsylvania State University, University Park, Pennsylvania

ABSTRACT

The luminescence of the compounds $2CdO \cdot B_2O_3$, $3CdO \cdot 2B_2O_3$, and $2CdO \cdot 3B_2O_3$ has been investigated under 2537Å radiation and cathode ray excitation for a wide range of manganese concentrations. Under 2537Å radiation, each compound emits in the orange or orange-red with a peak intensity near 6200Å at room temperature. For each composition there is a broad maximum in the relative intensity between MnO concentrations of 0.1-1%. The 3:2 compound appears to yield the brightest phosphor, but the 2:1 compound is only slightly less intense for equivalent manganese additions. The 2:3 compound yields only half the relative brightness of the 3:2 compound for equivalent manganese concentrations.

Under cathode ray excitation, the 2:1 and 3:2 compounds fluoresce orange and the 2:3 compound fluoresces green for manganese concentrations between 0.01 and 2%.

In a recent paper (1) thermal, optical, and x-ray data were provided for four compounds in the system CdO-B_2O_3. Three of the compounds ($2CdO \cdot B_2O_3$, $3CdO \cdot 2B_2O_3$, $2CdO \cdot 3B_2O_3$) are fluorescent when activated with Mn and it is the purpose of this paper to provide some quantitative data on their emission under 2537Å and cathode ray excitation over a wide range of Mn concentrations.

Many references to cadmium borate phosphors have been made in the literature but the present data demonstrate that their compositions have been primarily in terms of technical formulations and did not necessarily denote the constitution of compounds. A review of some of the more recent papers will make manifest the significance of the data of this paper in clarifying the situation.

Kroger (2) has indicated green cathodoluminescence for the "matrices" $3CdO \cdot B_2O_3$, $CdO \cdot B_2O_3$, and $CdO \cdot 2B_2O_3$ and orange for the "matrix" $2CdO \cdot B_2O_3$.

Botden and Kroger (3) stated that $2CdO \cdot B_2O_3$ is excited by $\lambda < 3200$Å and cathode rays and then shows an orange luminescence, whereas $CdO \cdot B_2O_3$, $2CdO \cdot 3B_2O_3$, and $3CdO \cdot B_2O_3$ show a green cathodoluminescence only.

Leverenz (4) has presented emission curves for $3CdO \cdot 2B_2O_3$: 0.018 MnO and $2CdO \cdot B_2O_3$: 0.012 MnO, indicating a peak at 6260Å under 6-kv, 1μa cm^2 C. R. $CdO \cdot 2B_2O_3$: 0.006 peaked at 5380 while $CdO \cdot B_2O_3$ had both the 5380Å peak and another near 6200Å. In speaking about luminescence as a function of time, Leverenz states, "In some cadmium-borate: Mn phosphors having both a green and an orange emission band, the orange band predominates during phosphorescence".

Fonda (5), working with Mn concentrations of 0.02-1.00% by weight, 2537Å excitation, and temperatures of 80°, 300°, and 375°K, showed that above 0.50% Mn, the peak of the emission of $2CdO \cdot B_2O_3$ at 80°K lies at 6300Å and is reduced to 6200Å on sufficient increase in temperature. Below 0.1% Mn, the peak is altered only insignificantly by change in temperature and persists at the stable value of 6200Å.

Experimental Procedure

The phosphors were prepared from the fluorescent grade materials $CdCO_3$, boric acid, and $MnCO_3$. The most significant impurity present may have been sulfate, introduced through the $CdCO_3$ and ranging in amount from 0.3-1% on the basis of $CdCO_3$. The Mn concentrations (MnO) investigated for each compound were 0.01, 0.02, 0.03, 0.04, 0.06, 0.08, 0.10, 0.12, 0.15, 0.20, 0.25, 0.50, 1.00, and 2.00%.

The $3CdO \cdot 2B_2O_3$ and $2CdO \cdot 3B_2O_3$ compositions were fired in fused silica crucibles at 810° ±10°C for 2 hr. The $2CdO \cdot B_2O_3$ phosphors were fired at 850° ±15°C for 2 hr. The higher firing temperature for the 2:1 compound was necessary in order to insure complete conversion to this stoichiometric ratio, since it is known from the previous phase equilibrium studies that this compound has a lower limit of stability near 780°C.

Three additional mixtures were made with 0.1% MnO at CdO: B_2O_3 ratios of 1:1, 1:2, and 1:3.

Emission curves for 2537Å and cathode ray excitation were obtained on a General Electric recording spectrophotometer, standardized with a commercial sample of cadmium borate.

Reproducibility of results was checked by measurements on the same composition prepared at intervals of two months or more, by firing at several different temperatures other than those listed above,

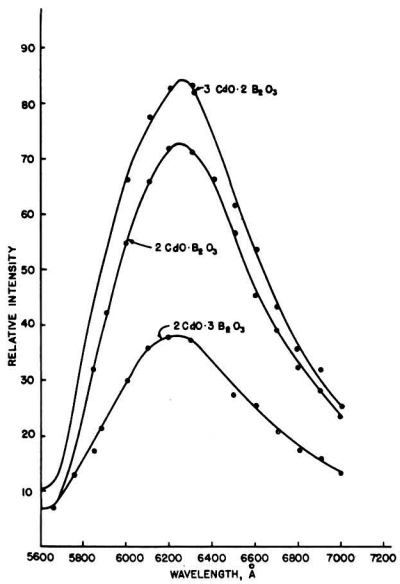

Fig. 1. Typical emission curves for three cadmium borate compounds activated with 0.25% MnO (2537Å excitation); intensity relative in terms of a commercial cadmium borate phosphor.

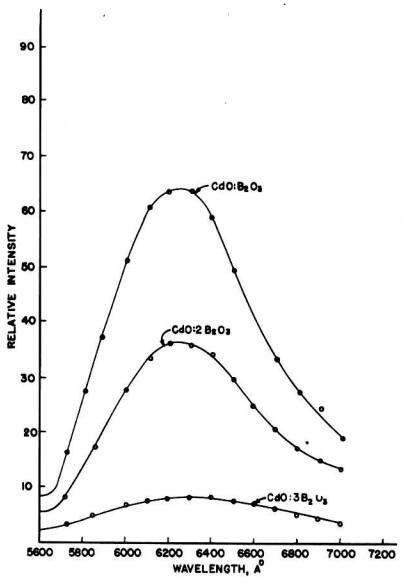

Fig. 2. Emission curves for $CdO:B_2O_3$ mixtures 1:1, 1:2, and 1:3 activated with 0.1% MnO (2537Å excitation); intensity relative in terms of a commercial cadmium borate phosphor.

and by comparing results from sintered samples with those which had been obtained on fused and recrystallized products.

Results and Discussion

2537Å Excitation.—The form of the emission curve which is typical for all three compounds for 2537Å excitation is shown in Fig. 1. The peak emission at room temperature occurred near 6200Å. It is interesting to note that, although the emission spectra for the 3:2 and 2:3 compounds are similar in form, the 2:3 preparation looks much "pinker" when made into lamps, relative to the 3:2 compound, due probably to the difference in brightness.

The emission curves for the 1:1, 1:2, and 1:3 mixtures for 2537Å excitation are shown in Fig. 2. It is noteworthy that the curve for 1:1 is intermediate between that for 3:2 and 2:3 as might be expected on the basis of a mechanical mixture. The peak intensity for the 1:2 mixture is comparable to that for the 2:3 compound, while the relative intensity falls off markedly for the 1:3 mixture.

The relative intensity vs. Mn concentration is shown for the three compounds in Fig. 3, using a log scale for the MnO content. There is a characteristically broad maximum between 0.1 and 1% MnO and a rapid drop above 2% MnO. In the previous paper on equilibrium relationships, it was estimated that the solid solubility of MnO in the 2:1 and 3:2 compounds was relatively low (possibly 1-3%) while perhaps 5-8% could be incorporated in the 2:3 lattice. In view of these figures it appears that the decrease in relative intensity above 1% MnO may not be related to the limit of solid solubility of MnO in these compounds.

Cathode ray excitation.—Under cathode ray excitation, for Mn concentrations ranging from 0.01-2%, the 2:1 and 3:2 compounds fluoresce orange (Fig. 4). The 2:3 compound ranges from a very pale green for low concentrations of MnO such as 0.01-0.1% to a stronger, but still not very intense green for MnO contents between 0.1 and 2%. These results are in total agreement with the data of Leverenz (6) who shows orange peaks at 6260Å for 2:1 and 3:2, green for 1:2, and both green and orange peaks for 1:1, indicating that the latter is actually a mixture of the two compounds, $3CdO \cdot 2B_2O_3$ and $2CdO \cdot 3B_2O_3$. He also indicates a much greater relative intensity (30 and 15) for the 2:1 and 3:2 compounds than for the matrices which yield the green band (5 for the 1:1 and 4 for the 1:2 mixture).

Activators other than Mn.—Brief experiments with 0.1% additions of other activators are sum-

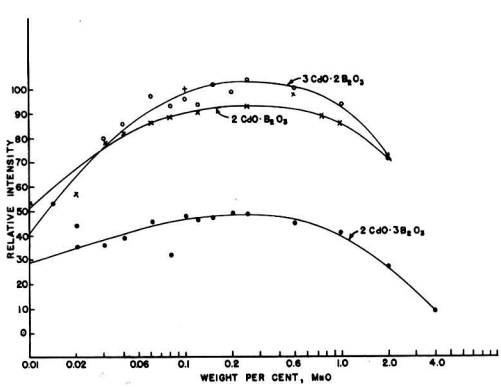

Fig. 3. Relative intensity vs. Mn concentration for the 2:1, 3:2, and 2:3 cadmium borate compounds (2537Å excitation).

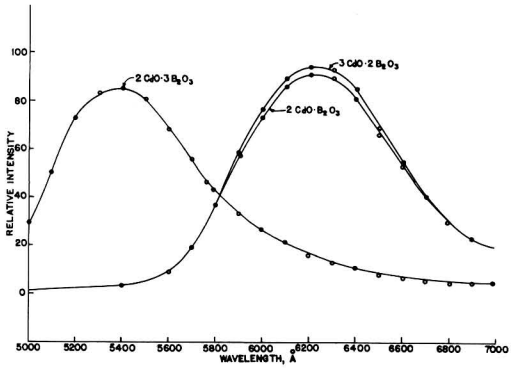

Fig. 4. Typical emission curves for three cadmium borate compounds (cathode ray excitation); [2:1 and 3:2 compounds activated with 0.15% MnO, 2:3 compound with 2.0% MnO]; intensity relative in terms of a commercial cadmium borate phosphor.

marized in Table I. Activators were added as C.P. compounds and each preparation was fired to 800°C for 2 hr in the case of the 3:2 and 2:3 compounds and at 850°C for 2 hr for the 2:1 compound.

Summary

Data are presented on the fluorescence of the three cadmium borate phosphors whose composition is that of specific compounds. It is now evident that previous data frequently have been in terms of technical formulations. It is now possible to associate characteristic emission color with a particular compound, and to describe the behavior of intermediate mixtures in terms of the 2:1, 3:2, and 2:3 compounds.

All three compounds are excited to orange emission by 2537Å radiation and the 2:1 and 3:2 compounds also emit in the orange region under cathode ray excitation. The 2:3 compound is distinct from the others in emitting in the green region under cathode ray excitation. Future work on the decay, temperature dependence, nature of the emitting centers, or other aspects of the luminescence of compositions in this system may be guided by these results for the pure compounds.

Acknowledgment

The authors wish to thank members of the Chemical Products Plant of the General Electric Company for their assistance in obtaining emission curves.

Manuscript received April 11, 1957. Contribution #56-28 from the Department of Ceramic Technology, College of Mineral Industries, Pennsylvania State University, University Park, Pennsylvania.

Any discussion of this paper will appear in a Discussion Section to be published in the June 1958 JOURNAL.

REFERENCES

1. E. C. Subbarao and F. A. Hummel, *This Journal*, **103**, 29 (1956).
2. F. A. Kroger, "Some Aspects of the Luminescence of Solids," pp. 60, 61, 270, Elsevier Publishing Co., New York (1948).
3. Th. P. J. Botden and F. A. Kroger, *Physica*, **13**, 216 (1947).
4. H. W. Leverenz, "An Introduction to Luminescence of Solids," pp. 233, 256, John Wiley & Sons, Inc., New York (1948).
5. G. R. Fonda, *J. Opt. Soc. Amer.*, **40**, 347 (1950).
6. Ref. (4), p. 234.

Table I. Fluorescence of cadmium borate compounds with various activators

Activator	2537	$2CdO \cdot B_2O_3$ 3650	C.R.	2537	$3CdO \cdot 2B_2O_3$ 3650	C.R.	2537	$2CdO \cdot 3B_2O_3$ 3650	C.R.
Sn	Weak blue	Weak orange	Weak orange	Dead	Weak orange	Weak orange	Dead	Dead	Weak blue
Sb	Weak blue	Weak orange	Weak orange	Dead	Weak orange	Weak orange	Dead	Dead	Weak blue
Ti	Weak blue	Weak orange	Weak orange	Dead	Weak orange	Weak orange	Dead	Dead	Weak blue
Hg	Weak blue	Weak orange	Weak orange	Dead	Weak orange	Weak orange	Dead	Weak orange	Weak blue
Sm	Weak blue	Weak blue	Grey	—	—	—	Dead	Dead	Weak blue
Bi	—	—	—	Dead	Weak blue	Weak orange	Dead	Dead	Weak blue
Ag	—	—	—	Dead	Weak blue	Weak orange	Dead	Weak orange	Brown(?)
Tl	—	—	—	Dead	Weak orange	Weak orange	Dead	Weak orange	Pale blue
Pb	—	—	—	Pale blue	Pale blue	Weak orange	Dead	Weak blue	Pale blue

Optical Measurement of Film Growth on Silicon and Germanium Surfaces in Room Air

R. J. Archer

Bell Telephone Laboratories, Incorporated, Murray Hill, New Jersey

ABSTRACT

The thickness and growth kinetics of oxide films on polished silicon and germanium exposed to room air after having been rinsed in hydrofluoric acid were obtained by measuring the ellipticity of reflected polarized light. Film growth obeys the Elovich equation. Plots of thickness vs. the logarithm of the time in air are linear after about 15000 sec with slopes of 6.8Å/decade (Si) and 8.1Å/decade (Ge). Immediately after the hydrofluoric acid rinses the films are 10-15Å thick and increase in thickness by about 11-12Å after one day in air. A small part of the films dissolves in certain organic liquids. Measurements of ellipticity at two angles of incidence during film growth gave an experimental check of the optical theory.

The rates of growth of films—presumably oxide films—on polished Si and Ge in room air following a rinse in HF were obtained by measuring the ellipticity of polarized light reflected from the surfaces. The measurements were undertaken because a simple experimental system was desired for evaluating the applicability of this optical technique for studying Si and Ge surfaces and because of interest in the system itself since the surfaces in these experiments are similar to etched surfaces in room air upon which the majority of physical measurements have been made and which are the most common device surfaces. Film thicknesses and growth rates have not been measured previously for such surfaces.

When plane polarized light, with the plane of oscillation of the electric field vector inclined at 45° to the plane of incidence, is reflected from a surface, the state of polarization, i.e., the ellipticity, of the reflected beam is characterized by the phase difference, Δ, and the amplitude ratio, $\tan \Psi$, between the two components of the electric field vector measured in and normal to the plane of incidence. The magnitudes of Δ and Ψ (expressed in degrees) depend on the angle of incidence, the optical constants of the reflecting substance, and the thickness and index of refraction of the surface film. For films thin compared to the wave length of the incident light, first order linear relationships between film thickness and the reflection parameters obtain. By expanding the exact equation and retaining only first order terms in thickness, the following equations, valid for films thinner than about 50Å, are derived (1)[1]

$$\Delta = \bar{\Delta} - \alpha L \qquad \text{(I)}$$

$$\Psi = \bar{\Psi} + \beta L \qquad \text{(II)}$$

[1] Reference (1a) gives simple derivation of exact equation, (1b) best expansion procedure. Above Eqs. (I) and (II) have same form as well-known Drude equations (1c). However, certain terms missing in Drude's equations are retained here which significantly affect the magnitude of the coefficients when evaluated for Si and Ge.

$$\alpha = \frac{720 \cos\phi \sin^2\phi \,(n_1^2 - 1)\,(1/n_1^2 - a)\,[\cos^2\phi - a + \sin^2\phi\,(a^2 - a'^2) + a'^2]}{\lambda([\cos^2\phi - a + \sin^2\phi\,(a^2 - a'^2)]^2 + a'^2)} \qquad \text{(III)}$$

$$\beta = \frac{720 \sin^2\bar{\Psi} \cos\phi \sin^2\phi \,(n_1^2 - 1)\,a'\,((1/n_1^2 - a)\,(1 - 2a\sin^2\phi) - [\cos^2\phi - a + \sin^2\phi\,(a^2 - a'^2)])}{\lambda([\cos^2\phi - a + \sin^2\phi\,(a^2 - a'^2)]^2 + a'^2)} \qquad \text{(IV)}$$

Film thicknesses are calculated from the experimental quantities Δ and Ψ using the relationships (I) and (II). The evaluation of the coefficients of these equations requires values for the optical constants of the film and subphase. $\bar{\Delta}$ and $\bar{\Psi}$ are calculated from standard formulas (2) and α and β from Eqs. (III) and (IV). Values for the optical constants are given in Table II along with the calculated coefficients for two angles of incidence.

Since $\alpha >> \beta$ and Δ and Ψ can be measured with about the same precision and accuracy, film thicknesses are obtained from measurements of Δ. n and κ were determined experimentally from measurements of Δ and Ψ using special techniques, and the problems attending the evaluation of these measurements—because of the unavoidable presence of surface films when high vacuum cleaning techniques

Table I. Glossary of symbols

ϕ —angle of incidence.
n_1—index of refraction of surface film.
L—film thickness expressed in Ångstrom units.
a —$(1-\kappa^2)/n^2(1+\kappa^2)^2$
a'—$2\kappa/n^2(1+\kappa^2)^2$
n —real part of complex index of refraction of reflecting substance
κ —absorption coefficient of reflecting substance. The complex index of refraction is written $\bar{n}=n(1-i\kappa)$.
$\bar{\Delta}$ —value of Δ for a film free surface.
$\bar{\psi}$ —value of ψ for a film free surface.
λ —vacuum wave length of light. In these experiments λ=5461Å.

Table II. Optical constants (λ=5461Å) and values for α, β, $\bar{\Delta}$, and $\bar{\psi}$ at two angles of incidence

	n	κ	n_1
Si	4.13 ± 1%	0.01 ± 50%	1.55 ± 5%
Ge	5.01 ± 2%	0.387 ± 6%	1.9 ± 10%

	Si		Ge	
ϕ	61.26°	70°	61.26°	70°
α deg/Å	0.140 ± 6%	0.325 ± 5%	0.154 ± 6%	0.276 ± 6%
β deg/Å	0.00010	0.0033	0.005	0.014
$\bar{\Delta}$	179.43° ± 0.28°	178.70° ± 0.64°	166.28° ± 0.81°	154.73° ± 1.08°
$\bar{\psi}$	23.40°	12.10°	29.58°	21.54°

are not applied—make uncertain the errors in the values obtained. The uncertainties given in Table II are for the most part estimated but are believed to be realistic. The indices of refraction of the films were obtained from measurements of Δ as a function of the refractive index of the mirror's ambient medium using a series of organic liquids. The values agree with the bulk values for quartz (1.55) and insoluble germanium dioxide (1.99-2.10). All of the constants, n, κ, and n_1 are from preliminary measurements and are qualified as tentative. More refined experiments are underway and a complete report of the problems, techniques, and results of the reflection measurement of the optical constants of Si and Ge and their surface films is forthcoming. For present purposes it is sufficient to state that the maximum possible errors in the constants will not significantly affect the values for α, given in Table II, so that relative thicknesses and changes in thickness can be calculated accurately. $\bar{\Delta}$ is more sensitive to the values for the optical constants used in its evaluation. Consequently, calculated total or absolute thicknesses have relatively large uncertainties.

Technique

The instrument for measuring Δ and Ψ, the ellipsometer, is shown in Fig. 1. It consists of a spectrometer fitted with two nicol prisms and a mica quarter-wave plate, all mounted in divided circles. The procedure is to align the fast axis of the mica plate at 45° to the plane of incidence and to adjust the azimuths of the nicol prisms until the reflected beam is extinguished. Δ and Ψ are directly measured by the orientations of the nicols at extinction (3). A photomultiplier microphotometric technique is used to obtain extinction settings, and Δ and Ψ can be measured with a precision of ±0.04° and ±0.02°, respectively. Therefore, from the magnitude of α in Table II, changes in thickness can be measured to ±0.15Å (for Ge at $\phi = 70°$).

The surfaces were polished mechanically using as a final abrasive Linde B in water and were judged adequately flat when straight parallel fringes were observed with an optical flat. After polishing, the mirrors were boiled in acetone and benzene, rinsed in hot tap water and deionized distilled water, refluxed over ethyl ether, and rinsed for several minutes in HF. The mirror to be studied was mounted and aligned at the spectrometer axis; Δ and Ψ were measured; while still aligned, the mirror was immersed for 1 min in CP quality concentrated HF and immediately rinsed in three separate portions of re-distilled acetone to remove the pendent HF. As soon as possible (about 200 sec) after this treatment, Δ and Ψ were again measured and followed as a function of time while the mirror was exposed to room air. A typical experiment lasted for two days.

The measurements were made in a closed room in which the relative humidity and temperature were maintained at 54% ±4% and 28°C ±2°. The Si mirror is 10 ohm-cm n-type, the Ge 6 ohm-cm p-type. The polished faces are of unknown orientation.

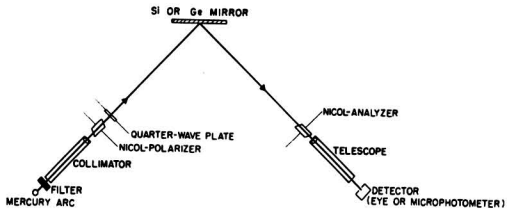

Fig. 1. Schematic representation of ellipsometer

Results

The results to be reported include film growth data, experimental verification of Eq. (I), and data demonstrating the partial solubility of the surface films in certain organic liquids.

Fig. 2 plots Δ, measured at $\phi = 61.26°$, as a function of the logarithm of time following the HF rinse.

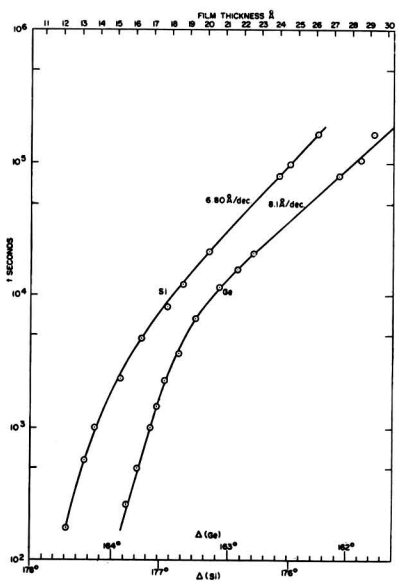

Fig. 2. Relative phase difference and calculated film thickness as a function of the time in air after an HF rinse. ϕ = 61.26°.

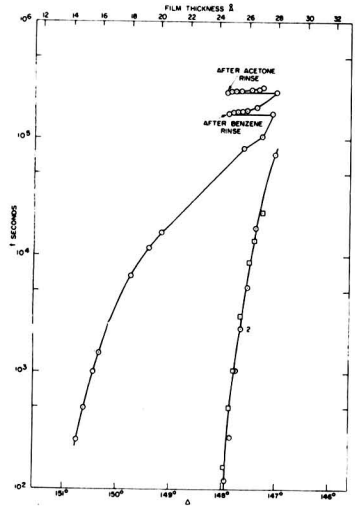

Fig. 3. Curve 1, film growth curve showing effects of 1-min benzene and acetone rinses; curve 2, Δ vs. log t for t = 0 instant of removal from organic liquid. Circle with dot = benzene, square with dot = acetone. Ge, $\phi = 70°$.

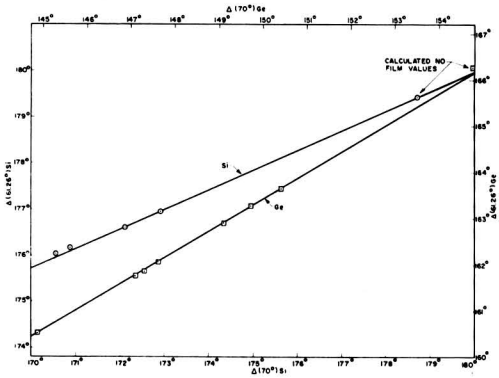

Fig. 4. Δ measured simultaneously at two angles of incidence during film growth. Fit of points to lines is degree to which experiment checks theory.

The zero of time is the instant of removal of the mirror from the HF. The two Δ axes are adjusted relative to each other so that the thickness axis at the top of the figure is for both the Si and Ge data. Thickness is obtained from Δ using Eq. (I) and the values of the coefficients given in Table II. Repeating the measurements several times on each mirror established their reproducibility, and the results of representative experiments are plotted. The linear parts of the curves (t>15000 sec) have slopes of 6.8Å/decade (Si) and 8.1Å/decade (Ge) which values were reproducible to about ±2% from experiment to experiment.

A reproducible decrease in the thickness of the regrown films on both Si and Ge accompanies rinsing in acetone, ether, benzene, hexane, and pentane. The latter two substances cause the smallest effect. Fig. 3 shows a film growth curve for Ge and the effect of rinses in acetone and benzene. The changes in Δ following the rinses are also plotted, taking as the zero

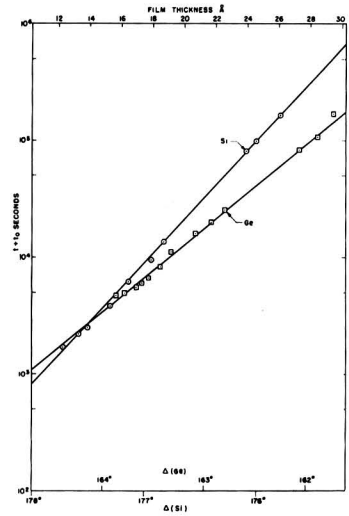

Fig. 5. Data of Fig. 2 plotted against t + t_0; t_0(Si)= 1500 sec, t_0(Ge) = 4500 sec.

of time the instant of removal from the organic liquid. The data following the benzene and acetone rinses are colinear and the slope decreases with time.

The measurement of each point on the film growth curve at two angles of incidence yielded the plots of Δ ($\phi = 61.26°$) vs. Δ ($\phi = 70°$), Fig. 4. Eq. (I) predicts the slope of these curves, $\alpha(61.26°)/\alpha(70°)$, so that comparison of experiment and theory serves to check the validity of Eq. (I). For Ge the data are fairly extensive and the agreement of theory and experiment is good. The slope of the Ge curve is 0.571 and, from Table II, the calculated value is 0.558. The best straight line through the Si points has a slope of 0.40 whereas the calculated slope is 0.430. There is not enough data to make this difference certain, and the line for Si is drawn to agree with theory. The fit is reasonably good. A further agreement with theory is obtained from the colinearity with the experimental data of the calculated clean surface points $\bar{\Delta}$ (61.26°), $\bar{\Delta}$ (70°). The displacement of this point from the experimental curve for Ge is within its limits of uncertainty.

The variation of Ψ is so small that no useful information was forthcoming from its measurement. However, the magnitudes of the changes observed are in agreement with that predicted by Eq. (II).

Discussion

The film growth data accord reasonably well with the Elovich (4) equation

$$dL/dt = A \exp(-BL) \qquad (V)$$

which, integrated, has the form

$$L = a + b \log(t + t_o) \qquad (VI)$$

Values for t_o are estimated from Fig. 2 and the data are re-plotted in Fig. 5 as Δ vs. $(t + t_o)$. The equations for these curves are

$$\text{Si: } L = -9.74 + 6.86 \log (t + 1500) \quad \text{(VII)}$$

$$\text{Ge: } L = -17.2 + 9.05 \log (t + 4500) \quad \text{(VIII)}$$

From these relationships are obtained the values 12.1Å and 15.8Å for film thickness at zero time for Si and Ge, respectively. From the uncertainties given for the coefficients of Eq. (I) in Table II, the uncertainty in calculated absolute thickness values is ±2Å for Si and ±5Å for Ge, and the uncertainty in the relative values is ±6%.

The changes in thickness accompanying the organic liquid rinses may result from the removal of a slowly growing "grease" film. Depending on the refractive index of such a film, curve 2 of Fig. 3 gives a growth rate of 1-2Å/decade between 10^4 and 10^5 sec with a total thickness of 3-4Å after 24 hr in air. Other explanations of the effect are possible, and the grease film hypothesis will not be further discussed.

These results can be compared with those of Green and Kafalas (5) on the oxidation of atomically clean Si and Ge. They measured oxygen uptake at relatively low pressures and reported logarithmic rates about an order of magnitude smaller than obtained here. The difference in rates may be due to a difference in mechanism. In the present case, the phenomenon observed is probably the growth of a nucleated oxide film accelerated by the relatively high humidity, whereas the data of Green and Kafalas measure oxygen chemisorption. The differences should be resolved by future experiments with the ellipsometer under controlled surface and ambient conditions.

Manuscript received April 26, 1957. This paper was prepared for delivery before the Washington Meeting, May 12-16, 1957.

Any discussion of this paper will appear in a Discussion Section to be published in the June 1958 JOURNAL.

REFERENCES

1a. O. S. Heavens, "Optical Properties of Thin Solid Films," p. 55, Butterworths Scientific Publications, London (1955).
1b. C. E. Leberknight and B. Lustman, *J. Opt. Soc. Amer.*, **29**, 59 (1939).
1c. P. Drude, *Wied. Ann.*, **36**, 532, 865 (1889); *ibid.*, **39**, 481 (1890).
2. R. W. Ditchburn, *J. Opt. Soc. Amer.*, **45**, 743 (1955).
3. A. B. Winterbottom, *ibid.*, **38**, 1074 (1948).
4. S. Yu Elovich and G. M. Zhabrova, *Zhur. fiz. Khim. USSR*, **13**, 1761, 1775 (1939).
5. M. Green and J. A. Kafalas, *Phys. Rev.*, **98**, 1566 (1955).

Electrical Conductivity of Molten Fluorides

I. Apparatus and Method

Ernest W. Yim and Morris Feinleib

Chemical Research Department, Kaiser Aluminum & Chemical Corporation, Permanente, California

ABSTRACT

A method and apparatus have been developed for determining the electrical conductivity of cryolite-base melts and other fluorides. Hot-pressed boron nitride was used to fabricate high-resistance cells with constants ranging from 17 to 39 cm^{-1}. Such cells must be used under an inert atmosphere, and correction must be made for the conductance of the cell body proper. A furnace and apparatus for accomplishing these objectives are described. An a-c Wheatstone bridge is used for measurements. In spite of the fact that Inconel electrodes were employed, resistance values were found to be independent of frequency above 1000 cycles.

The many attempts to measure the conductivity of cryolite-base melts and the importance of these measurements have been summarized by Edwards, *et al.* (1). They point out the wide discrepancy in the conductance results coming out of various laboratories.

The major difficulty in determining conductivities of fused fluorides is to find a suitable conductance cell material. It should not be attacked by the melts, should be an electrical insulator at temperatures of the order of 1000°C, and should have dimensional stability at those temperatures. Until recently, no such material was available. Accordingly, most investigators sidestepped the problem by using Pt cells (1). Such cells have a very low resistance, and electrode polarization becomes a major problem. Other difficulties with this type of cell are the lack of dimensional stability at high temperatures, and the fact that the electrodes may no longer be strictly equipotential surfaces.

Cuthbertson and Waddington (2) attempted to get away from the limitations of the Pt cell by using a magnesia tube. However, magnesia is attacked by cryolite rather rapidly, and therefore reproducibility was limited. A similar attempt with a quartz cell was not successful (1).

Lately, electrolysis of fused fluorides has been applied to several new fields. Yet a recent exhaustive compilation of data on alkali halide systems (3) shows a conspicuous lack of data on fluorides due to the absence of a suitable measuring tool. While the present work is concerned primarily with systems of

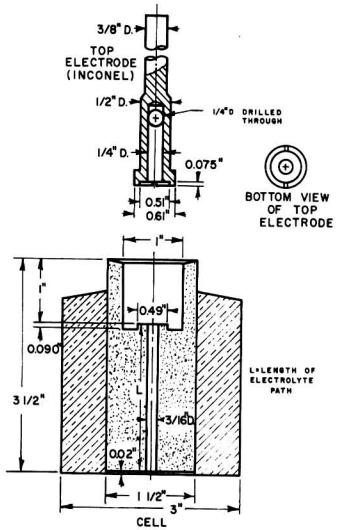

Fig. 1. Boron nitride conductivity cell with graphite jacket

interest to the aluminum industry, the method and apparatus described are applicable to measurements of electrical conductance in many fused fluorides.

Conductivity Cell and Electrodes

After examining a great number of standard and special materials, it was decided that hot-pressed BN was the most promising refractory for a conductance cell. Laboratory tests indicate that this material is not attacked by molten cryolite, and that it is readily drilled and machined.

The properties of hot-pressed BN have been described (4). Its electrical resistivity has been reported to be 3.1 x 10^4 ohm-cm at 1000°C. This value is sufficiently high so that the conductance of a BN cell could be neglected in comparison to that of most fused salts. However, even hot-pressed BN bodies have some porosity and, therefore, become impregnated with melts gradually. As a result, the conductance of the cell body becomes appreciable and needs to be taken into account. This was achieved by lowering the cell assembly into the melt under investigation and measuring the combined conductance of the electrolyte and cell body, then lifting the cell out of the melt and determining the "empty cell conductance".

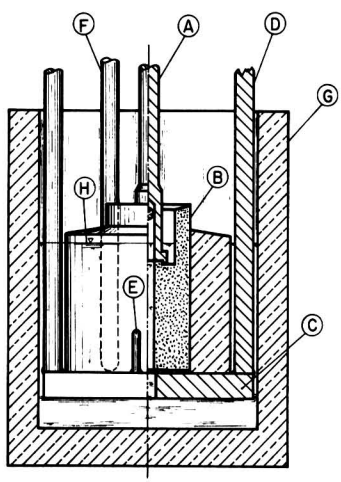

Fig. 2. Cell assembly in melt. A, top electrode; B, boron nitride cell; C, Inconel carriage and bottom electrode; D, bottom electrode leads, and supports; E, cell positioning studs; F, thermocouple tube; G, graphite crucible; H, melt level.

In the final design, the BN cell was surrounded by a graphite jacket. This jacket served a dual purpose: (*a*) it retarded the rate of melt penetration and, therefore, decreased the magnitude of the empty cell correction; and (*b*) in a graphite-jacketed cell, the paths of flow of current through impregnated cell walls are almost the same whether the cell is immersed in a melt or out of the melt, so that a representative empty cell correction can be measured.

Boron nitride is normally hot-pressed inside a graphite mold. Some of the cells were machined from 1 in. BN cylinders which had been left inside their original 3 in. mold. Boron nitride has a radial coefficient of expansion (perpendicular to pressing direction), which is much smaller than that of graphite (4); therefore, in a cold cell, the graphite is under considerable tensile stress, and the assembly must be machined carefully.

For pressing 1½ in. BN cylinders, a 5 in. graphite mold is needed. When attempting to machine this graphite down to 3 in., as required by furnace size limitations, it was impossible to avoid cracking the graphite. As an alternative, a graphite sleeve was machined separately and then slipped over an unjacketed BN cylinder to make a tight-fitting jacket.

A typical cell with matching top electrode is shown in Fig. 1. The reasons for its particular shape will become apparent during the discussion of the operating procedure. Alternate designs were also used successfully. Fig. 2 shows the cell and electrode assembly immersed in melt.

The top electrode was made of Inconel. The cell rested on an Inconel carriage which also constituted the bottom electrode (Fig. 2). Platinum electrodes were used initially, but it was soon found that BN reacts with Pt at about 1000°C; this embrittles the Pt and causes erosion of the BN; also the Pt sticks to the BN after prolonged contact. The use of Inconel was made possible by the fact that a relatively high-constant cell was available and that the polarization of Inconel was therefore of a tolerable order of magnitude. Inconel had the advantages of relatively good strength and dimensional stability at the temperatures of the experiments.

Most of the dimensions given in Fig. 1 are typical, but by no means critical. The electrolyte path consisted of a nominal 3/16 in. D. hole; its actual bore and length were carefully measured for each cell. The 3/16 in. dimension was a compromise; the smaller the bore, the higher the resistance of the electrolytic path and, therefore, the smaller the relative effect of electrode polarization. On the other hand, in smaller bores, gas bubbles tend to become trapped when the cell is lowered into a melt, and the effect of cell contamination by previously used melts may become serious. In this connection, the

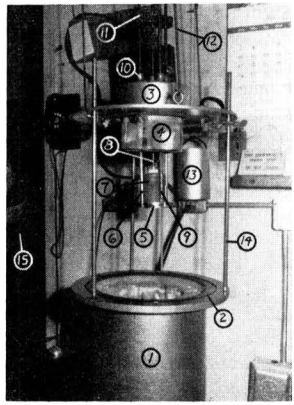

Fig. 3. Furnace and cell assembly ready for a conductivity determination. 1, Furnace shell; 2, O-ring (Neoprene); 3, furnace cover; 4, top insulator; 5, carriage and bottom electrode; 6, bottom electrode leads; 7, cell; 8, top electrode; 9, thermocouple protection tube; 10, Condulets; 11, clamping block; 12, lifting rig for furnace cover; 13, counterweight for furnace cover; 14, furnace cover guide rods; 15, fan.

holes through the bottom part of the top electrode are designed to facilitate the escape of gas bubbles from the cell bore as it is being immersed, and to hasten drainage as the carriage is being lifted out of the fused salt.

Precautions are needed against the tendency of melts to creep and thus provide an extra path between top electrode and graphite jacket. This is minimized by tapering both the graphite and the BN, and by designing the cell so that the melt level stays ¾ in. below the top of the BN.

Furnace

Boron nitride is oxidized at an excessive rate at about 1000°C, as is graphite. Therefore, it was necessary to make the conductivity measurements in an inert atmosphere.

A special furnace was built (Fig. 3) for taking resistance readings in or out of melts. It consists essentially of a flanged can, 1, and a matching cover, 3, built sufficiently strong to stand vacuum. Through the bottom, connections were made to a vacuum pump and to an argon tank. The furnace element consisted of heavy Nichrome V wire (#1 or #2 gauge): the ends of the wire were welded to ½ in. Inconel rods, which also came out through the bottom. To insure a vacuum-tight fit where the element is brought in, "Condulets" (waterproof electrical conduit fittings) were used in connection with specially fabricated Teflon compression grommets. The control thermocouple was also brought in through a Condulet provided with a rubber stopper. Since the heat generated in the furnace is normally sufficient to cause plastic deformation of the sealing grommets and stoppers (with resulting loss of vacuum), these connections were water-cooled through loops of Cu tubing soldered to the outside of the fittings.

The cover, 3, consisted of a central recessed portion and a machined flange to match that of the furnace. Thermal insulation, 4, filled the central portion and projected below the flange; it was supported by Inconel strips bolted to the underside of the cover and was therefore readily replaceable.

The conductivity cell electrode leads and an Inconel thermocouple protection tube were led in through the furnace cover; Condulets, 10, with rubber grommets were used to achieve a vacuum-tight seal and to permit vertical motion of the cell and electrode assembly. Again, there was the problem of keeping heat away from the rubber grommets. The use of Teflon grommets with movable rods was not satisfactory from the sealing standpoint. The difficulties were overcome by a combination of the following steps: (*a*) the cover was designed with the recessed central portion to remove the sealing fittings from the hot zone of the furnace; (*b*) the Inconel rods were kept down to ⅜ in. in order to decrease heat conduction along the metal; this is also the reason for reducing the diameter of the top electrode, as shown in Fig. 1; the ⅜ in. dimension was a compromise: with a smaller cross section, the electrical resistance of the Inconel would become appreciable in comparison to that of the cell, and the mechanical stability of the assembly at high temperatures would not be satisfactory; and (*c*) a fan, 15, cooled the furnace cover during runs.

Electrical Circuit

For many measurements, a self-contained conductivity bridge was used (Model RC-16, Industrial Instruments Inc.). This bridge is normally accurate to 1% of its reading, but its lower recommended limit of measurement is 0.2 ohm. In the case of highly conductive melts, cell resistances were of the order of 3 to 6 ohms and, therefore, this accuracy was no longer adequate. Accordingly, the circuit shown in Fig. 4 was used in such cases. Another reason for using the latter circuit was to determine the effects of a-c frequency on the readings. By using 4 precision resistors (General Radio, one 1Ω, two 10Ω, and one 100Ω), the scale factor for the decade box could be varied from 0.01 to 100. In this particular circuit, in view of other experimental limitations, the oscilloscope null detector was sufficiently sensitive (±0.5%) so that it was not necessary to use a variable capacitor in order to increase the sharpness of the null point. It was determined that resistance readings did not vary appreciably between 1,000 and 20,000 cycles; accordingly, a 2,000-cycle oscillator setting was normally used.

The total lead resistance, including the Inconel rods, was less than 0.04 ohm. A blanket value of 0.04Ω was subtracted from all resistance readings.

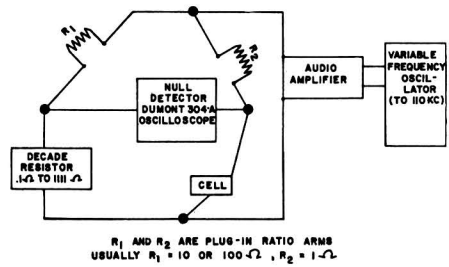

Fig. 4. Electrical circuit for conductivity measurements

This never amounted to more than a 1% correction; its variation with temperature is entirely negligible.

Care had to be taken to eliminate any unintentional grounding of the conductivity cell. This was especially true when using the RC-16 bridge, which already has an internal ground connection. A low-resistance path to the grounded furnace shell can exist at high temperatures by way of the crucible containing the melt and the insulation which becomes impregnated with fluorides. It becomes, therefore, necessary to change the insulation at times. Similarly, the top insulator (4, Fig. 3) may provide an electrical path between top and bottom electrode leads when it becomes impregnated with salt vapors. Finally, the a.c. going through the furnace element interferes with the balancing of the conductivity bridge; therefore, readings were normally taken during the off-cycle of the furnace controller.

Experimental Procedure

(*a*) *Setting up a determination.*—Fig. 2 and 3 show the way the cell and electrodes are assembled prior to making a determination. It is essential to press the top electrode down firmly against the cell, and to lock it to the carriage and bottom electrode leads by means of a Bakelite clamping block, 11, provided with thumbscrews. This prevents any motion of the top electrode relative to the cell when the assembly is raised or lowered inside the furnace. The Inconel thermocouple protection tube, 9 (which has been tested for tightness to vacuum) is lowered against the carriage and, therefore, the thermocouple indicates the temperature of the bottom electrode at all times.

After making sure that the graphite crucible containing the bath is properly centered under the carriage, the furnace cover is lowered, and the chamber is pumped down to approximately 200μ. The furnace is then flushed with argon and heated to 300°C, while again pumping to 200μ or less. After refilling the furnace with argon, the temperature is raised to 600°C; the furnace is pumped to 100 mm, and argon is again admitted until the pressure reaches about 600 mm. Finally the temperature is raised to the desired level. The argon pressure inside the furnace is kept slightly below atmospheric in order to make sure that the cover is properly seated at all times. The proper positioning of the top electrode is again tested by loosening the clamping block, 11, pushing the top electrode down, and retightening the thumbscrews.

(*b*) *Determination of cell resistance.*—When the bath inside the furnace is molten, the cell assembly is slowly lowered into the melt. An ohmmeter is connected across the electrode leads; a sharp jump of the ohmmeter pointer indicates that the top electrode has become immersed into the melt. It is important not to lower the cell too fast, since liquid may rise faster on the outside of the cell than in the small central hole and actually flow over the top of the BN. This will create a parallel path through a film of salt which drains only gradually and makes it extremely difficult to determine the true cell resistance.

After the cell has been lowered the first time, the ohmmeter is removed, and either the RC-16 conductivity bridge or the decade bridge and variable frequency source are connected to the electrode leads. A reading of resistance and temperature is taken. An adjustable pointer is lined up with a reference mark on the electrode lead rods to indicate how far the carriage should be lowered during subsequent immersions. The carriage is then raised, allowed to drain, and reimmersed. If the second resistance reading approximates the first one and is steady, it means that the assembly has been lowered to the correct level. It is necessary to lower and raise the cell two or three times (*a*) to make sure that no gas bubbles are trapped in the bore of the cell, and (*b*) to rinse off any residue of melt from a previous run. Such residues rarely amount to more than 0.1 g, and usually less than that. After about two immersions, the effect of such residues is entirely negligible.

At this point, initial cell resistance readings are taken for the record. Usually the immersed cell resistance shows very little variation at a given temperature. Normally, about 3-5 successive readings at a given temperature are taken over a period of 5-10 min.

The cell is then raised and the empty cell resistance is measured every minute for about 3-4 min. This resistance drifts for several reasons: [1] At first, the liquid film on the walls of the cell bore will be draining. [2] After a while, some liquid impregnating the cell body (and which, therefore, properly contributes to the empty cell resistance value) will also start to drain. [3] The cell is more responsive to temperature fluctuations when out of the bath since the thermal mass is smaller.

It is usually found that the rate of increase of empty cell resistance tapers off after about 2 min. Therefore, it is assumed that at that time any liquid remaining in the cell bore has drained, whereas the walls are still impregnated, and that the 2-min value of empty cell resistance is the most representative value.

It is important to secure a low and reproducible contact resistance between top electrode and cell body. This is no problem when the cell is immersed; the melt automatically makes for a low-resistance contact. In order to achieve a similar condition when the assembly is out of the melt, the cell in Fig. 1 was provided with an annular top groove to trap a small amount of melt. The matching top electrode seats in this groove when pressed against the cell body. The clamping block helps to maintain a good contact.

The contact between the bottom of the cell and the Inconel carriage is essentially made through the graphite jacket when the cell is empty, and is inherently low in resistance. However, the axial coefficient of thermal expansion of BN (i.e., parallel to the direction of pressing) is higher than that of graphite (4) unlike the radial expansion coefficient. Therefore, the bottom of the BN cylinder is 0.02 in. above the bottom of the graphite (Fig. 1), so that,

on heating, the BN expansion does not cause the graphite jacket to lift off the bottom electrode.

If a cell impregnated with one melt is used in a bath of a different composition, it takes considerable time for the original melt within the pores to be replaced by the new melt. The effect on the composition of the new melt is negligible, but the effect on the empty cell resistance is considerable. Thus, the empty cell resistance varies during the course of a run because of melt replacement as well as temperature variations. It is, therefore, necessary to determine the empty cell resistance after each reading of total resistance.

(c) *Measurement of cell constant.*—In most cases, the cell constant (length/cross sectional area) was calculated from the dimensions of the central bore which were accurately measured. From thermal expansion data (4), the constant increases by about 0.5% between room temperature and 1000°C.

In a few cases, cells were also standardized in molten KCl. Their constants were determined using published conductivity values for KCl (1, 5, 6). The values thus obtained checked with the values calculated from cell dimensions to better than 1%.

Cell constants ranged from about 17 to 39 cm^{-1}.

Reproducibility and Errors

In the absence of cracking in the cell, unintentional grounding, or parallel paths, the reproducibility between duplicate runs was usually 2% or better; in many cases, it was better than 1%. Typical standard deviations of the mean ranged from 0.3% to 1.4%. A good run was always characterized by steady, reproducible readings when the cell was immersed in melt. When the readings were erratic, one could usually ascribe this to a damaged cell body, or to stray electrical paths; such runs were discarded.

Most of the sources of error have been discussed. It is believed that the measurement of empty cell resistance contributes the most to errors. From the fact that readings did not vary with frequency between 1,000 and 20,000 cycles, polarization is not considered a major factor. Melt composition changes were found to be small in all systems investigated.

Acknowledgment

The authors wish to acknowledge the helpful suggestions of B. Porter and other members of the Chemical Research Department in designing the apparatus. Machining of the cells was performed by K. I. Booth and G. D. Wilson who also helped in the construction of the apparatus. The Carborundum Company, Niagara Falls, N. Y., and the Norton Company, Worcester, Mass., were most cooperative in supplying the BN cell bodies.

Manuscript received Jan. 8, 1957. This paper was prepared for delivery before the Washington Meeting, May 12-16, 1957.

Any discussion of this paper will appear in a Discussion Section to be published in the June 1958 JOURNAL.

REFERENCES

1. J. D. Edwards, C. S. Taylor, A. S. Russell, and F. Maranville, *This Journal*, **99**, 527 (1952).
2. J. W. Cuthbertson and J. Waddington, *Trans. Faraday Soc.*, **32**, 745 (1936).
3. E. R. Van Artsdalen and I. S. Yaffe, *J. Phys. Chem.*, **59**, 118 (1955); **60**, 1125 (1956).
4. K. M. Taylor, *Ind. Eng. Chem.*, **47**, 2506 (1955).
5. R. W. Huber, E. V. Potter, and H. W. St. Clair, *U. S. Bur. Mines Rept. Investig.* 4858.
6. E. K. Lee and E. P. Pearson, *Trans. Electrochem. Soc.*, **88**, 171 (1945).

Electrical Conductivity of Molten Fluorides

II. Conductance of Alkali Fluorides, Cryolites, and Cryolite-Base Melts

Ernest W. Yim and Morris Feinleib

Chemical Research Department, Kaiser Aluminum & Chemical Corporation, Permanente, California

ABSTRACT

The electrical conductivities of molten LiF, NaF, KF, Li_3AlF_6, Na_3AlF_6, and K_3AlF_6 have been determined. The effect of alumina, CaF_2, and NaF: AlF_3 ratio on the conductivity of cryolite-base melts has been studied. Molar and equivalent conductances have been calculated for several melts, and their significance is discussed.

A previous paper (1) described a new technique and apparatus for determining electrical conductivities of fused fluorides. The present work deals with the conductance of pure alkali fluorides and cryolites as well as cryolite-base melts of interest in the electrolytic production of aluminum.

A comprehensive investigation of the conductivity of sodium cryolite, with and without additives, was reported by Edwards, *et al.* (2, 3). For their determinations, these authors used a Pt dip cell, limitations of which have been discussed previously (1). Drossbach (4) reported values for the conductivity

of LiF, NaF, and KF, without indicating the source of the data. No conductivity values for lithium and potassium cryolites have been found in the literature.

Experimental

The apparatus and general procedure have been described in detail (1). The conductance cell was made of hot-pressed BN; all measurements were carried out in an inert atmosphere.

The usual practice was to make at least two runs for each melt composition. Furthermore, the temperature was lowered from maximum to minimum and then raised again; data were taken on both the descending and the ascending temperature cycles. In a typical run, data were usually taken over a span of 3 hr.

The following raw materials were used:

LiF, NaF, KF, CaF_2, KCl: Baker's reagent grade;

Alumina: Kaiser reduction grade;

Cryolite: natural hand-picked crystals, obtained from Pennsylvania Salt Mfg. Company, were further sorted in the laboratory, and the selected fraction was ground for use. This material has a melting point of 1005°C [cf. a mp of 1009° reported by Phillips, Singleton, and Hollingshead (5) for the purest available natural cryolite]. Analysis corresponds to the theoretical composition of pure cryolite within the limits of experimental error.

AlF_3: Alcoa X-2A grade powder containing approximately 97% AlF_3, about 1.2% NaF and 1.5% Al_2O_3. In view of the relatively large quantity of melt required for each run, and the number of experiments performed, it was not practical to use vacuum-sublimed AlF_3. The error introduced by the use of Alcoa X-2A grade AlF_3 was negligible except in the case of conductance determinations for Li_3AlF_6 and K_3AlF_6.

Melts whose main constituent was sodium cryolite were synthesized from this material and additives such as AlF_3, NaF, CaF_2, or Al_2O_3. Li_3AlF_6 and K_3AlF_6 were prepared starting from LiF or KF and AlF_3. In view of the relatively large proportions of impure AlF_3 required to prepare the cryolites of Li and K, conductance values reported for these two compounds are less reliable than for the rest of the fluoride melts.

In all cases, even with pure salts, melts were fused before each determination. A furnace was preheated to about 50°C above the melting point of the composition under investigation. The melt constituents were mixed in the dry state and placed in a graphite crucible, which was then placed inside the hot furnace. As soon as melting occurred, the crucible contents were stirred with a graphite rod to insure homogeneity and then chilled. This procedure was designed to cut down the time that the melts were at high temperatures; consequently composition changes due to volatilization or hydrolysis were kept to a minimum.

The chilled melt was pulverized, thoroughly mixed, and sampled. It was then placed in another graphite crucible which served as the container for conductance determinations. After one or more runs, the melt was again pulverized and sampled.

Table I. Comparison of alkali fluoride conductivities

	Conductivity in $ohm^{-1}cm^{-1}$		
	LiF at 900°C	NaF at 1020°C	KF at 900°C
This work	8.43	5.15	3.80
Drossbach (4)	19.8	3.32	4.32
Edwards, *et al.* (3)	—	5.63	—

Cryolite-base melts were analyzed by control methods used in the aluminum industry. The NaF: AlF_3 ratio was determined by pyrotitration (6), and the "free alumina" (7) was also determined. In all cases, little or no melt composition change was found, in spite of the fact that each run lasted several hours (it is important to remember here that the experiments were carried out in a closed furnace under an inert atmosphere). In the case of Li_3AlF_6 and K_3AlF_6, it was assumed that the composition did not change during runs.

Conductivity of alkali fluorides.—The specific conductances of LiF, NaF, and KF are plotted in Fig. 1. Table I shows wide differences between these values and Drossbach's (4). The conductivity of NaF reported by Edwards, *et al.* (3) is appreciably higher than that determined in the present study.

Specific conductance of cryolites without additives.—The conductivity of pure lithium, sodium, and potassium cryolites is shown in Fig. 2. Values for a mixture of 60% Li_3AlF_6 and 40% Na_3AlF_6 by weight have also been included in Fig. 2: this composition is close to the eutectic reported by Drossbach (8).

The conductance of sodium cryolite determined in this laboratory is in good agreement with that reported by Edwards, *et al.* (2).

It is interesting to note the high conductivity of lithium cryolite. The data for this compound have been extrapolated to 1010°C, at which temperature the conductivity of Li_3AlF_6 is almost 1.5 times that of Na_3AlF_6.

Effect of alumina on the conductivity of cryolite and cryolite-CaF_2 melts.—The conductivities of cryolite-alumina melts are plotted in Fig. 3, and for cryolite-alumina-8% CaF_2 melts in Fig. 4.

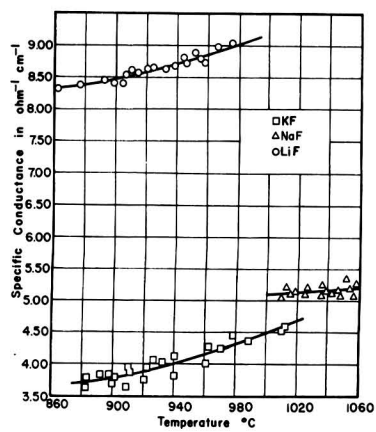

Fig. 1. Conductivity of alkali fluorides

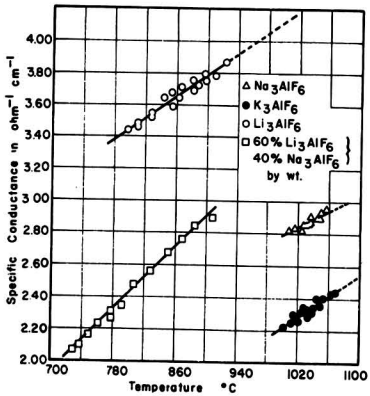

Fig. 2. Conductivity of cryolites

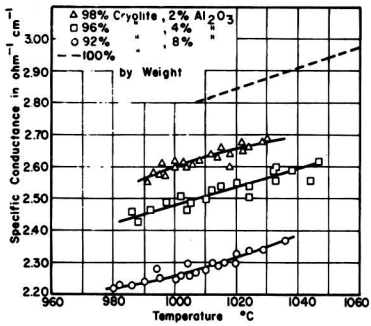

Fig. 3. Conductivity of cryolite-alumina melts (The line for 100% cryolite is taken from Fig. 2.)

These data are replotted in Fig. 5 to show the effect of alumina additions on the conductivity of cryolite and cryolite-8% CaF_2 melts. The conductivity of a typical aluminum reduction bath at 980°C decreases by 13% when the alumina concentration increases from 2% to 8%. This rate of decrease is somewhat greater than the one reported by Edwards, *et al.* (3).

Effect of $NaF:AlF_3$ *ratio on the conductivity of cryolite-base melts.*—The conductivity of NaF-AlF_3 melts without additives was determined at several $NaF:AlF_3$ ratios (Fig. 6).

The $NaF:AlF_3$ ratio was also varied in a typical aluminum reduction bath containing 8% CaF_2 and 4% Al_2O_3. Results have been plotted in Fig. 7.

The data of Fig. 6 and 7 have been rearranged in Fig. 8 to show the effect of $NaF:AlF_3$ ratio on the conductivity of cryolite-base melts. Comparing the conductivity of pure cryolite and that of a melt whose $NaF:AlF_3$ weight ratio is 1.22, the present study indicates that the effect of AlF_3 in decreasing the conductivity of cryolite is greater than reported by Edwards, *et al.* (3). On the other hand, the effect of NaF on conductivity, at a $NaF:AlF_3$ ratio of 1.76, appears to be smaller than shown by Edwards, *et al.* For the time being, no good explanation can be given for the shape of the curves shown in Fig. 8.

Molar and Equivalent Conductances

A. Definitions and calculations.—For a binary mixture of A and B, the molar conductance is

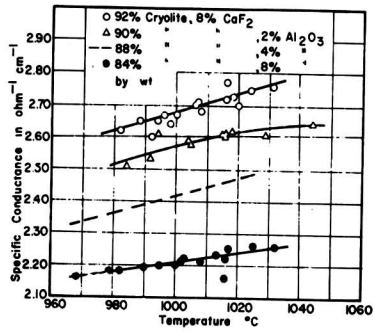

Fig. 4. Conductivity of cryolite-Al_2O_3-CaF_2 melts. (The line for 4% Al_2O_3 is taken from Fig. 7.)

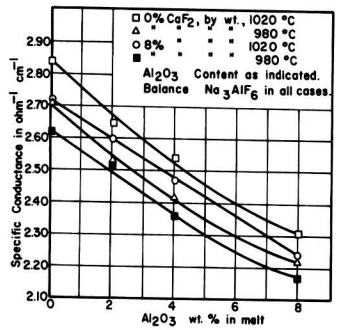

Fig. 5. Effect of alumina on the conductivity of Na_3AlF_6-CaF_2-Al_2O_3 melts.

$$\mu = \frac{N_A \times MW_A + N_B \times MW_B}{d} \times K$$

where N_A and N_B are mole fractions, MW molecular weights, K the specific conductance, and d the melt density.

In terms of weight fractions W_A and W_B

$$\mu = \frac{1}{\left[\frac{W_A}{MW_A} + \frac{W_B}{MW_B}\right] \times d} \times K$$

Similarly, for equivalent conductance,

$$\Lambda = \frac{1}{\left[\frac{W_A}{EW_A} + \frac{W_B}{EW_B}\right] \times d} \times K$$

where EW_A and EW_B represent equivalent weights.

For more than two components

$$\Lambda = \frac{1}{\left[\frac{W_A}{EW_A} + \frac{W_B}{EW_B} + \frac{W_C}{EW_C} + \ldots.\right] \times d} \times K$$

and a similar expression can be obtained for μ

Density data were obtained from published values by Drossbach (4), Edwards, *et al.* (2, 3) and Vajna (9), as well as from unpublished work carried out in this laboratory.

B. Equivalent conductances of fluorides and cryolites.—Yaffe and Van Artsdalen (10) have proposed to compare melts at "corresponding tempera-

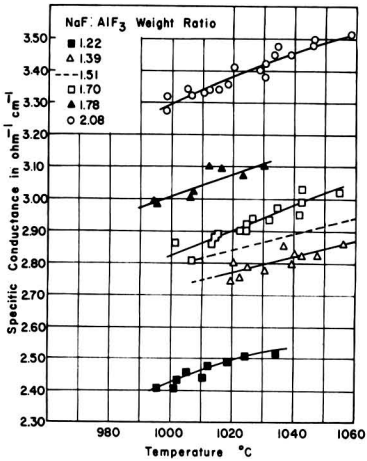

Fig. 6. Conductivity of AlF_3-NaF melts as a function of NaF:AlF_3 ratio (no additives). The line for a ratio of 1.51 is taken from Fig. 2.

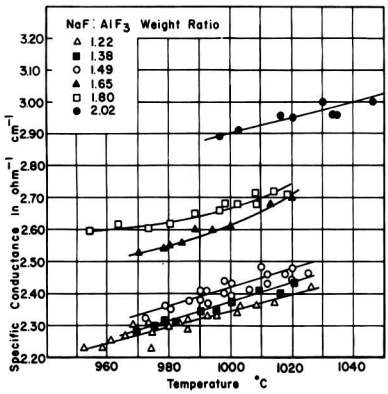

Fig. 7. Conductivity of a typical aluminum reduction bath as a function of NaF:AlF_3 ratio. Composition: 8% CaF_2, 4% Al_2O_3; balance AlF_3 + NaF by weight.

tures", i.e., at equal fractions above their melting point:

$$\theta = \frac{T°K}{T_m °K}$$

where T_m is the melting point. The equivalent conductances of the fluorides and cryolites of Li, Na, and K have been plotted in Fig. 9. It shows that, at a given temperature, the equivalent conductance of each cryolite is somewhat lower than that of the fluoride of the same cation. This relationship also holds true at "corresponding temperatures". A possible explanation is that the F^- ion is more mobile than a complex fluoaluminate ion (e.g., $AlF_6^{\equiv}$), and/or that the latter exerts more of an attractive force on the cations than the former.

Comparing the alkali fluorides, Table II shows that NaF has a smaller equivalent conductance than either LiF or KF, even at "corresponding temperatures". Equivalent conductances of other halides were taken from Yaffe and Van Artsdalen (10).

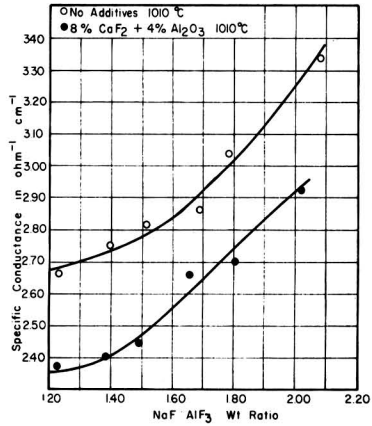

Fig. 8. Effect of NaF:AlF_3 ratio on the conductivity of cryolite-base melts.

Both LiF and NaF have a considerably lower equivalent conductance than the rest of the corresponding halides, even though one might expect the F^- ion to be more mobile than the other halide ions. It may be that the attractive forces between the small F^- ion and other small ions such as Li^+ and even Na^+ are the determining factor here. In the case of the larger K^+ ion, the interionic forces may be less important, and the greater mobility of the F^- ion may now become the dominant factor: this may account for the fact that the equivalent conductance of KF is higher than that of the other potassium halides.

C. Effect of alumina on molar conductance of cryolite.—The molar conductance of cryolite-alumina melts is shown in Fig. 10, as is the theoretical effect of an inert diluent. It is apparent that alumina depresses the molar conductance of cryolite considerably more than an inert diluent does. This effect is especially pronounced at low alumina concentrations; above a certain point, e.g. 8 mole % Al_2O_3, further additions of Al_2O_3 do not depress the conductance much more than an inert diluent would. Edwards, *et al.* (3) reported similar findings.

D. Effect of CaF_2 on molar conductance of cryolite.—The effect of CaF_2 on molar conductance of cryolite can be calculated from Fig. 2 and 4, as

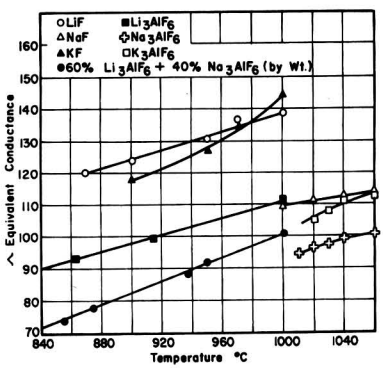

Fig. 9. Equivalent conductance of fluorides and cryolites

Table II.—Equivalent conductances of alkali halides at $\theta = T\ °K/T_m\ °K = 1.05$

LiF	**NaF**	**KF**
128	113	124
LiCl	**NaCl**	**KCl**
170	143	114
LiBr	**NaBr**	**KBr**
170	136	99
LiI	**NaI**	**KI**
163	132	94

shown in Table III. The values for 19% inert unionized diluent are obtained by taking 81% of the molar conductance of cryolite.

Within the limits of experimental error, it appears that CaF_2 acts as an inert diluent when added to neutral cryolite ($NaF:AlF_3$ mole ratio = 3:1). The situation is different in "acid baths", where the $NaF:AlF_3$ ratio is smaller than 3:1.

Table IV compares the conductances of two melts, both having a $NaF:AlF_3$ mole ratio of 2.57, but one of them containing CaF_2.

The conductivity of melt 1 can be taken from Fig. 8. The conductivity of melt 2 was determined separately but was not plotted in this paper. The effect of 17.7 mole % inert diluent on melt 1 would have been to lower the molar conductance to 206. Calculations at different temperatures, or in acid melts containing both CaF_2 and Al_2O_3, show a similar trend; at $NaF:AlF_3$ mole ratios lower than 3, CaF_2 decreases the molar conductance to a lesser extent than an inert diluent would.

To explain the behavior of CaF_2 in acid melts, the following hypothesis is offered.

The ionization of CaF_2 is repressed in neutral or alkaline cryolite-base melts, where sufficient F^- ions are present. In baths containing excess AlF_3, the activity of free F^- ions is low because of the complexing power of AlF_3 to form fluoaluminate ions (e.g., $AlF_6^{\equiv}$), and CaF_2 may ionize. This is equivalent to saying that CaF_2 may react with excess AlF_3 to form a calcium cryolite, which is partially ionized.

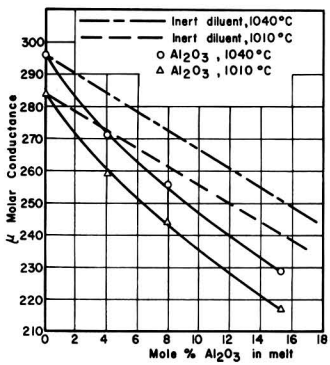

Fig. 10. Molar conductance of cryolite-alumina melts

Table III. Effect of CaF_2 on molar conductance of Na_3AlF_6

Mole % additive to cryolite	Molar conductance 1010°C	1040°C
0	284	296
19% CaF_2	232	242
19% Inert diluent	230	240

Table IV. Effect of CaF_2 on "Acid" $NaF:AlF_3$ Melt

Melt No.	1	2
Composition	$Na_3AlF_6 + AlF_3$ $NaF:AlF_3$ mole ratio = 2.57 Mole % CaF_2 = 0	$Na_3AlF_6 + AlF_3 + CaF_2$ $NaF:AlF_3$ mole ratio = 2.57 Mole % CaF_2 = 17.7
K ohm^{-1}cm^{-1} at 1010°C	2.69	2.70
μ at 1010°C	250	218

Acknowledgment

The authors wish to acknowledge the assistance of R. Lum, M. Waggoner, and P. Robba in performing the analyses, and of B. Porter in carrying out the calculations. Some of the density data used in the calculations of molar and equivalent conductances were determined by W. M. Lafky and J. L. Henry.

Manuscript received Jan. 8, 1957. This paper was prepared for delivery before the Washington Meeting, May 12-16, 1957.

Any discussion of this paper will appear in a Discussion Section to be published in the June 1958 JOURNAL.

REFERENCES

1. E. W. Yim and M. Feinleib, *This Journal*, **104**, 622 (1957).
2. J. D. Edwards, C. S. Taylor, A. S. Russell, and F. Maranville, *ibid.*, **99**, 527 (1952).
3. J. D. Edwards, C. S. Taylor, L. A. Cosgrove, and A. S. Russell, *ibid.*, **100**, 508 (1953).
4. P. Drossbach, "Elektrochemie Geschmolzener Salze," Julius Springer, Berlin (1938).
5. N. W. F. Phillips, R. H. Singleton, and E. A. Hollingshead, *This Journal*, **102**, 648 (1955).
6. M. Feinleib and B. Porter, *ibid.*, **103**, 234 (1956).
7. J. L. Henry and W. M. Lafky, *Ind. Eng. Chem.*, **48**, 126 (1956).
8. P. Drossbach, *Z. Elektrochem.*, **42**, 65 (1936).
9. A. Vajna, *Alluminio*, **6**, 541 (1950).
10. I. S. Yaffe and E. R. Van Artsdalen, *J. Phys. Chem.*, **60**, 1125 (1956).

Contribution to the Theory of Cathodic Protection, II

Carl Wagner

Department of Metallurgy, Massachusetts Institute of Technology, Cambridge, Massachusetts

ABSTRACT

The distribution of the electrical potential inside an electrolytic solution has been calculated for typical cases of cathodic protection involving an impressed current. In particular, it is shown under which conditions the differences in the local single electrode potential are sufficiently low so that complete cathodic protection without significant hydrogen evolution can be accomplished by using an automatic control of the impressed current.

Corrosion of a metal in an electrolyte may be prevented by cathodic protection, i.e., by providing a sufficiently negative electrode potential. This may be accomplished by passing electrical current from an auxiliary anode through the electrolyte to the metal to be protected as cathode. The minimum current required for complete protection is determined by the condition that the local single electrode potential $E_1(X)$ of metal 1 to be protected must be more negative (less noble) at any point X than its equilibrium single electrode potential $E_{1(eq)}$ in the given electrolyte (1),

$$E_1(X) < E_{1(eq)} \qquad [1]$$

The local single electrode potential $E_1(X)$ is defined as the voltage of the cell

standard hydrogen electrode	salt bridge	electrolyte	metal 1

where the opening of the capillary leading from the electrolyte to the salt bridge is located next to point X at the surface of metal 1.

If the anodic dissolution rate of metal 1 rises rather slowly with increasing potential, virtually complete cathodic protection may be accomplished at a potential above $E_{1(eq)}$. Then Eq. [1] and likewise Eq. [2] below may be replaced by less rigorous conditions where $E_{1(eq)}$ is replaced by E_1' defined as the highest single electrode potential at which the anodic dissolution rate is negligibly small in the environment under consideration. It has been shown previously (1) how the values of $E_{1(eq)}$ and E_1' can be estimated.

The minimum current for complete cathodic protection can be calculated readily if the geometry is such that the current density and the single electrode potential are the same at all points of the cathode, e.g., when the inner side of a tube as cathode is protected by means of an anode located in the axis of the tube. In this case, the current required for complete cathodic protection is equal to the product of area and the sum of the current densities at potential $E_{1(eq)}$ for all possible reduction processes of oxidizers present in the electrolyte. If hydrogen evolution is negligible at this potential and oxygen dissolved in the electrolyte is the only oxidizer, the minimum current is equivalent to the diffusion rate of oxygen to the metal.

In general, conditions are more involved. In particular, when a local electrode potential $E_1(X) < E_{1(eq)}$ at points remote from the anode is maintained, the local potential at points close to the anode may be considerably more negative than $E_{1(eq)}$ and accordingly an appreciable portion of the current may be used for cathodic evolution of hydrogen. Since hydrogen evolution may cause undesirable effects such as blistering of paint and embrittlement of steel, it is of interest to know under which conditions complete cathodic protection can be accomplished without significant hydrogen evolution when the local electrode potential at points most remote from the anode is made equal to $E_{1(eq)}$. Under most conditions the rate of hydrogen evolution rises exponentially when the electrode potential is made more negative. For practical purposes an electrode potential E^* for the onset of significant hydrogen evolution may be introduced. For instance, E^* may be defined as the potential at which the current density used for hydrogen evolution is equal to the current density J_{ox} used for reduction of oxygen, or a certain fraction thereof. Then the first requirement is that the equilibrium potential $E_{1(eq)}$ is more positive (more noble) than E^*. In addition, the difference $E_{1(eq)} - E^*$ must be greater than the maximum variation of the local single electrode potential, ΔE_{max}, under conditions providing complete cathodic protection. Thus the condition for insignificant hydrogen evolution becomes

$$\Delta E_{max} < E_{1(eq)} - E^* \qquad [2]$$

The following cases are amenable to a theoretical treatment and may be considered as a basis for a qualitative discussion of more complex situations.

Wire Anodes in Front of the Metal to Be Protected

Oxygen reduction as the only cathodic process.— To protect the surface of an infinite plate of metal 1, equidistant auxiliary anodes in the form of wires parallel to the surface of metal 1 may be provided (*see* Fig. 1). It is assumed that the oxidizer, e.g., oxygen, is readily reduced if $E_1(X) \leqq E_{1(eq)}$, i.e., the

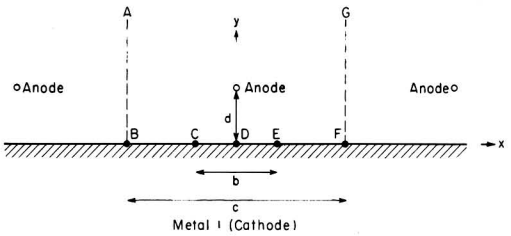

Fig. 1. Metal 1 protected by equidistant auxiliary wire anodes. Hydrogen evolution is supposed to take place between points C and E.

current density J_{oz} for the reduction of the oxidizer, is supposed to be determined by the maximum diffusion rate for zero concentration of the oxidizer at the surface of metal 1 and to be independent of the local electrode potential $E_1(X)$. Moreover, a virtually uniform effective thickness of the diffusion boundary layer is assumed so that the current density J_{oz} is the same at all points along the surface of metal 1. The surface may involve microscopic inhomogeneities, e.g., inclusions of a second phase, but the dimensions of inclusions are supposed to be less than the thickness of the hydrodynamic boundary layer. In this case, the local single electrode potential is not affected by the heterogeneity of the surface (2-4).

The potential ϕ in the electrolyte has to satisfy the Laplace differential equation

$$\partial^2\phi/\partial x^2 + \partial^2\phi/\partial y^2 = 0 \qquad [3]$$

where x and y are the coordinates shown in Fig. 1.

For negligible hydrogen evolution, the boundary conditions are

$$\partial\phi/\partial y = 0 \text{ at } y = \infty \qquad [4]$$

$$\partial\phi/\partial y = J_{oz}/\sigma \text{ at } y = 0 \qquad [5]$$

where σ is the electrical conductivity of the electrolyte and Eq. [5] is a consequence of Ohm's law. For equidistant auxiliary anodes as line sources shown in Fig. 1, the potential distribution in the electrolyte ($y > 0$) is found to be

$$\phi(x,y) = \text{constant} + J_{oz}\,y/\sigma - \frac{J_{oz}c}{2\pi\sigma} Re\left[\ln\sin\frac{\pi(z-id)}{c} + \ln\sin\frac{\pi(z+id)}{c}\right] \qquad [6]$$

where c is the distance between adjacent anodes, d is their distance from the metal to be protected, $z = x + iy$, $i = (-1)^{1/2}$, and $Re[..]$ denotes the real part of the complex function in brackets. The term $J_{oz}y/\sigma$ represents a uniform field which gives the potential gradient at the surface of metal 1 in accord with Eq. [5]. The following term represents the field resulting from an infinite series of positive line sources at $x = \pm nc$, $y = d$ where $n = 0, 1, 2$, etc., and their images at $\pm nc$, $y = -d$. The latter term does not give a contribution to the potential gradient at $y = 0$. The intensity of these line sources is chosen so that the potential gradient at infinite distance y vanishes in accord with Eq. [4].

From Eq. [5] the potential in the electrolyte at the surface of metal 1 is obtained as

$$\phi(x, y=0) = \phi(x=0, y=0) - \frac{J_{oz}c}{2\pi\sigma}\ln\left[1 + \frac{\sin^2(\pi x/c)}{\sinh^2(\pi d/c)}\right] \qquad [7]$$

According to Eq. [7] the potential ϕ in the electrolyte along the surface of metal 1 is a periodic function of distance x. The maximum potential difference occurs between points opposite to auxiliary anodes (e.g., $x = 0$, $y = 0$) and points located half way between the anodes (e.g., $x = \frac{1}{2}c$, $y = 0$). Inside metal 1 a virtually constant potential is assumed. Hence the local single electrode potential $E_1(X)$ is equal to a constant value minus the local electrical potential in the electrolyte. The maximum difference ΔE_{max} of the local single electrode potential between different points of metal 1 is, therefore, found to be

$$\Delta E_{max} = E(x = \tfrac{1}{2}c) - E(x = 0)$$
$$= \phi(x=0, y=0) - \phi(x = \tfrac{1}{2}c, y = 0)$$
$$= (J_{oz}c/\pi\sigma)\ln\coth(\pi d/c) \qquad [8]$$

Upon introducing the dimensionless group

$$f_1 = \pi^{-1}\ln[\coth(\pi d/c)] \qquad [9]$$

the maximum difference of the local single electrode potentials may be calculated as

$$\Delta E_{max} = (J_{oz}c/\sigma)f_1 \qquad [10]$$

A graph for f_1 as a function of the distance ratio d/c is shown in Fig. 2.

If the ratio d/c is much less than unity, the hyperbolic cotangent in Eq. [9] may be replaced by the reciprocal of its argument as a close approximation. Thus

$$f_1 \cong (1/\pi)\ln(c/\pi d) \text{ if } d << c \qquad [11]$$

i.e., f_1 is of the order of unity if $d/c << 1$.

If the distance d of the auxiliary anodes from metal 1 is greater than half the distance c between neighboring anodes, the following approximation holds

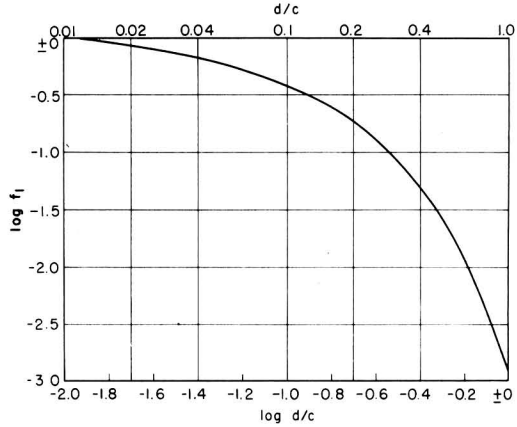

Fig. 2. Dimensionless group f_1 vs. ratio d/c according to Eq. [9].

$$\ln[\coth(\pi d/c)] = -\ln[\tanh(\pi d/c)] \cong -\ln[1-2\exp(-2\pi d/c)] \cong 2\exp(-2\pi d/c) \quad [12]$$

Upon substitution of Eq. [12] in Eq. [8], it follows that

$$\Delta E_{max} \cong (2J_{oz}c/\pi\sigma)\exp(-2\pi d/c) \text{ if } d/c > 0.5 \quad [13]$$

Hence ΔE_{max} may be decreased to very low values by increasing the anode-cathode distance d.

If the value of ΔE_{max} is less than the difference $E_{1(eq)} - E^*$ in Eq. [2], complete cathodic protection can be accomplished without significant hydrogen evolution. Upon combining Eqs. [2] and [10], the condition for the possibility of complete cathodic protection without significant hydrogen evolution becomes

$$E_{1(eq)} - E^* > (J_{oz}c/\sigma)f_1 \quad [14]$$

With the aid of Eq. [14] it is possible to calculate the minimum distance d for this condition. For instance, if $E_{1(eq)} - E^* = 0.2$ volt, $J_{oz} = 10^{-4}$ amp/cm^2, $c = 200$ cm, and the corroding solution is sea water having a specific electrical conductivity $\sigma = 0.1$ ohm^{-1}cm^{-1}, it follows from Eq. [14] that $f_1 \leqq 1$, or $d/c \geqq 0.01$ according to Fig. 2, and $d \geqq 2$ cm. If, however, the corroding solution is fresh water having a low conductivity, e.g., $\sigma = 10^{-4}$ ohm^{-1}cm^{-1}, hydrogen evolution can be avoided only if $f_1 \leqq 0.001$, or $d/c \geqq 1$ according to Fig. 2 and $d \geqq 200$ cm.

If the value of ΔE_{max} is below the limit stated in Eq. [2], cathodic protection without significant hydrogen evolution may be accomplished by making the current equal to the product of J_{oz} and the area of metal 1, e.g., by using an automatic control of the current so that at points most remote from the anodes, i.e., at $x = \frac{1}{2}c, y = 0$, the local single electrode potential measured with the help of a probe is equal to or slightly lower than the equilibrium potential $E_{1(eq)}$. This may be accomplished with the help of a potentiostat as described by Hickling (5) and others (6-8). Use of a circuit involving a magnetic amplifier (9, 10) may be particularly appropriate. In spite of higher costs, an automatic control of the current may be economical because sufficient current for cathodic protection without significant hydrogen evolution is provided even under variable conditions which result, for instance, from different rates of oxygen diffusion toward the surface when a ship travels at different speeds, or is at rest.

Simultaneous reduction of oxygen and evolution of hydrogen.—If an automatic current control is not provided, it is necessary to apply a constant current which is greater than the product of the maximum value of J_{oz} expected under practical conditions and the area A of metal 1. Use of excess current necessarily results in evolution of hydrogen. Hydrogen evolution will be nearly uniform along the surface of metal 1 if the potential of the solution and accordingly the single electrode potential $E_1(X)$ varies only slightly, e.g., if $\Delta E_{max} < 0.02$ volt.

On the other hand, if $\Delta E_{max} > 0.1$ volt, hydrogen evolution will predominate in the vicinity of the anodes, whereas at points more remote from the anodes hydrogen evolution may be negligible. For regions with significant hydrogen evolution the single electrode potential of metal 1 is nearly equal to E^* irrespective of the local current density since a very steep rise of the current density-potential curve below E^* is assumed. Accordingly, for the sake of mathematical simplification, the potential in the electrolyte along sections of metal 1 where hydrogen is evolved may be considered to be constant, i.e., equal to $\phi(x = 0, y = 0)$ as a fair approximation. On the other hand, at points more remote from the auxiliary anodes, the potential gradient in the electrolyte is determined essentially by the current density used for cathodic reduction of oxygen.

For the strip ABCDEFG between $y = -\frac{1}{2}c$ and $y = \frac{1}{2}c$ with significant hydrogen evolution between $y = -\frac{1}{2}b$ and $y = \frac{1}{2}b$ (*see* Fig. 1), the boundary conditions are, therefore, assumed to be

$$\phi = \phi(x = 0, y = 0) \text{ at } |x| < \frac{1}{2}b, y = 0 \quad [15a]$$

$$\partial\phi/\partial y = J_{oz}/\sigma \text{ at } \frac{1}{2}b \leqq |x| \leqq \frac{1}{2}c \quad [15b]$$

which replace Eq. [5].

A solution for conditions stated in Eq. [15a] and [15b] but without a line source at $x = 0$, $y = d$ has already been obtained in Eq. (36) of a previous paper (1). On this solution, the solution for a line source at $x = 0$, $y = d$ satisfying the boundary conditions $\phi = 0$ along the line CDE and $\partial\phi/\partial y = 0$ along the lines BC and EF in Fig. 1 is superimposed. In the z'' plane of Fig. 6 of the previous paper the boundary conditions are satisfied by a line source at

$$x'' = 0, y'' = \sinh^{-1}(\sinh\alpha/\sin\beta) = v$$

and its negative image at

$$x'' = 0, y'' = -\sinh^{-1}(\sinh\alpha/\sin\beta) = -v$$

where

$$\alpha = \pi d/c \quad [16a]$$

$$\beta = \pi b/2c \quad [16b]$$

$$v = \sinh^{-1}(\sinh\alpha/\sinh\beta) \quad [17]$$

The corresponding solution in the z plane is obtained by using the pertinent relation between z and z''. Thus the complete solution is found to be

$$\phi(x,y) = \phi(x = 0, y = 0) + \frac{J_{oz}}{\sigma}\left\{y + \frac{c}{\pi} Re\left[i\sin^{-1}\left(\frac{\sin\zeta}{\sin\beta}\right)\right]\right\} - \frac{J_{oz}c}{2\pi\sigma} g\, Re\left\{\ln\sin\left[\sin^{-1}\left(\frac{\sin\zeta}{\sin\beta}\right) - iv\right] - \ln\sin\left[\sin^{-1}\left(\frac{\sin\zeta}{\sin\beta}\right) + iv\right]\right\} \quad [18]$$

where

$$\zeta = \pi z/c \quad [19]$$

The factor g in Eq. [18] is proportional to the strength of the line source at $x = 0$, $y = d$. Upon

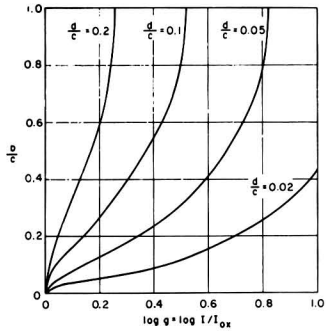

Fig. 3. Ratio b/c vs. log g = log I/I_{ox} according to Eq. [21]

using the condition that $\partial\phi/\partial y$ must be continuous at $x = b, y = 0$, it follows that

$$g = \coth v \qquad [20]$$

Since $g = 1$ for $b = 0$ according to Eqs. [17] and [20], it follows that g is equal to the ratio of the current I for conditions involving hydrogen evolution to the current I_{ox} for exclusive reduction of oxygen,

$$I/I_{ox} = g = \coth\{\sinh^{-1}[\sinh(\pi d/c)/\sin(\pi b/2c)]\} \qquad [21]$$

Eq. [21] has been used in order to draw graphs shown in Fig. 3 from which one may read the width b of the section of metal 1 at which hydrogen is evolved if the current ratio I/I_{ox} and the distance ratio d/c are given.

Inspection of Fig. 3 shows that a high increase of the current is required in order to obtain significant hydrogen evolution along the entire surface of metal 1 if the distance d of the auxiliary anodes is small as compared to the distance c between neighboring anodes. On the other hand, a moderate increase of the current leads to hydrogen evolution along the entire surface of metal 1 if the distances c and d are of the same order of magnitude.

For the section of metal 1 at which hydrogen is evolved, the single electrode potential $E_1(X)$ is assumed to be equal to E^*. The single electrode potential $E_1(X)$ at any point is equal to a constant value minus the local electrical potential in the electrolyte. Thus, $E_1(X)$ for the section of metal 1 at which cathodic reduction of oxygen prevails is obtained from Eq. [18] as

$$E(X) = E^* - [\phi(x, y = 0)^* - \phi(x = 0, y = 0)]$$
$$= E^* + (J_{ox}c/\pi\sigma)\{u - g\tanh^{-1}[(\tanh v)(\tanh u)]\}$$

$$\text{if } \frac{1}{2}b \leqq |x| \leqq \frac{1}{2}c \qquad [22]$$

where

$$u = \cosh^{-1}[\sin(\pi x/c)/\sin(\pi b/2c)] \qquad [23]$$

and v is defined by Eq. [17].

Upon substituting Eq. [21] in Eq. [22] and letting $x = \frac{1}{2}c$, the maximum difference of the local single electrode potential is found to be

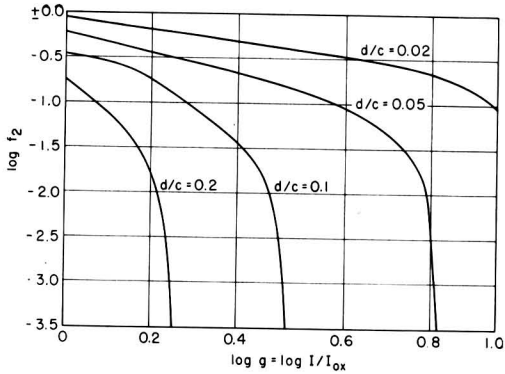

Fig. 4. Dimensionless group f_2 vs. log g = log I/I_{ox} according to Eq. [26].

$$\Delta E_{max} = E(x = \frac{1}{2}c) - E^*$$
$$= \frac{J_{ox}c}{\pi\sigma}\left[w - \frac{I}{I_{ox}}\tanh^{-1}\left(\frac{I_{ox}}{I}\tanh w\right)\right] \qquad [24]$$

where in view of Eq. [21]

$$w = u(x = \frac{1}{2}c) = \cosh^{-1}\left\{\frac{\sinh[\coth^{-1}(I/I_{ox})]}{\sinh(\pi d/c)}\right\} \qquad [25]$$

Upon introduction of the dimensionless group

$$f_2 = \frac{1}{\pi}\left[w - \frac{I}{I_{ox}}\tanh^{-1}\left(\frac{I_{ox}}{I}\tanh w\right)\right] \qquad [26]$$

the values of ΔE_{max} may be calculated as

$$\Delta E_{max} = (J_{ox}c/\sigma)f_2 \text{ if } I > I_{ox} \qquad [27]$$

Fig. 4 shows curves for f_2 as a function of the applied current according to Eq. [26]. Thus one may calculate ΔE_{max} with the help of Eq. [27]. Values of f_2 are equal to values of f_1 if $I = I_{ox}$, and decrease if $I > I_{ox}$, i.e., ΔE_{max} decreases with increasing current. Consequently, the necessary condition for complete cathodic protection in Eq. [2] may not be satisfied for $I = I_{ox}$ but may be satisfied by increasing the current. If $d/c \ll 1$, f_2 is of the order of unity, and a decrease of f_2 may be very desirable in order to satisfy Eq. [2], but for small d/c ratios f_2 decreases only slowly with increasing current. Unless the excess current is very high, hydrogen evolution is confined to the vicinity of the anodes and, therefore, the potential distribution along the cathode is changed only slightly. Only when hydrogen is evolved along most of the surface of metal 1, do the values of f_2 and ΔE_{max} drop markedly. Calculated values of ΔE_{max} and f_2 become zero according to Eqs. [24] and [26] if $b = c$, but this results only from the simplifying presupposition that the variation of the single electrode potential with current density used for hydrogen evolution is negligible.

On the other hand, if the anode-cathode distance d is of the same order of magnitude as the distance c between neighboring anodes, a relatively small increase of the current suffices to obtain significant hydrogen evolution along the entire surface of

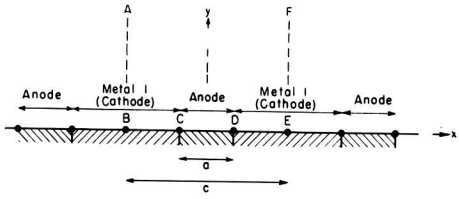

Fig. 5. Metal 1 as a cathode protected by auxiliary anodes at the surface of metal 1.

metal 1 and a considerable decrease of f_2 as shown in Fig. 3 and 4. Since the value of $f_1 = f_2 (I = I_{ox})$ for $d \sim c$ is small and, therefore, Eq. [2] is easy to satisfy, a decrease of f_2 and ΔE_{max} due to a current $I > I_{ox}$ is, in general, not of practical importance.

Anodes in the Plane of the Metal to Be Protected

A periodic array of strips of metal 1 and anodes lying in the same plane is shown in Fig. 5. Calculations are confined to the strip ABCDEF. Insulating sections between cathodes and anodes are assumed to be negligibly small. The width of the anodes is designated by a and the distance between the midlines of sections of metal 1 by c. At the cathodic areas of metal 1, only reduction of oxygen is supposed to occur. Thus, the boundary condition is analogous to that stated in Eq. [5]

$$\partial\phi/\partial y = J_{ox}/\sigma \text{ at } \frac{1}{2}a < |x| < \frac{1}{2}c,\ y = 0 \quad [28]$$

At the anodes either a constant electrode potential or a constant current density may be assumed. For a constant electrode potential, the solution obtained in Eqs. [38] and [39] of the previous paper (1) may be used. With the present notation, the maximum difference of the single electrode potential of metal 1 is found to be

$$\Delta E_{max} = (J_{ox}c/\sigma) f_3 \quad [29]$$

where

$$f_3 = \pi^{-1} \cosh^{-1}[1/\sin(\pi a/2c)] \quad [30]$$

On the other hand, there may be considered a uniform current density along the anode, which is $(c-a)/a$ times greater than the cathodic current density J_{ox} corresponding to the area ratio of anodes and cathodes. Thus

$$\partial\phi/\partial y = -(c-a)J_{ox}/a\sigma \text{ at } 0 < |x| < \frac{1}{2}a,\ y = 0 \quad [31]$$

A solution of the Laplace equation [3] for boundary conditions [28] and [31] may be obtained by a superposition of line sources at the surface of anodes and line sinks at the surface of cathodes.

$$\phi = \text{constant} + \frac{J_{ox}}{\sigma}\left[y - \frac{c}{\pi a} Re \int_{-\frac{1}{2}a}^{\frac{1}{2}a} \ln \sin \frac{\pi(z-\xi)}{c}\, d\xi\right] \quad [32]$$

where the variable of integration ξ is the distance of a line source from the origin.

To find the potential at the surface of cathodes and anodes, $\eta = \pi(x-\xi)/c$ is substituted as the variable of integration. Thus

$$\phi(x, y=0) = \text{constant} - \frac{J_{ox}c}{\sigma}\frac{c}{\pi^2 a} \mathrm{Re} \int_{\pi(x-\frac{1}{2}a)/c}^{\pi(x+\frac{1}{2}a)/c} \ln \sin \eta\, d\eta \quad [33]$$

Hence the maximum difference of the single electrode potential at the surface of metal 1 is

$$\Delta E_{max} = \phi(x = \frac{1}{2}a, y = 0) - \phi(x = \frac{1}{2}c, y = 0) = (J_{ox}c/\sigma) f_4 \quad [34]$$

where

$$f_4 = \frac{c}{\pi^2 a}\left\{\int_{\frac{1}{2}\pi(1-a/c)}^{\frac{1}{2}\pi(1+a/c)} \ln \sin \eta\, d\eta - \int_0^{\pi a/c} \ln \sin \eta\, d\eta\right\} \quad [35]$$

The integrals in Eq. [35] can be evaluated readily by means of numerical methods.

Graphs of f_3 and f_4 vs. a/c are shown in Fig. 6. The difference between the curves for f_3 and f_4 is relatively small. It is, therefore, irrelevant whether a constant electrode potential or a constant current density at the anodes is assumed.

In the foregoing calculation the effect of insulating strips between cathodes and anodes has been neglected. The effect is of minor importance if the width of the anodes is much less than that of the cathodes. As a limiting case, wire anodes in the plane of metal 1 as shown in Fig. 7 are considered. The width of insulating sections between metal 1 and a wire anode is denoted by $\frac{1}{2}s$. Thus the boundary conditions for the strip ABCDEF are

$$\partial\phi/\partial y = J_{ox}/\sigma \text{ at } \frac{1}{2}s < |x| < \frac{1}{2}c,\ y = 0 \quad [36]$$

$$\partial\phi/\partial y = 0 \text{ at } 0 < x < \frac{1}{2}s,\ y = 0 \quad [37]$$

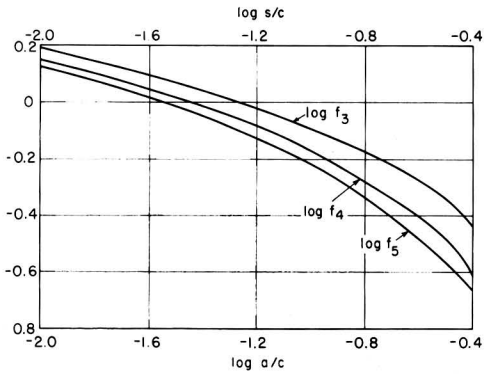

Fig. 6. Dimensionless groups f_3, f_4, and f_5 vs. log a/c and log s/c according to Eqs. [30], [35], and [41], respectively.

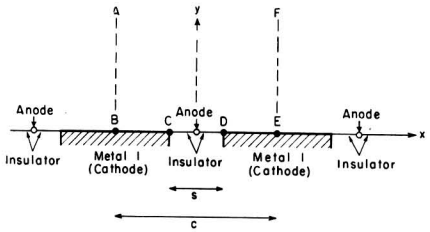

Fig. 7. Metal 1 as a cathode protected by wire anodes at the surface of metal 1.

Since all current lines originating from the anode are supposed to enter metal 1 as cathode, the potential gradient at infinite distance y must vanish,

$$\partial\phi/\partial y = 0 \text{ at } y = \infty \qquad [38]$$

The latter condition determines the strength of the line source at $x = 0$, $y = 0$ where the wire anode is located.

The Laplace equation [3] and the boundary conditions [36] to [38] are satisfied by

$$\phi = (J_{oz}/\sigma)\left\{ y - \pi^{-1} Re \int_{-\frac{1}{2}s}^{\frac{1}{2}s} \ln\sin\left[\pi(z-\xi)/c\right] d\xi \right.$$
$$\left. -(c-s)\pi^{-1} Re \ln\sin(\pi z/c) \right\} + \text{constant} \qquad [39]$$

Hence the maximum difference of the local single electrode potential at the surface of metal 1 is found to be

$$\Delta E_{max} = \phi(x = \frac{1}{2}s,\ y = 0) - \phi(x = \frac{1}{2}c,\ y = 0)$$
$$= (J_{oz}c/\sigma) f_5 \qquad [40]$$

$$f_5 = -\left[(c-s)/c\right]\pi^{-1} \ln\sin(\pi s/2c)$$
$$+ \pi^{-2} \int_{\frac{1}{2}\pi(1-s/c)}^{\frac{1}{2}\pi(1+s/c)} \ln\sin y\, dy - \pi^{-2} \int_0^{\pi s/c} \ln\sin y\, dy \qquad [41]$$

A graph for f_5 as a function of s/c is shown in Fig. 6. Since the curves for f_3, f_4, and f_5 lie relatively close together, it follows that the value of ΔE_{max} is determined mainly by the width of the section where metal 1 is not present, regardless of the width of the anodes.

Moreover, curves in Fig. 6 show that the factors f_3, f_4, and f_5 are of the order of unity except for very small values of a/c or s/c. For anodes located in or close to the surface plane of the metal to be protected, ΔE_{max} is, therefore, of the order of $J_{oz}c/\sigma$. Hence the distance c between neighboring anodes is the most important controllable factor in order to make ΔE_{max} sufficiently small as a necessary requirement for the possibility of complete cathodic protection without significant hydrogen evolution. In particular, a low conductivity of the electrolyte requires small distances between neighboring anodes.

If $E_{1(eq)} - E^* = 0.2$ volt, $J_{oz} = 10^{-4}$ amp/cm^2, and the corroding solution is sea water with a specific electrical conductivity $\sigma = 0.1$ ohm^{-1}cm^{-1}, the permissible maximum value of c is of the order of 200 cm. A low conductivity of the electrolyte, however, requires much smaller distances between neighboring anodes located in the plane of the metal to be protected. In fresh water with an electrical conductivity of 10^{-4} ohm^{-1} cm^{-1}, the permissible maximum value of c under the aforementioned conditions would be of the order of 0.2 cm. Under these conditions, anodes located in the plane of the metal to be protected are not helpful and anodes must be placed at a sufficient distance in front of the metal to be protected.

For the configurations shown in Fig. 5 and 7, the potential distribution for conditions involving hydrogen evolution has not been calculated. If only oxygen is reduced, values of f_3, f_4, and f_5 for small values of a/c or s/c are of the same order of magnitude as the values of f_1 for comparable values of d/c. Thus it may be concluded that conditions involving hydrogen evolution for configurations shown in Fig. 5 and 7 and small values of a/c or s/c are similar to those for wire anodes in front of the metal to be protected. By and large, a significant decrease in ΔE_{max} will require a current I much greater than I_{oz} with significant hydrogen evolution along most of the surface of metal 1.

Cathodic Protection of Bare Sections of a Painted Metal

In many cases, most of the metal is painted and there are only small bare sections for which cathodic protection is needed. In what follows it is shown that the potential distribution in the electrolyte and the value of ΔE_{max} are determined mainly by equations derived above if the current density in these equations is replaced by $J_{oz(av)}$, i.e., the current density for oxygen reduction averaged over painted and bare sections.

Fig. 8 shows a periodic array of bare and painted sections of metal 1 with wire anodes in front of metal 1. The distance between anodes is denoted by c, the width of bare sections by p, and the distance between the midlines of neighboring bare sections of metal 1 by q. Thus the boundary conditions for the strip ABCD in Fig. 8 are

$$\partial\phi/\partial y = J_{oz}/\sigma \text{ at } \mu q - \frac{1}{2}p < |x| < \mu q + \frac{1}{2}p \qquad [42]$$

$$\partial\phi/\partial y = 0 \text{ at } \mu q + \frac{1}{2}p < |x| < (\mu+1)q - \frac{1}{2}p \qquad [43]$$

$$\partial\phi/\partial y = 0 \text{ at } y = \infty \qquad [44]$$

where μ is 0, ±1, ±2, . . . , or $\pm m$ corresponding to $2m = c/q$ bare sections per length c.

The potential distribution may be represented by a superposition of line sources and line sinks,

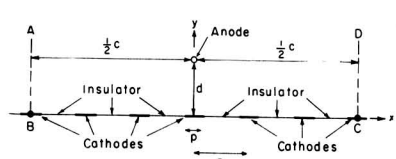

Fig. 8. Periodic array of bare and painted sections of metal 1 with wire anodes in front of metal 1.

$$\phi = \text{constant} + Re\{-(mp\,J_{oz}/\pi\sigma)\ln\sin[\pi(z-id)/c] - (mp\,J_{oz}/\pi\sigma)\ln\sin[\pi(z+id)/c] + \frac{J_{oz}}{\pi\sigma}\sum_{\mu=-m}^{\mu=+m} I_\mu(z) \quad [45]$$

where the integral $I_\mu(z)$ involving the serial number μ is

$$I_\mu(z) = \int_{\mu q-\frac{1}{2}p}^{\mu q+\frac{1}{2}p} \ln\sin\frac{\pi(z-\mu q-\xi)}{c}\,d\xi \quad [46]$$

In Eq. [45] the first two terms result from line sources located at the positions of the anodes at $x = \pm nc, y = d$ and their images at $x = \pm nc, y = -d$. The integrals result from line sinks located at bare sections of metal 1. The validity of Eq. [45] may be verified by substituting Eq. [45] in Eqs. [42] to [44].

Hence the difference ΔE in the single electrode potential between points at $x = \frac{1}{2}c$ and $x = 0$ is found to be

$$\Delta E = \phi(x=0, y=0) - \phi(x=\frac{1}{2}c, y=0) = (2mp\,J_{oz}/\pi\sigma)\ln\coth(\pi d/c) + \frac{J_{oz}}{\pi\sigma}\sum_{\mu=-m}^{\mu=+m}\left[I_\mu(z=0) - I_\mu(z=-\frac{1}{2}c)\right] \quad [47]$$

Shifting the origin of the coordinate system and substituting $\xi' = \xi - \frac{1}{2}c$ as the variable of integration in the integrals for $z = \frac{1}{2}c$, it can be shown that the two sums of integrals in Eq. [47] are equal and, therefore, cancel each other. Upon substituting

$$J_{oz(av)} = J_{oz}(2mp/c) = J_{oz}(p/q) \quad [48]$$

as the current density averaged over bare and painted sections, it follows that

$$\Delta E = (J_{oz(av)}\,c/\pi\sigma)\ln\coth(\pi d/c) \quad [49]$$

This is the same result that has been found above in Eq. [8] for a completely bare surface of metal 1.

In addition, it can be shown with the help of Eq. [45] that local differences of the single electrode potential along an individual section of metal, e.g., between $x = \frac{1}{2}p$, $y = 0$, and $x = 0$, $y = 0$ are insignificant in comparison to the value of ΔE calculated in Eq. [49].

Similar calculations can be made for the configurations shown in Fig. 5 and 7. By and large, the foregoing equations for ΔE_{max} remain valid for partly painted structural components if $J_{oz(av)}$ is substituted for J_{oz}.

Concluding Remarks

In the present paper, variations in the local single electrode potential of cathodes have been calculated (*a*) for anodes placed in front of the cathodes as shown in Fig. 1 and (*b*) for anodes and cathodes lying in the same plane as shown in Fig. 5 and 7. In both cases, the maximum variation in the local potential of the cathodes is found to be

$$\Delta E = J_{oz(av)}\,(c/\sigma)f \quad [50]$$

where the dimensionless factor f depends on length ratios characteristic of the geometries shown in Fig. 1, 5, and 7.

If anodes are placed in front of the cathodes, the value of $f = f_1$ shown in Fig. 2 can always be made sufficiently small by providing an anode-cathode distance d comparable to or greater than the distance c between neighboring anodes. Under these conditions, hydrogen evolution may be avoided easily by automatic adjustment of the impressed current so that a predetermined single electrode potential of the cathodes is maintained.

In contrast, if anodes and cathodes lie in the same plane, the value of the factor $f = f_3$, f_4, or f_5 shown in Fig. 6 is in general of the order of unity. Consequently, in order to keep ΔE_{max} within limits required for the suppression of hydrogen evolution, it is necessary to make the width c of the cathodic areas sufficiently small. A small width c is especially necessary if the conductivity σ of the electrolyte is low. Consequently, if anodes and cathodes lie in the same plane, cathodic protection is, in general, practical only in electrolytes which have a high electrical conductivity as, e.g., sea water, and the average current density for reduction of oxygen is relatively low owing to painting most of the metal which is to be protected.

Manuscript received Dec. 3, 1956.
Any discussion of this paper will appear in a Discussion Section to be published in the June 1958 JOURNAL.

REFERENCES

1. C. Wagner, *This Journal*, **99**, 1 (1952).
2. C. Wagner, "Chemische Reaktionen der Metalle," in "Handbuch der Metallphysik," edited by G. Masing, Vol. 1, Part 2, pp. 196-199, Akademische Verlagsgesellschaft Becker & Erler, Leipzig (1940).
3. A. Frumkin and B. Levich, *Acta Physicochim. U.R.S.S.*, **18**, 325 (1943).
4. J. T. Waber, *This Journal*, **101**, 271 (1954).
5. A. Hickling, *Trans. Faraday Soc.*, **38**, 27 (1942).
6. J. J. Lingane, "Electroanalytical Chemistry," pp. 214 ff, Interscience Publishers, Inc., New York (1953).
7. J. Schoen and K. E. Staubach, *Regeltechnik*, **2**, 7 (1954).
8. W. Vielstich and H. Gerischer, *Z. physik. Chem. N.F.*, **4**, 10 (1955).
9. C. J. Penther and D. J. Pompeo, *Anal. Chem.*, **21**, 178 (1948).
10. M. H. Aronson, *Instruments*, **25**, 608 (1952).

APPENDIX

Errata in Eqs. [29] and [36] of the previous paper (1) have occurred. The correct form of Eq. [29] is

$$z'' = \sin^{-1}\left\{\frac{z'}{\sin\left[\frac{1}{2}\pi b/(a+b)\right]}\right\} \quad [29]$$

In Eq. [36] x is to be replaced by z.

Technical Note

The Silver and Thallium Oxide Coulometer

W. T. Foley

Chemistry Department, St. Francis Xavier University, Antigonish, Nova Scotia

The standard instrument for measuring quantity of electricity is the silver coulometer, but the iodine coulometer is of equally high precision (1). The copper coulometer is subject to secondary chemical reactions at the electrode, and it suffers from the disadvantage of a low equivalent weight. The water coulometer is subject to a negative error which increases rapidly with decreasing current (2).

A simple and precise coulometer using Ag and Tl salts at *p*H 9.5 is described here. It possesses the advantage of adherent Ag deposits and the use of conventional Pt gauze electrodes. The cell reaction is as follows:

$$4Ag^+ + 2Tl^+ + 6OH^- = Tl_2O_3 + 3H_2O + 4Ag$$

The value of the normal potential for the reaction

$$2Tl^+ + 6OH^- = Tl_2O_3(s) + 3H_2O + 4e^-$$

is -0.23 ± 0.02 vs. S.C.E. (3). Hence, at unit activity of thallous ion the oxidation potential at *p*H 9.5 is +0.40 v. At the same *p*H and in the absence of overvoltage, which is usually high, the oxidation potential of hydroxide to oxygen is +0.67 v. Thus thallous ion is an excellent depolarizer to prevent the formation of oxygen at the anode. The potential for the reaction

$$Tl = Tl^+ + e^-$$

is −0.33 v. A solution containing 0.1M $AgNO_3$, 0.5M NH_4OH, and 0.2M NH_4NO_3 will have a Ag ion concentration of, say, 10^{-8}M. At this concentration the plating of Ag on the cathode will occur at a potential of about 0.3 v. If these solutions are stirred, there is no danger of plating Tl or H_2.

Apparatus.—Reagent grade $AgNO_3$, Tl_2SO_4, NH_4NO_3, and NH_4OH were used without further purification. Before the start of each of the first few runs the solution was scavenged electrolytically; this was later abandoned as unnecessary. The electrolyte was prepared by dissolving in 300 ml of water 4 g Tl_2SO_4, 4 g $AgNO_3$, 4 g NH_4NO_3, and 8 ml 15M NH_4OH. The Pt gauze cathode was 40 cm^2 and the anode was 23 cm^2; they were attached to the holder concentrically. A magnetic stirrer was used. Electrical energy was obtained from six 2-v storage batteries of 900 amp-hr capacity. The standard resistors[1] with conventional current and potential leads were 1 ohm and 10 ohms in nominal value. A Rubicon type B potentiometer was used for all measurements except one in which a L&N K2 was used. The limit of accuracy of calibration was ±0.0001%. Two saturated Weston cells were used, one for preliminary adjustment of the potentiometer and the other for actual measurements. Time was measured by means of the WWV time signal.

Procedure.—The current through the electrolysis cell ran through the standard resistor across which the potential drop was measured. A DPDT switch in series with the resistor had across two of its terminals a dummy electrolysis cell with the same electrolyte and the same size electrodes as the working cell. Current was allowed to flow until all adjustments had been made and then at zero time the switch was made to the working coulometer. The potentiometer was read every 30 sec. The start and finish of the electrolysis was timed by the time signal from radio station WWV. At the conclusion of the electrolysis the electrodes were removed and washed with distilled water. The cathode, whose deposit was a beautiful silvery white, was dried at 110°C and weighed. If the deposit is not silvery white, the rate of stirring or the area of the cathode should be increased. The Tl_2O_3 is jet black except when very thin and it may be removed with H_2SO_3 or more conveniently with HCl.

Results.—The IR drop through the calibrated resistor enabled one to calculate the value of the current. The product of the average current and the time gave the quantity of electricity passed. The value of 107.88 was taken as the atomic weight of

Table I. Observed and calculated weights of Ag

Current, amp	Grams, Ag	Calculated Ag	Δ mg
1.0	1.0154	1.0153	+0.1
0.37	0.7496	0.7494	+0.2
0.28	1.0436	1.0429	+0.7
0.25	0.9235	0.9239	−0.4
0.22	1.1790	1.1794	−0.4
0.20	0.2550	0.2552	−0.2
0.19	0.3725	0.3725	0.0
0.18	0.2827	0.2827	0.0
0.16	0.2507	0.2505	+0.2
0.009	0.0958	0.0958	0.0

[1] Calibrated by the Applied Physics Division of the National Research Council of Canada.

Ag and 96,492 absolute coulombs (4) was taken as the value of the Faraday. Results are given in Table I.

Acknowledgment

This work was supported by the Defence Research Board of Canada Grant No. 7510-19, Project D-44-75-10-19.

Manuscript received July 27, 1956. This paper was prepared for delivery before the Washington Meeting, May 12-16, 1957.

Any discussion of this paper will appear in a Discussion Section to be published in the June 1958 JOURNAL.

REFERENCES

1. E. W. Washburn and S. J. Bates, *J. Am. Chem. Soc.*, **34**, 1341 (1912).
2. J. A. Page and J. J. Lingane, *Anal. Chim. Acta*, **16**, 175 (1957).
3. I. M. Kolthoff and J. Jordan, *J. Am. Chem. Soc.*, **74**, 382 (1952).
4. D. M. Craig and J. I. Hoffman, *Natl. Bur. Standards Circ.*,**524**, 13 (1953).

The Past and Future of Silicon Carbide

G. M. Butler

Research and Development Division, The Carborundum Company, Niagara Falls, New York

When, in 1891, E. G. Acheson first found tiny, shining crystals on the electrode in his furnace made from a plumber's bowl, he did not know that the new compound was silicon carbide or that it was to prove the most versatile of all carbides. Within a few years, however, he himself found that his new crystals were not only very hard, but also possessed unique refractory, electrical, chemical, and metallurgical properties.

While calcium carbide and tungsten carbide, the two other really important carbides of commerce, have contributed greatly to the world's economy, each of them can do only one job well: calcium carbide is the basis of acetylene chemistry, and tungsten carbide yields hard, wear-resistant tools, dies, and similar parts.

Silicon carbide, on the other hand, can do many tasks well. Its attributes challenge the imagination:

Extreme hardness and resistance to wear and abrasion.

High strength and very slow oxidation rate at extremely high temperatures.

Chemical inertness to all acids and many other corrodants.

Chemical reactivity with chlorine and other halogens, and with several metal oxides.

Electrical semiconductive and rectifying properties.

Low absorption or "capture" of thermal neutrons.

High thermal conductivity.

High thermal emf when paired with graphite.

Low density and thermal expansibility.

Raw materials abundant and cheap.

Surely such a material is uniquely valuable to mankind! Even today its valuable characteristics are not fully exploited, although the demand for silicon carbide taxes every manufacturer.

Those who work with SiC believe that its future holds uses as yet only dimly foreseen. By outlining the extent to which its abilities are now utilized, and by showing wherein greater knowledge of it should lead to enhancement of these good properties, the author hopes to encourage workers in many fields to explore this unusual "man-made mineral."

Synthesis.—Although SiC has been manufactured for 65 years, the process of making it has changed little. Silica and carbon are still packed around a graphite resistor and heated to cause the reaction, $SiO_2 + 3C \rightarrow SiC + 2CO$. While some of the characteristics of the product, such as crystal size, purity, and resistivity, can be varied to a limited degree by furnacing practice and choice of raw materials, the manufacturer cannot yet persuade his furnaces to yield crystals of controlled size, density, shape, and other properties. He can select from the crude "ingot" various areas differing in character, but this is at best a compromise.

In the research laboratory many investigators have formed SiC crystals of higher purity than can be made easily commercially. They have used a variety of methods: heating mixtures of high purity SiO_2 and C in crucibles or packed around resistors; substituting Si for the SiO_2 to avoid the need for additional C; use of the "hot wire" process to reduce volatile Si halides in hydrogen; sublimation and recrystallization of previously formed SiC; adding C to a molten high-Si alloy; reacting molten or vaporized Si with C, etc.

No one has yet announced a method by which large, flawless single crystals of SiC can be synthesized, comparable to those grown from oxides by the flame-fusing process. This should be feasible, once a solution is found to the mechanical problem of providing a continuous, uniform flow of vapors containing Si and C, within which the crystal can grow as desired.

All evidence indicates that the commercial hexagonal crystal product is the result of a vapor-phase reaction in which Si unites with C. Some uncertainty exists as to the form in which C is present in the vapor, since the vapor pressure of elemental C at the reaction temperature range of 1800°-2400°C (3270°-4350°F) seems to be too low to provide the necessary concentration for crystal growth. Nevertheless, SiC crystals will grow whenever vapors carrying Si pass over C or when a mixture of C and SiO_2 is sufficiently hot.

Availability of large, ultrapure crystals would free the researcher from the vexing limitations imposed by the lack of high purity except in tiny crystals. Laboratory quantities of silicon carbide are available with moderately high purity, probably better than 99.9% SiC but only in particle sizes of about 80 mesh.

Of equal interest would be a way to grow large crystals of the low-temperature primary or cubic form of SiC. Apparently all SiC first forms as tiny cubic crystals, which transform at higher temperatures to the hexagonal or rhombohedral crystal forms. The largest cubic crystals seem to be less than 0.02 in. across, so they have little use at present.

These cubic crystals differ from the usual hexagonal product in electrical properties and perhaps also in chemical reactivity. Theoretically, large cubic crystals should make beautiful gem stones; DeMent (1) has presented arguments for this contention. Cubic crystals appear to grow from a liquid, such as molten Si or Si alloy, thus offering promise of growing large ones by techniques used to grow other crystals from molten baths.

Silicon carbide can be formed in high-Si alloys, both ferrous and nonferrous, in the presence of C. For many years after Moissan (2) first claimed to have found tiny crystals of SiC in meteoric iron, no other occurrence in nature was known. Later, Baumann (3) summarized the work of investigators who were able to produce SiC crystals in various Al-Si alloys, and also showed evidence for its formation in such alloys at temperatures as low as 525°C (977°F). Fulton and Chipman (4) recently showed that high-Si irons can contain small SiC crystals.

Loose grain.—One major division of SiC uses is as loose grits or "grain." Acheson first used his SiC crystals in loose form for the lapping and polishing of diamonds. Today substantial quantities of graded grits are sold for lapping, polishing, sawing, and similar operations using grits either loose or in a vehicle such as tallow, grease, or other lubricant and carrier. Rock sawing, stone and gem polishing, glass grinding, valve lapping, and other familiar operations make use of the hard, sharp crystals. Challenges to these uses of loose grain are coming from improved bonded abrasive materials and from new mechanical methods for grinding and polishing; but the low cost and convenience of loose grain methods will ensure them popularity for a long time to come.

Acheson also soon learned that his new product had interesting chemical properties. Before the turn of the century, he established that it would react with molten Fe with deoxidizing effect, and that numerous metal oxides, which might otherwise be lost in slags, could be reduced to metal by SiC additions. From this knowledge grew the widespread usage of specially processed SiC grain and briquettes in iron foundries and steel plants, and in certain nonferrous smelting processes, as a metallurgical additive, amounting to thousands of tons annually.

Another unusual chemical property, that of vigorous reaction with halogens such as chlorine at elevated temperatures, was utilized in World War I to produce $SiCl_4$, which was released into the air to produce smoke screens. Nowadays $SiCl_4$ is an industrial chemical of rapidly increasing importance, from which fine silica for rubber reinforcement, ethyl silicate for foundry sand binder, and silicon itself for transistor and rectifier use are made. Simply by "burning" SiC in Cl_2, $SiCl_4$ can be manufactured easily and cheaply. Recent developments in elemental Si technology, leading to huge potential use in solar batteries and rectifiers, offer promise of great expansion in this use of SiC.

Acheson knew that SiC was an electrical conductor, but he could hardly have foreseen that nearly every major high-voltage power distribution line in the world would be protected against lightning damage by arresters made with loose SiC grain, or with grain bonded with clays. SiC grains in contact with each other will conduct almost no current at low voltages, but the contact resistance decreases very rapidly with increasing voltage. When a voltage surge caused by lightning hits an arrester, current jumps across spark gaps in series with the grain column or stack of bonded disks, then through the grain, and harmlessly to ground. When the surge decreases, the grain column regains its high resistance and cuts off the current flow to ground, an action which it can perform many times without damage.

The important commercial uses of loose grain are summarized in Table I. There are, however, other potentially important uses. Older radio fans remember crystal sets, in many of which the sensitive detector was SiC, carefully selected and mounted with the "Cat's Whisker" permanently sealed in contact with an active spot on the crystal surface. With the passing of crystal sets, this rectification ability of SiC has been little utilized. Materials such as Si and Ge have been refined until they demonstrate dramatically valuable rectification properties, opening up the whole transistor development. When comparable progress is made in purifying SiC and controlling the introduction of certain trace impurities into its structure, a new transistor material, stable to higher temperatures, may result. The importance of high temperature transistors in high-speed aircraft and missiles could be enormous.

Such controlled-purity SiC, in the form of fine powder, may become an important source of illumination. Like certain other compounds, it has the property of electroluminescence, or glowing when subjected to a small electrical current. Recent developments promise large panels of electroluminescent material glowing over whole ceilings; perhaps SiC will prove suitable for this use.

Coated abrasives using SiC.—"Sandpaper" was once a properly descriptive name for coated abra-

Table I. Important uses of loose SiC grain

Abrasive:	Lapping and polishing Wire sawing of stone Abrasive blasting Non-slip additive for concrete
Metallurgical:	For deoxidation of steels and reducing agent in alloy steel and ferroalloy manufacture
Chemical:	For chlorination to produce silicon tetrachloride, made into silicones, silicon metal, ethyl silicate, and fine silica
Electrical:	Lightning arresters

sives. Sand or crushed flint was sprinkled on a paper coated with wet glue and then dried. Nowadays, coated abrasives include products whose backings may be paper, of a wide variety of types, but also cloths and vulcanized fiber, and the abrasive particles may be flint, garnet, fused alumina, SiC, or even diamond.

Silicon carbide coated abrasives find their greatest usefulness in grinding very hard or very soft materials. One of the important uses is for sanding hard undercoat primer paint of automobile bodies, which is done wet, by hand, with flexible papers coated with fine-grit SiC. On the other hand, the leather industry is a big user of SiC coated abrasives, especially in shoe manufacturing and repairing. Soft metals like aluminum, brass, and copper are best ground with this material, as is also cast iron.

Grinding the edges of plate glass, especially for automobile use, is done very effectively by belts coated with SiC, which are also used for grinding and finishing marble and other decorative stone. Power-driven floor sanders equipped with drums or disks coated with SiC, are familiar to do-it-yourself fans, who have seen how the coarse open-coat papers rip through old paint and warped wood floors. The advent of resins reinforced with glass fibers, for cars, boats and other uses, opens additional markets for SiC belts and disks, especially in fine finishing operations.

Coated abrasive uses in general are expected to grow moderately as novel materials are developed which need the sharp, brittle cutting action of SiC. The important present uses are listed in Table II.

Bonded SiC

Abrasives: Acheson soon incorporated his newly discovered SiC into grinding wheels. He used the techniques and bonding agents of the emery wheel industry. This practice was based on natural clays and other minerals mixed with the abrasive grain, formed into wheels, and fired to "mature" the bond and cause it to wet the grains and join them together. Even today most SiC articles are bonded with such materials. The abrasive applications listed in Table III are mostly carried out with vitrified wheels. Other bonding materials, such as resins and rubbers, are displacing some of the vitrified materials, especially where toughness is desired.

Table II. Principal coated abrasive SiC applications

Auto body undercoat sanding
Glass edging
Leather grinding and finishing
Floor sanding
Stone grinding and polishing
Grinding soft nonferrous metals and alloys; also cast iron
Finish-grinding glass-reinforced resins

Table III. Principal bonded SiC abrasive uses

Wheels:	Tungsten carbide rough-grinding
	Grinding and cutting glass, gems, marble, ceramics, stone
	Grinding cast iron and hard cast alloys
	Wood pulp grinding; leather, rubber and plastic grinding
	Aluminum, copper, brass, bronze grinding
Sticks and stones:	Cast iron cylinder honing
	Sharpening stones
Nonslip uses:	Stair treads and floor inserts

The properties of SiC fit it best for grinding either very hard and brittle materials such as cemented carbides, stone, glass, ceramics, cast iron, and hard alloys, or at the other extreme of the scale for very soft materials like resins, leather, rubber, and soft nonferrous metals. The consumption of SiC in bonded form as abrasives is apt to increase only in proportion to the general growth of business, without dramatic possibilities for rapid upswings.

Refractories.—The high temperature resistance and good heat conductivity of SiC were long ago put to service in the form of vitrified "super-refractory" wares. Today the possibilities for growth of this outlet for SiC are impressive. The super-refractories are formulated for resistance to deformation, corrosion, and other destructive effects of service at extremely high temperatures.

The standard products made by several companies are bonded with mixtures of minerals and clays which form silicates during firing. These wares have become widely accepted for good strength, oxidation resistance, heat conduction, and ability to withstand wear and corrosion. They go into kiln furniture, retorts, and condensers in zinc refining, linings for blast furnace dust cyclones, and a host of other specialized uses.

The softening temperature of the silicate bond imposes a definite limit on the temperature which these refractories can endure. New and more severe demands have pushed these materials to their limit. It was evident that the potentialities of SiC could be realized only by drastically improved bonding techniques.

Silicon nitride bonding.—The first major "breakthrough" came when it was proved that a new silicon carbide-silicon nitride material[1] made an outstandingly successful nozzle and combustion chamber liner for rockets. It can now be revealed that rocket nozzle production from this material has become "big business."

This new composition, in which silicon nitride is formed *in situ*, is itself a great advance over conventional SiC refractories bonded with silicates formed from clays. Whereas the older materials weaken seriously at temperatures of 2500°-2700°F (1480°-1590°C), the new silicon nitride bond does not melt up to its dissociation point of 3450°F (1900°C), and retains useful strength to much higher temperatures. Even more important, it will withstand the stresses of rapid heating and cooling, with much less tendency to crack than conventional bonds.

Once thoroughly proved in the inferno of rocket motors, modifications of this novel super-refractory began to find important roles in jobs formerly done only by metals (5). Jet engine makers used to bemoan the high cost of maintaining cast alloy jigs used for brazing together the halves of hollow

[1] Niafrax® silicon carbide, a trade mark of The Carborundum Company.

blades for the compressor. After a few trips through the brazing furnaces, the alloy jigs were so warped that they had to be recut to dimensions, and the blades came out so distorted they had to be coined to restore them to accurate shape. Now silicon nitride-bonded silicon carbide[2] jigs make hundreds of trips through the furnaces with no distortion, generating accurate blades which require no dimensional correction.

The new nitride-bonded material has unusual resistance to corrosion by molten aluminum and fluxes used with it. Now the aluminum industry is carrying on extensive tests which may result in many new applications for this product.

Other bonds.—SiC can be bonded with elemental Si. One such body[3] has been used for years as terminals for SiC heating elements and to a limited extent for igniters and heating elements, using its capacity to generate heat by resistance to electric current (6). This composition is now under investigation as a container for nuclear fuel, to make ceramic fuel elements for nuclear reactors (7).

Carbon also is used to bond SiC, especially for the familiar graphite-silicon carbide crucibles used for nonferrous metal melting.

Table IV summarizes these bonds and their major fields of usefulness. Efforts to use refractory metals to bond SiC have not yet yielded results of commercial importance.

Self-bonded silicon carbide.—Although silicon nitride-bonded SiC is a great advance over conventional refractories, it still is bonded with a material with less heat resistance than itself, and it cannot be made impermeable to gases and liquids. Self-bonded SiC recrystallized in such a way that the interstices are filled completely with more SiC should be a still more valuable material.

[2] Refrax® silicon carbide, a trade mark of The Carborundum Company.

[3] Durhy® silicon carbide, a trade mark of The Carborundum Company.

Table IV. Refractory uses for SiC wares

Silicate bond:	Kiln furniture (tiles, posts, saggers)
	Muffles, hearths, skid rails in furnaces
	Retorts and condensers for zinc distillation
	Heat recuperator tubes and core-busters
	Wear and erosion-resistant parts such as hot cyclones and downcomers for blast furnaces; acid domes
	Boiler settings
Silicon nitride bond:	Rocket motor nozzles and combustion chambers
	Brazing jigs
	Containers, pump parts, protection tubes and allied parts for molten aluminum and zinc
	Acid burner tips and spray nozzles
Silicon bond:	Heating elements
	Thermocouple protection tubes
	Nuclear fuel elements (possibility)
Carbon bond:	Graphite-silicon carbide crucibles

Tinklepaugh (8, 9), at Alfred University, was able to produce such a body by hot pressing fine SiC grains at very high temperatures and pressures. The limitations of this technique prevent production of pieces of large or complicated nature, but his work directly inspired the development of a practical method to produce a wholly dense, self-bonded SiC body.

This revolutionary new material, christened KT[4] (the initials of its inventor, Kenneth Taylor), consists of SiC with less than 5% of any other material. It is wholly impervious to gases and liquids, has great strength at high temperatures, better thermal conductivity at high temperatures than any other known ceramic and most metallic heat-resisting alloys, and other properties such as great resistance to abrasion and corrosion. It was first described publicly before the Electrochemical Society in May 1956, in San Francisco, and in an article recently published (10).

KT silicon carbide is the first commercial material utilizing to the fullest the valuable properties of SiC. One can confidently expect tremendously wide application of it, as its properties become better known and adequate capacity is installed for its production.

Some of the uses now being explored are shown in Table V.

Electrical uses of bonded silicon carbide.—Nonmetallic heating elements of SiC are widely used in furnaces operating above the useful temperature of metallic resistors. They are composed of grains recrystallized together at high temperatures into self-bonded, porous rods, which are usually equipped with terminal ends of lower electrical resistance made of siliconized SiC. Continued improvement in these elements is extending their useful life to temperatures approaching 3000°F (1650°C), and steady expansion of volume is to be expected.

Heating elements are formulated to have relatively small change in electrical resistance with temperature; at temperatures reached in service they resemble metallic elements in displaying increase of resistance as the temperature goes up.

Changes in manufacturing techniques, raw materials, or use of bonding agents can give drastically different resistance characteristics. At low voltages resistance can be very high but can drop rapidly as voltage is increased. An electrical "safety valve" such as this has many uses in electronic design, plus the very important use in lightning arresters.

The unusual electrical properties of SiC derive in part from the phenomena associated with surface contacts between semiconductive materials and in

[4] KT silicon carbide, a trade mark of The Carborundum Company.

Table V. Potential uses for dense, impervious SiC ware

Valves and piping for corrosive and erosive materials
Pumps and related parts for handling molten alumina
Sandblast nozzles
Rocket nozzles
Fuel elements and structural members in gas-cooled nuclear reactors
Thermocouple protection tubes
Heat exchangers

Table VI. Predicted areas for increased SiC consumption

Chemical:	Rapid growth as raw material for silicon tetrachloride production, ending up as silicon metal and as fine silica.
	Piping, valves, and other parts for corrosion and heat resistance, out of dense, self-bonded silicon carbide.
Metallurgical:	Marked upswing as addition to ferrosilicon furnaces to increase production.
	Continued growth in briquette use in iron foundry practice.
	Possible new source of silicon metal by thermal dissociation.
Electrical:	Transistor and rectifier use at elevated temperatures, if necessary purity can be achieved.
	Electroluminescent powder for low-intensity area lighting.
	Increased use of nonlinear resistors.
Nuclear Energy:	Fuel element sheaths or fuel carriers for high temperature gas-cooled reactors; also structural parts.

part from the basic properties of the material itself. Much can be done by control of purity of the crystals, with resistivity variable over several orders of magnitude.

Transistors have been made experimentally with selected SiC crystals, but their performance has not been good enough to compete with Si or Ge. Here again lack of ability to regulate what is in the crystal may be at fault. Theoretical considerations suggest great promise for this application when crystal growing becomes better controlled.

The ability of certain silicon carbide crystals to emit light when excited by a weak electric current has been long known but never used commercially. Since not all crystals can be so excited as to be electroluminescent, more must be learned about the effects of impurities and structure variations before such uses are perfected.

The Future

Those most familiar with this remarkable compound are confident that it will grow into new and even more valuable uses. Likewise, one can confidently predict continued growth in its nonabrasive uses. These are summarized in Table VI.

Acheson, imaginative scientist that he was, could hardly foresee all the possibilities for the compound he discovered. Emphasis on high temperature technology will present further new and important uses for this compound which will keep it at the front of modern man-made minerals.

Manuscript received April 5, 1957. This paper was prepared for delivery before the Cleveland Meeting, Sept. 30-Oct. 4, 1956.

Any discussion of this paper will appear in a Discussion Section to be published in the June 1958 JOURNAL.

REFERENCES

1. J. DeMent, *Mineralogist*, **16**, 211 (1948).
2. Henri Moissan, *Compt. rend.*, **140**, 405 (1905).
3. H. N. Baumann, Jr., *This Journal*, **99**, 109 (1952).
4. J. C. Fulton and J. Chipman, *J. Metals*, **6**, 356 (1954).
5. W. L. Wroten, *Materials & Methods*, **40**, 83 (1954).
6. C. G. Rose, *Brick & Clay Record*, **117**, 62 (1951).
7. J. R. Johnson, *J. Metals*, **8**, 660 (1956).
8. R. A. Alliegro and J. R. Tinklepaugh, *WADC Tech. Report 53-5*, Jan. 1953.
9. R. E. Wilson, L. B. Coffin, and J. R. Tinklepaugh, *WADC Tech. Report* 54-38, Part 2, Jan. 1955.
10. K. M. Taylor, *Materials & Methods*, **44**, 92 (1956).

FUTURE MEETINGS OF
The Electrochemical Society

New York, N. Y., April 27, 28, 29, 30, and May 1, 1958

Headquarters at the Statler Hotel

Sessions probably will be scheduled on Electric Insulation, Electronics, Electrothermics and Metallurgy, Industrial Electrolytics, and Theoretical Electrochemistry (including a symposium on "Electrokinetic and Membrane Phenomena")

★ ★ ★

Ottawa, Canada, September 28, 29, 30, October 1, and 2, 1958

Headquarters at the Chateau Laurier

★ ★ ★

Philadelphia, Pa., May 3, 4, 5, 6, and 7, 1959

Headquarters at the Sheraton Hotel

★ ★ ★

Columbus, Ohio, October 18, 19, 20, 21, and 22, 1959

Headquarters at the Deshler-Hilton Hotel

★ ★ ★

Chicago, Ill., May 1, 2, 3, 4, and 5, 1960

Headquarters at the Lasalle Hotel

★ ★ ★

Houston, Texas, October 9, 10, 11, 12, and 13, 1960

Headquarters at the Shamrock Hotel

★ ★ ★

Papers are now being solicited for the meeting to be held in New York, N. Y., April 27-May 1, 1958. Triplicate copies of each abstract (*not exceeding 75 words in length*) are due at the Secretary's Office, 1860 Broadway, New York 23, N. Y., *not later than January 2, 1958* in order to be included in the program. *Please indicate on abstract for which Division's symposium the paper is to be scheduled.* Complete manuscripts should be sent in triplicate to the Managing Editor of the JOURNAL at 1860 Broadway, New York 23, N. Y.

Current Affairs

Dr. Eugene Willihnganz Assumes New Post of Director of Research at C & D Batteries, Inc.

Dr. Eugene Willihnganz has been appointed to the new post of Research Director at C & D Batteries, Inc., Conshohocken, Pa. The firm specializes in the design and manufacture of storage batteries for industrial use and specialized applications such as telephone, control, and auxiliary power.

For the past 25 years he has been connected with the battery industry, first in charge of battery research for the National Lead Co. and later as Director of Research and then Staff Consultant for Gould-National Batteries, Inc.

His work on the theory of negative plate operation in the lead-acid storage battery and his method of measuring the electrical resistance

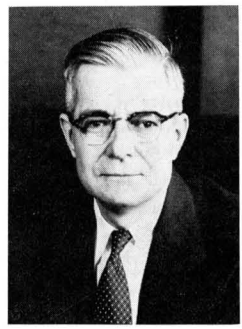

Eugene Willihnganz

of storage batteries are listed among some of Dr. Willihnganz's outstanding accomplishments. A considerable proportion of the storage batteries being manufactured today incorporates directly or indirectly the results of his work somewhere in their construction.

Dr. Willihnganz feels that the storage battery, notwithstanding its advanced state of development today, is still surrounded by a number of fundamental, complex, unsolved problems. By conducting basic research into these problems he is certain many new things will be discovered about batteries. Application of this new knowledge will lead to even more advanced batteries which will provide greater capacity, higher efficiency, and longer life.

Dr. Willihnganz is a member and Past Chairman of the Battery Division of our Society.

Meetings of Interest to Electrochemists

Chemical Industries Align for Huge Exposition

The 26th Exposition of Chemical Industries will be held at the Coliseum in New York City, December 2 to 6. The Exposition will occupy all four floors of the Coliseum and, with spaces assigned to 530 exhibitors up to the end of July, it will be the largest display of its kind ever staged.

Several new sections have been added to this year's exposition. They include the Chemical and Chemical Materials Section, which is already well filled; the Rocket and Satellite Section, which is being sponsored by the American Rocket Society; and the Laboratory Materials and Supplies Section, which will reveal advances in apparatus for research and development.

Norman Hackerman, President of The Electrochemical Society, and Sidney D. Kirkpatrick, editorial director "Chemical Engineering" and "Chemical Week," are members of the Advisory Committee for the exposition.

Marshall Sittig Appointed Chairman of ACS Symposium on Alkali Metals

Marshall Sittig, of the American Lithium Institute, Inc., has been appointed Chairman of a symposium on alkali metals to be held at the 133rd National Meeting of the American Chemical Society slated for San Francisco in April 1958.

The symposium will be concerned with a wide range of technical subjects surrounding all of the alkali metals—lithium, sodium, potassium, rubidium, cesium, and francium. Some of the topics tentatively planned for the program are: new developments in the analysis of the alkali metals; the outlook for lithium in alloys; new developments in liquid metals handling equipment; alkali metals as polymerization catalysts; sodium as a nuclear reactor coolant; manufacture of titanium by sodium reduction; manufacture of isosebacic acid; alkali metals derivatives as components of Ziegler-type polymerization catalysts; manufacture of synthetic natural rubber; large-scale manufacture of sodium borohydride; and the outlook for rubidium and cesium metals.

Anyone interested in contributing material for the symposium on alkali metals should write: Marshall Sittig, American Lithium Institute, Inc., 32 Nassau St., P. O. Box 549, Princeton, N. J.

Reactive Metals Conference

The Third Annual Reactive Metals Conference in scheduled for May 27, 28, and 29, 1958, at the Hotel Statler, Buffalo, N. Y., under the sponsorship of the Niagara Frontier Section of the AIME.

Those metals which by present standards are difficult to process by conventional means due to their reactivity with the more common refractories, oxygen and nitrogen, are the subject of this conference. The production, properties, fabrication, and application of tantalum, niobium, titanium, zirconium, hafnium, vanadium, molybdenum, tungsten, thorium, uranium, and their alloys will be discussed during the various technical sessions.

The General Chairman is Dr. S. F. Urban of the Titanium Alloy Manufacturing Division, National Lead Co.

Corrosion Convention in London

Britain is holding National Anti-Corrosion Week from October 14 to 19, 1957. The principal features of this campaign are a Corrosion Convention, to be held at Central Hall Westminster, London, on October 15 and 16, and a Corrosion Exhibition, at the Royal Horticultural Society's Old Hall, from the 15th to the 17th. A number of overseas delegates have been registered for the Convention, and it is hoped that many U. S. visitors will attend.

Papers by leading British experts will cover many aspects of corrosion, including: The Protection of Plant in the Oil and Chemical Industries; Corrosion in the Atomics Industry; Paints and Corrosion; Packaging and Corrosion; Metals and Alloys; Metal and Plastics Spraying and Finishing; High Polymers vs. Corrosion; Cathodic Protection; Water Treatment; and Galvanized Coatings.

This campaign against industry's losses from corrosion is being supported by many British technical associations and engineering societies and was organized by the Leonard Hill Technical Group.

Special Libraries Association Metals Division Meeting

The Metals Division of Special Libraries Association will be in session during the Second World Metallurgical Congress to be held in Chicago, November 6, 7, and 8, 1957. A library display booth and information center will be available at the International Amphitheater.

Speakers from England, France, and Germany, as well as from the United States and Canada, will be on the program.

Tours have been arranged through the Armour Research Foundation Labs., International Harvester's New Research Center, and several other research organizations in the Chicago area. A tour of The John Crerar Library, the largest technical library in the world, should be included while in Chicago.

New Sustaining Member

Minnesota Mining & Manufacturing Co., St. Paul, Minn., recently became a Sustaining Member of The Electrochemical Society.

Polystyrene Plant in India Now Operating

The first polystyrene plastic manufacturing plant in the middle east and southeast Asia recently started production in Bombay, India.

About a year in construction, the new plant is owned by Polychem Ltd., formed in 1955 by The Dow Chemical Co. and Kilachand Devchand & Co. Ltd., an Indian firm.

Dow supplied the technical know-how for producing Styron as well as technical assistance in designing and equipping the plant. It also has provided training for Indians comprising the key operating personnel. Fifty per cent of the company's common stock is held by the Indian public while the Dow and Kilachand group share its remaining stock.

Division News

Electronics Division

The annual business meeting of the Electronics Division was held in Washington, D. C., on May 15, 1957.

The Chairman reported on the activities of the Division as follows.

The Electronics Division sponsored a symposium on Semiconductors at the Fall Meeting of the Society in Cleveland. Thirty-two papers, all of the "late news" type, were presented. Keynote speakers were: Dr. G. K. Teal, Texas Instruments, Inc., and Dr. J. W. Faust, Jr., Westinghouse Electric Corp.

At the Washington Meeting, the Electronics Division presented five symposia. There were thirty-three papers on Luminescence, nineteen on Semiconductors, along with twelve "late news" papers, thirteen papers on Thermionic Cathodes, five on Screen Applications, and seven on Instrumentation.

The practice of having keynote speakers has been continued. Dr. H. F. Ivey, Westinghouse, keynoted the Luminescence Symposium. Dr. D. A. Jenny, RCA Labs., was keynote speaker for Semiconductors, and Dr. J. J. Lander, Bell Telephone Labs., was keynote speaker for Thermionic Cathodes.

The November 1956 issue of the JOURNAL, compiled by Dr. H. Bandes, Semiconductor Editor, featured semiconductor papers. It is distinguished by the fact that it was the first issue on this subject ever published by the JOURNAL.

Planning for a symposium on "Surface Phenomena" or "Surface Reactions" is under way. It is hoped to develop the symposium into an international event, supported by other Divisions of the Society.

An Electronics Division Cocktail Mixer was scheduled for the Washington Meeting for the purpose of bringing the various groups of the Division closer together and encouraging membership in the Society.

The Division again published its booklet of Enlarged Abstracts. As in past years, the composition and printing were both done by Edwards Brothers. Last year's booklet has shown a profit, which can be attributed to its small size and low cost. This year's booklet is about three times the size of last year's, resulting in a much higher cost. Nevertheless, the price is being maintained at $2.00 per copy. The loss is being supported by the profit from sales of last year's booklet.

The 1955 "Semiconductor Abstracts" is just being published by John Wiley & Sons. This issue contains 1258 abstracts. Mr. E. Paskell of Battelle Memorial Institute, Chairman of the "Abstracts" Committee, has compiled and edited the 1955 issue with the help of his committee and the excellent services at Battelle. Sales of the 1953 and 1954 issues, as of January 1, 1957, are: 1953—1142 copies; 1954—1107 copies. Break-even points for the 1953 and 1954 issues are about 1650 and 670 copies, respectively.

An addition to the Bylaws of the Division was proposed by the Bylaws Committee in order to incorporate the Semiconductor Abstracts Committee into the structure of the Division. The proposal was referred to a special committee for study and recommendations. The following committee was appointed by the Chairman of the Division: E. Paskell, Chairman, P. H. Keck, M. F. Lamorte, and J. R. Musgrave.

The Membership Committee of the Division has been very active, with the result that the Division membership has increased by almost 100 in the past year. The Division membership as of May 10, 1957, is 445.

Symposia planned for next year include: Luminescence and Semiconductors. If sufficient interest is shown, symposia on other interests of the Division may be held. A symposium on Semiconductors will be held at the Buffalo Meeting.

The new officers of the Division, elected for a two-year term (1957-59) at the business meeting, are:

Chairman—Herbert Bandes, Sylvania Electric Products Inc., Woburn, Mass.

Vice-Chairman (Luminescence)—Robert J. Ginther, Naval Research Labs., Washington 25, D. C.

Vice-Chairman (General Electronics)—Charles T. Lattimer, Radio Corp. of America, Marion, Ind.

Vice-Chairman (Semiconductors)—J. W. Faust, Jr., Westinghouse Research Labs., Pittsburgh 35, Pa.

Secretary-Treasurer—Martin F. Quaely, Westinghouse Electric Corp., Bloomfield, N. J.

The fiscal year of the Division ends on May 31. Since the results of the sale of 1957 abstract booklets are not yet complete, the financial report given below does not include data of these transactions:

Balance reported at San Francisco Meeting	$ 749.20
Net profit from 1956 booklet	269.02
Additional payments on 1955 booklets	4.00
Interest on bank balance	22.48
Total receipts and assets	$1,044.70
Total paid out	53.26
Balance carried forward	$ 991.44

M. F. Quaely, *Secretary-Treasurer*

Theoretical Electrochemistry Division

Spring 1958 Symposium

A symposium on **Electrokinetic and Membrane Phenomena** is being arranged by the Theoretical Electrochemistry Division for the meeting of the Society to be held in New York, N. Y., April 27 to May 1, 1958. The program is to include invited and contributed papers.

The committee arranging this pro-

1958 Bound Volume

Members and subscribers who wish to receive bound copies of Vol. 105 (for 1958) can receive the volume for the low, prepublication price of $6.00 if their orders are received at Society Headquarters, 1860 Broadway, New York 23, N. Y., *by December 1.* After that date members will be charged $12.00, and nonmembers, including subscribers, $18.00.

Bound volumes are *not* offered independently of JOURNAL subscription.

Battery Division Extended Abstracts Booklet

The Battery Division has prepared an extended abstracts booklet of the 28 papers to be presented at the fall meeting of the Society in Buffalo, October 6-10, 1957.

This bulletin was expected to be available after September 15, at $2.00 per copy, and can be obtained by sending a check to the Secretary of the Battery Division:

E. J. Ritchie
Eagle-Picher Research Lab.
Joplin, Mo.

gram is: *Chairman,* Dr. Paul Delahay, Louisiana State University, Baton Rouge, La.; Professor J. J. Hermanns, Rijks University, Leiden, Netherlands; Dr. R. M. Hurd, University of Texas, Austin 12, Texas; Dr. T. Shedlovsky, The Rockefeller Institute for Medical Research, New York 21, N. Y.

Abstracts (not exceeding 75 words in length) of contributed and invited papers for this symposium and papers for the general sessions of the Theoretical Division should be submitted to the Secretary's Office, 1860 Broadway, New York 23, N. Y., in triplicate, *not later than January 2, 1958.*

Ralph Roberts, *Secretary-Treasurer*

Section News

India Section Symposium on Electrodeposition and Metal Finishing

A two-day Symposium on Electrodeposition and Metal Finishing has been planned by India Section during December 1957 at the Central Electrochemical Research Institute, Karaikudi. This is the fourth symposium to be arranged by the Section. Papers will be invited on the following aspects, theoretical and industrial: (*a*) Electrodeposition—electroplating, electrorefining, electrowinning, electroforming, metal powders, electroanalysis; (*b*) Metal Finishing—electropolishing, anodizing, protective coatings.

T. L. Rama Char,
Regional Editor, India

Pacific Northwest Section Participates in Regional Meeting

The Pacific Northwest Section of The Electrochemical Society and the Inland Empire Section of the American Chemical Society were hosts at a very successful joint Northwest Regional Meeting held in Spokane on June 13 and 14. In addition to a large number of papers presented at sessions sponsored by the Northwest region sections of the American Chemical Society, an Electrochemical Society Session, arranged by the Pacific Northwest Section, occupied one morning. Papers presented at this session were:

"Formation Fields and Current Efficiency in Anodic Oxidation of Zirconium," Geo. B. Adams, T. S. Lee, Pierre Van Rysselberghe, University of Oregon.

"Interference Color and Other Methods of Determining the Thickness of Anodic Oxide Films on Tantalum," L. Young, British Columbia Research Council.

"Capacity of Solid-Metal Solution Interfaces," J. J. McMullen, Kaiser Aluminum & Chemical Corp.; Norman Hackerman, University of Texas.

"Equilibrium in the System Fe^{+++}—H^{+}—Dowex 50," R. C. Vasishth, M. M. David, University of Washington.

"Anodizing of Aluminum for Decorative and Functional Applications," G. H. Kissin, Kaiser Aluminum & Chemical Corp.

At this meeting the following Pacific Northwest Section officers were elected for 1957-58:

Chairman—George B. Adams, Jr., University of Oregon, Dept. of Chemistry, Eugene, Ore.

Vice-Chairman—Cornelius Groot, General Electric Co., Richland, Wash.

Secretary-Treasurer — Michael J. Pryor, Kaiser Aluminum & Chemical Corp., Dept. of Metallurgical Research, Spokane 69, Wash.

G. H. Kissin, *Past Chairman*

Notice to Subscribers

Your subscription to the JOURNAL of The Electrochemical Society will expire on *December 31, 1957.* Avoid missing any issue. Send us your remittance now in the amount of $18.00 for your 1958 subscription. (Subscribers located outside the United States must add $1.00 to the subscription price for postage, and payment must be made by Money Order or New York draft, not local check.) An expiration notice has been mailed to all subscribers.

A bound volume of the 1958 JOURNALS can be obtained at a prepublication price of $6.00 by adding this amount to your remittance. However, no orders will be accepted at this rate after *December 1, 1957,* when the price will be increased to $18.00 subject to prior acceptance. Bound volumes are *not* offered independently of your JOURNAL subscription.

India Section

The Second Technical Meeting of the Section for 1957 was held on May 1 at the Indian Institute of Science, Bangalore. Dr. K. S. Rajagopalan, Senior Scientific Officer, Central Electrochemical Research Institute, Karaikudi, delivered a lecture on "Vapor Phase Corrosion Inhibitors."

The speaker referred to the importance of corrosion studies and the considerable saving in money and material effected by the use of measures to prevent or minimize the effects of corrosion. He then briefly dwelt on the use of inhibitors like sodium chromate, silicate, and nitrite in industry. While these rendered satisfactory protection in liquid media, parts of components not directly in contact with the liquid and places not readily accessible for protection were not protected. Researches of Wachter at Shell Development Co. and similar experimentation at the U. S. Naval Research Lab. resulted in the realization of the potentialities of amine nitrites, and culminated in the discovery of diisopropylamine nitrite, diisobutylamine nitrite, and dicyclohexylammonium nitrite. Dr. Rajagopalan also mentioned the other compounds like salicylal, ethanolamine, sodium mercapto benzothiazole, etc. He then discussed the three important requirements of a vapor phase inhibitor, viz., volatility, nontoxicity, and stability, and described the use of the two commonly marketed materials VPI260 and VPI220 in various applications like packaging of machine tools, aero engines, rifles, C.K.D. packaging of cars, etc., pointing out the application of the material in different forms, as powder, coating, and solution. While discussing advantages such as ease of application, protection of inaccessible parts, and the absence of need for removal of the material, the lecturer referred to the two prerequisites for the use of V.P.I., viz., relatively enclosed space and the effective distance of 1 ft. While the V.P.I. had many attractive features, he cautioned against the limitations with respect to their use in protection of nonferrous metals and alloys and multiple assemblies. He then referred to the effective life of the V.P.I. under different conditions, the method developed by him for estimation of the active ion, and some laboratory tests carried out for evaluation of relative merits of indigenous inhibitors.

Future possibilities in the development of specific inhibitors for nonferrous metals, oil soluble inhibitors,

and mixed inhibitors were touched upon in conclusion. The lecture was followed by an interesting discussion on the mechanism of protection and the economic aspect of this new type of protection against corrosion.

T. L. Rama Char,
Editor, Bulletin

Personals

L. J. Balasundaram has joined the Physical Metallurgy Division, National Metallurgical Lab., Jamshedpur, as Senior Scientific Officer.

Edward F. Foley, Jr., formerly Research Chemist, has been appointed Production Manager and Purchasing Agent for Enthone, Inc., New Haven, Conn.

Norbert D. Greene has joined the Metals Research Labs. of the Electro Metallurgical Co., a division of Union Carbide Corp., Niagara Falls, N. Y., as an assistant research metallurgist. He has been assigned to the Metals Research Group.

Joseph T. Gushue recently became Assistant Sales Manager of the Battery Separator Division of Texon, Inc., South Hadley Falls, Mass. He formerly was with the United States Rubber Co.

James H. Jacobs has been appointed Manager of the newly formed Chemical Engineering Group in the Product and Process Development Dept., Electro Metallurgical Co., Niagara Falls, N. Y. Under Mr. Jacobs' direction, the new group will be responsible for titanium development and bench-scale development in other chemical engineering fields.

H. J. Jendrzynski, formerly of Detroit, Mich., recently accepted a position as Research Engineer with R. R. Donnelley & Sons in Chicago, Ill.

Herbert Miller has joined the Monsanto Chemical Co., Research and Engineering Division, Special Projects' Solid State Section, Boston, Mass. His position entails the development of the Solid State Chemistry group of the Solid State Section. He had been with Sylvania Electric Products Inc.

Stanley M. Norwood has been appointed Assistant to the President of Electro Metallurgical Co., New York, N. Y. In addition to his new responsibilities, Mr. Norwood will continue as Vice-President of this division of Union Carbide Corp.

M. J. Pryor has been promoted to Head of a newly formed branch, Basic Physics and Physical Chemistry, at the Dept. of Metallurgical Research, Kaiser Aluminum & Chemical Corp., Spokane, Wash.

William D. Robertson has been promoted from Associate Professor to the rank of full Professor of Metallurgy at Yale University. At present he is directing research, conducted by graduate students, in the fields of deformation and fracture, the physical constitution of liquid metals, and the structural mechanism of corrosion phenomena.

S. Sathyanarayana has been appointed Senior Scientific Assistant, Central Electrochemical Research Institute, Karaikudi.

Edward S. Shanley has joined the staff of Arthur D. Little, Inc., Cambridge, Mass., as a chemist in the Research and Development division. Previously he worked in the Becco Chemical Division of Food Machinery and Chemical Corp.

Martin E. Straumanis, research professor of metallurgy at the Missouri School of Mines and Metallurgy, Rolla, Mo., recently accepted an invitation to go to the Vienna Institute of Technology, Austria, for one year as a visiting professor (Fulbright). He will be in Vienna up to July 1958.

M. S. Thacker has been appointed Secretary, Dept. of Technical Education and Scientific Research, Government of India, in addition to his duties as Director General, C.S.I.R.

Hans Thurnauer has been appointed section leader of the newly formed ceramics section of Minnesota Mining & Manufacturing Co., St. Paul, Minn.

G. Lloyd Martin has joined National Research Corp. as Assistant Director of the Chemistry Dept., where he will be responsible for inorganic chemistry and process development. Previously, he was associated with Mallinckrodt Chemical Works in analytical research, inorganic research and development, and as a research supervisor in its uranium division.

J. Vaid has left the Plating Section, Indian Telephone Industries Ltd., Bangalore, and joined the Central Electrochemical Research Institute, Karaikudi, as Junior Scientific Officer.

Notice to Members

By now you have received your official voting ballot from Society Headquarters. If you have not already done so, please return the ballot by *December 15* so that your vote can be included in the final election count.

John Gering Cashell

John Gering Cashell, Junior Fellow, Mellon Institute of Industrial Research, Pittsburgh, Pa., died on Monday, June 24, 1957. He was 34 years old.

He was born on September 16, 1922, and was raised in the Washington, D. C., area. His undergraduate work, begun at The Citadel, Charleston, S. C., and interrupted by three years' military service in Europe, was completed at Johns Hopkins University. Following this he took a position as a Development Engineer with the General Electric Co. in Schenectady, N. Y. After leaving G. E. in 1953, he joined the Mellon Institute, where he was associated with Ted LeLoup on the Power Rectifiers Fellowship. He became a member of The Electrochemical Society in July 1955. In June 1957 Mr. Cashell received his Masters' degree in natural science from the University of Pittsburgh.

He is survived by his wife, Sylvia, and three small children.

Book Reviews

Theoretische Metallkunde by Ulrich Dehlinger. Published by Springer-Verlag, Berlin/Göttingen/Heidelberg, 1955. IV + 250 pages, 82 figures, DM 27.- (about $6.45).

The scope and material covered in this book can be seen best from the Table of Contents. The headings of the six chapters are as follows: I. Crystallographic foundations (lattices, symmetry, interference), 15 pp. II. Electrons in the lattice (electron gas, lattice potential, Fermi statistics, Brillouin zones, rule of Hume-Rothery, atom functions, polyhedron method, correlation of electrons, spin distribution), 46 pp. III. Structure of elements within the periodic system (types of bonding, bonding through *s*- and *p*- functions, transition metals, allotropy), 24 pp. IV. Heats of formation and structure of alloys (electron theory of alloys, alloy groups), 23 pp. V.

(Continued on page 226C)

Committees of The Electrochemical Society, Inc., 1957-58

Acheson Award Committee

	Term expires
J. C. Warner, Chairman	Nov. 1957
H. J. Read	Nov. 1957
G. W. Heise	Nov. 1958
C. L. Faust	Nov. 1958
M. J. Udy	Nov. 1959
H. M. Scholberg	Nov. 1959
R. M. Hunter	Nov. 1960
E. M. Sherwood	Nov. 1960

Admissions Committee

Louis Weisberg, Chairman
L. I. Gilbertson
M. F. Quaely

F. M. Becket Award Committee

	Term expires
A. T. Hinckley	1958
A. C. Haskell	1959
G. M. Butler, Chairman	1960

Subcommittee on Revision of Constitution and Bylaws

R. A. Schaefer, Chairman
R. M. Hunter

Committee for the Administration of the Corrosion Handbook Fund

Norman Hackerman — J. E. Draley
R. M. Burns — H. H. Uhlig

Finance Committee

L. I. Gilbertson, Chairman
H. B. Linford — R. A. Schaefer
W. C. Gardiner — Hans Neumark

Investment Advisory Panel

	Term expires
Clyde Williams	Spring 1958
G. W. Heise, Chairman	Spring 1959
A. K. Graham	Spring 1960
M. J. Udy	Spring 1961
Hans Thurnauer	Spring 1962

Membership Committee

F. W. Koerker, Chairman
Cleveland Section—John Yeager
Electrothermics & Metallurgy Division—Morris Steinberg
Niagara Falls Section—Les Juel
Ontario-Quebec Section—H. A. Timm
Philadelphia Section—F. X. McGarvey and C. L. Scheer
San Francisco Section—T. R. Beck
Theoretical Electrochemistry Division—S. Schuldiner and R. R. Roberts

Nominating Committee
(Discharged at annual meeting)

H. H. Uhlig, Chairman
C. L. Faust — A. U. Seybolt
A. E. Middleton — U. B. Thomas

Palladium Medal Award Committee

H. A. Laitinen, Chairman
T. P. May — Norman Hackerman
E. B. Yeager — J. P. Fugassi

Perkin Medal Committee

Norman Hackerman, Chairman — Alternates: F. A. Lowenheim
S. Swann, Jr. — L. I. Gilbertson
Hans Thurnauer — C. V. King

Publication Committee

R. J. McKay, Chairman
Norman Hackerman — H. B. Linford

Resolutions Committee

H. B. Linford
William Blum
H. R. Copson (appointment to be approved at October 6 Board Meeting)

Sustaining Membership Committee

F. L. LaQue, Chairman
(Appointment of Hans Thurnauer as new Chairman to be approved at October 6 Board Meeting.)

Ways and Means Committee

W. C. Gardiner, Chairman
R. A. Schaefer — C. L. Faust
H. H. Uhlig — S. Swann, Jr.
F. A. Lowenheim — Hans Thurnauer

Council of Local Sections

H. T. Francis, Chairman
M. F. Quaely, Vice-Chairman
K. S. Willson, Secretary
Representatives on Board, Lee O. Case (2 yr) and R. A. Woofter (1 yr)

Representatives in Other Societies

American Association for the Advancement of Science
George Heise—expires spring 1960
Harry Alsentzer—expires spring 1958

American Institute of Electrical Engineers
Committee C-40—Eugene Willihnganz

American Standards Association
Sectional Committee C-18—J. M. Booe
Sectional Committee Y-10 and Y-32—W. J. Hamer
Sectional Committee C-42—W. C. Vosburgh
Sectional Committee C-67—Guy Fetterley
Sectional Committee C-34.1—W. E. Gutzwiller

Inter-Society Corrosion Committee
Paul Delahay
K. G. Compton

National Research Council
Division of Chemistry and Chemical Technology—J. C. Warner

Research Council on the Causes and Methods of Prevention of Internal Corrosion of Water Pipes
F. L. LaQue

(Continued from page 224C)

Physical properties of elements and alloys (conductivity, Hall effect, magnetism, optical properties, x-ray spectra), 17 pp. VI. Phase equilibrium and kinetics of transition (fundamental laws of statistical thermodynamics, specific heat of lattice oscillations, phase equilibria, diffusion, nucleation, precipitation in saturated mixed crystals, chain reactions due to migrating dislocations, lattice imperfections, grain boundaries, surfaces, relaxation processes), 83 pp. Tables, literature references, indexes occupy 42 pages.

The content shows that extensive material is treated in only 208 pages. The reader is assumed to be acquainted not only with advanced physical metallurgy, but also with theoretical physics (in the scope of the textbook of Joos) and with advanced calculus. Although the author has tried not to shield the "physical melody with its empirical contrapoint" by a thick barrier of equations, the book is nevertheless mathematical, although some sections are quite elementary. The book is written mainly for the solid state physicist. It is very systematic and the treatment is novel in many places and reflects in an excellent way the work which is done at the Institute of the author in Stuttgart. As such the book also has its limitations, as, for instance, very little can be found about the physics of the deformed state, deformation mechanisms, strength of metallic crystals, etc. The chapter on imperfections is short and the results of recent x-ray investigations are not used.

Foreign authors are frequently mentioned in the text and a list of references is given for each paragraph. However, not always is an observation attributed to its original author, as it is for instance in the case of eutectic crystallization, p. 199. This may be explained by the brevity of the book. Even so, the book should be valuable for those working in various fields of physical metallurgy.

M. E. Straumanis

Physical Methods in Chemical Analysis, Vol. III. Edited by Walter G. Berl. Published by Academic Press, Inc., New York, 1956. xii + 652 pages. $15.00.

The current interest in instrumental methods of chemical analysis has resulted in the publication of a series of books which cover subject matter in this general field. The present volume, like the two that preceded it, has the distinction of emphasizing the analytical aspects of each technique as well as presenting the fundamental concepts. In addition, the present volume includes a discussion of several techniques which have not as yet appeared in other collections. As a result, its publication at this time is very welcome.

The volume deals with the following 12 topics: gas chromatography (Phillips), electrochromatography (Wieland and Dose), electroanalytical methods in trace analysis (Cooke), high-frequency methods of chemical analysis (Blaedel and Petitjean), field emission microscopy (Muller), theory and principles of sampling for chemical analysis (Benedetti-Pichler), flame photometry (Gardiner), microwave spectroscopy (Dailey), and analytical applications of nuclear magnetic resonance (Gutowsky), fluorescent x-ray spectrometric analysis (Clark), analytical distillation (Podbielniak and Preston), and neutron spectroscopy and neutron interactions in chemical analysis (Taylor and Havens).

The chief criticism that one might level at such a list is the random placement of the topics. For example, the chapter on sampling is found between two chapters on optical methods, while the chapter on distillation is far removed from the two on chromatography, all of which deal primarily with separations. On the other hand, the editor has compensated for this deficiency by maintaining a high level of clarity and conciseness within each chapter.

L.B. Rogers

Thermodynamics and Statistical Mechanics, by A. H. Wilson. Published by Cambridge University Press, New York, 1957. 495 pages, $9.50.

In the author's words, this is a book written "mainly for theoretical physicists" and, although physical chemists will find the treatment of many chemical subjects such as solution theory somewhat sketchy, there is much interest to chemists in the book. Especially is this true if one wishes to review or to be brought up to date on the foundations of thermodynamics and statistical mechanics. The first four chapters contain a critical and penetrating discussion of the first and second laws and related material, then come two chapters reviewing very concisely statistical mechanics, chapters which pave the way for the seventh on the Third Law. This is an interesting chapter and should be read by every chemist whose knowledge and understanding of the Third Law stopped with the exposition of Lewis and Randall.

The remainder of the book deals with applications, mainly those subjects which are now usually classed under the subject "Statistical Thermodynamics." Outstanding chapters here are those on imperfect gases and on electric and magnetic phenomena. In the latter chapter is a discussion of perhaps the latest new subject of thermodynamics, negative absolute temperatures which must be used in the Boltzmann equation to describe the distribution or population of nuclei among their allowed spin states in a magnetic field when the field is suddenly reversed.

There is very little in this book of direct interest to the electrochemist. As mentioned above, the treatment in the realm of electrolytes is not authoritative. For example, the method of calculating K_c for acetic acid from electrical conductance measurements given on p. 425 fails to include modern methods of correcting Λ_∞ for slight decreases in mobility of the ions as the concentration increases. The author's treatment of a cell with transference on p. 443 is correct only if the transference number of zinc ion in zinc sulfate solution is independent of concentration, a stipulation which is never exactly true. The author dislikes standard free energies saying "this nomenclature is unilluminating and is best avoided." A final chapter on solids completes the book.

On the whole, this is a masterly work and would be a valuable addition to the library of any chemist.

Malcolm Dole

Extraction and Refining of the Rarer Metals (Proceedings of a Symposium). Published by the Institution of Mining and Metallurgy, 44 Portland Place, London, W. 1; 1957. 444 pages, $8.50.

This interesting volume contains 22 papers with accompanying discussion on the extraction and refining of the rarer metals, with particular emphasis on uranium, niobium, and beryllium and, to a lesser extent, vanadium, thorium, titanium, zirconium, and other metals. The book is similar in concept to its predecessor, "The Refining of Non-Ferrous Metals," also published by the Institution of Mining and Metallurgy. The older book has been of great value as a reference, and there is no doubt that the present volume will have a similar application, although it is

concerned to a greater extent with experimental procedures rather than established practice.

The papers cover a wide range, in that there are general reviews, theoretical papers, descriptions of small-scale laboratory experiments, details of construction and operation of pilot plants, and papers based on actual commercial practice. Some are concerned with groups of metals, others with one metal. As a result, the book is not meant to serve as a textbook with a balanced survey of the field, but rather as a compendium of recent work and thought in the field of the rarer metals.

The carefully recorded discussions and authors' replies are of great interest and value just as they were in the older volumes of the TRANSACTIONS of The Electrochemical Society. Ofttimes, points are brought out that are not clear or not even mentioned in the original article.

Because of the rapid progress in the production of the rarer metals, in a few instances the papers seem a bit dated, but this is a fault that cannot be avoided. The various authors and their organizations are doing a valuable service in describing their work so that others just entering the field can avoid unnecessary and expensive duplication of effort.

All workers in the field of rare metals will want this book as a source of valuable information and as an inspiration for novel and unusual approaches to metal production and refining.

A. W. Schlechten

Announcements from Publishers

The Making, Shaping and Treating of Steel. A complete one-volume reference work relating to the iron and steel industry, published in its seventh edition by United States Steel Corp. Copies of the volume, priced at $7.50 each, can be obtained from United States Steel, Office Service-Stores, 525 William Penn Place, Pittsburgh 30, Pa. Students of accredited educational institutions can obtain the book for $5.00 per copy, providing each order is countersigned by a faculty member.

Completely revised since its sixth edition was issued in 1951, the new volume offers users and makers of steel a comprehensive summary of present-day theory and practice covering all phases of iron and steel production from raw materials to finished products. The new edition is the result of team effort by nearly 200 technical representatives of U. S. Steel, its operating divisions and subsidiaries, co-ordinated by H. E. McGannon, technical editor, under the direction of Dr. E. C. Bain, Assistant Executive Vice-President—Operations.

Engineering Properties and Applications of Plastics, by G. F. Kinney. Published by John Wiley & Sons, Inc., New York, 1957. 278 pages, $6.75.

Metallurgical Progress-3. Published by Philosophical Library Inc., New York, 1957. 88 pages, $6.00.

A third series of reviews, reprinted from "Iron & Steel"; eight authors; deals with the following topics: refractories in the iron and steel industry, nondestructive testing, metallurgical coke, and various phases of foundry practice.

Guide to Atomic Energy Literature for the Civilian Application Program, TID-4575. A 74-page booklet which can be obtained without charge from the U. S. Atomic Energy Commission, Technical Information Service Extension, P. O. Box 1001, Oak Ridge, Tenn.

Department of Defense Titanium Sheet-Rolling Program: Status Report No. 1, Titanium Metallurgical Lab., Battelle Memorial Institute,

for Dept. of Defense, March 1957. Report PB 121624,* 43 pages, $1.25.

This report reviews progress during 1956 in the three phases of the titanium sheet-rolling program: study of the process variables in melting and working selected alloys; collection of design data on those alloys; and evaluation of the material in the aircraft industry. Detailed information is included on sheet sizes and gauges, statistical sampling procedures, mechanical properties, and target reproducibility of mechanical properties.

Corrosion and Ignition of Titanium Alloys in Fuming Nitric Acid, J. B. Rittenhouse and others, Wright Air Development Center, Feb. 1957. Report PB 121940,* 67 pages, $1.75.

Previous studies have noted that although the corrosion resistance of titanium is usually good, the metal reacts explosively and has a susceptibility to stress-corrosion cracking after exposure to red fuming nitric acid. This research examined the corrosion, ignition reactions, and stress-corrosion cracking of titanium and its alloys resulting from storage in fuming nitric acid.

Permeability of Barrier Materials to Volatile Corrosion Inhibitors at Various Humidities, A. S. Mohaupt and J. P. Hohf, Forest Products Labs., U. S. Dept. of Agriculture, for Wright Air Development Center, Dec. 1956. Report PB 121893,* 90 pages, $2.25.

* Order from Office of Technical Services, U. S. Dept. of Commerce, Washington 25, D. C.

Meetings of Other Organizations

Oct. 7-9—National Association of Corrosion Engineers Northeast Regional Meeting, Pittsburgh, Pa.

Nov. 13-15—American Standards Association, Annual Meeting and National Conference on Standards, St. Francis Hotel, San Francisco, Calif.

Dec. 8-11—American Institute of Chemical Engineers, Annual Meeting, Conrad Hilton Hotel, Chicago, Ill.

Dec. 26-31—American Association for the Advancement of Science, Annual Meeting, Indianapolis, Ind.

Employment Situations

Positions Available

PHYSICAL-ELECTROCHEMIST

Ph.D. with 1-3 years' experience. Interested in electrochemical process research. Responsible for planning and directing process improvement program on electrolytic caustic-chlorine cells. Senior project chemist level supervising other chemists and technicians.

Location in divisional research laboratories at Charleston, W. Va. Salary commensurate with training and experience. Liberal corporate benefit plans.

Please send qualification details to:
Research and Development Dept.—
Attention A.A.
Westvaco Chlor-Alkali
Division
Food Machinery and Chemical
Corporation
South Charleston, W. Va.

Electronic Scientists, Metallurgists, Physicists, Technologists, and **Engineers** (Aeronautical, Electrical, Electronic, Industrial, General, Mechanical, and Power Plant). The Naval Air Material Center, Philadelphia 12, Pa., has an urgent need for qualified engineering and scientific personnel to fill vacancies in the above positions. The Center is currently engaged in an extensive program of aeronautical research, development, experimentation, and test operations for the advancement of Naval aviation. Starting salaries range from $4480 to $7570 per annum. Application for Federal Employment, Standard Form 57, should be filed with the Industrial Relations Dept., Naval Air Material Center, Naval Base, Philadelphia 12, Pa. Applications may be obtained from the above address or information as to where they are available may be obtained from any first or second class post office.

Advertisers' Index

The Electrochemical Society

Patron Members

Aluminum Co. of Canada, Ltd., Montreal, Que., Canada
International Nickel Co., Inc., New York, N. Y.
Union Carbide Corp.
  Divisions:
    Electro Metallurgical Co., New York, N. Y.
    National Carbon Co., New York, N. Y.
Westinghouse Electric Corp., Pittsburgh, Pa.

Sustaining Members

Air Reduction Co., Inc., New York, N. Y.
Ajax Electro Metallurgical Corp., Philadelphia, Pa.
Allied Chemical & Dye Corp.
  General Chemical Div., Morristown, N. J.
  Solvay Process Div., Syracuse, N. Y. (3 memberships)
Alloy Steel Products Co., Inc., Linden, N. J.
Aluminum Co. of America, New Kensington, Pa.
American Machine & Foundry Co., Raleigh, N. C.
American Metal Co., Ltd., New York, N. Y.
American Platinum Works, Newark, N. J. (2 memberships)
American Potash & Chemical Corp., Los Angeles, Calif. (2 memberships)
American Zinc Co. of Illinois, East St. Louis, Ill.
American Zinc, Lead & Smelting Co., St. Louis, Mo.
American Zinc Oxide Co., Columbus, Ohio
Auto City Plating Co. Foundation, Detroit, Mich.
Bart Manufacturing Co., Bellville, N. J.
Bell Telephone Laboratories, Inc., New York, N. Y. (2 memberships)
Bethlehem Steel Co., Bethlehem, Pa. (2 memberships)
Boeing Airplane Co., Seattle, Wash.
Burgess Battery Co., Freeport, Ill. (4 memberships)
Canadian Industries Ltd., Montreal, Que., Canada
Carborundum Co., Niagara Falls, N. Y.
Chrysler Corp., Detroit, Mich.
Columbia-Southern Chemical Corp., Pittsburgh, Pa.
Consolidated Mining & Smelting Co. of Canada, Ltd., Trail, B. C., Canada (2 memberships)
Corning Glass Works, Corning, N. Y.
Cramet, Inc., Chattanooga, Tenn.
Crane Co., Chicago, Ill.
Diamond Alkali Co., Painesville, Ohio (2 memberships)
Dow Chemical Co., Midland, Mich.
Wilbur B. Driver Co., Newark, N. J. (2 memberships)
E. I. du Pont de Nemours & Co., Inc., Wilmington, Del.
Eagle-Picher Co., Chemical Div., Joplin, Mo.
Eaton Manufacturing Co., Stamping Div., Cleveland, Ohio
Electric Auto-Lite Co., Toledo, Ohio
Electric Storage Battery Co., Philadelphia, Pa.
The Eppley Laboratory, Inc., Newport, R. I. (2 memberships)
Food Machinery & Chemical Corp.
  Becco Chemical Div., Buffalo, N. Y.
  Westvaco Chlor-Alkali Div., South Charleston, W. Va.
Ford Motor Co., Dearborn, Mich.
General Electric Co., Schenectady, N. Y.
  Chemistry & Chemical Engineering Component, General Engineering Lab.
  Chemistry Research Dept.
  Metallurgy & Ceramics Research Dept.
General Motors Corp.
  Brown-Lipe-Chapin Div., Syracuse, N. Y. (2 memberships)
  Guide Lamp Div., Anderson, Ind.
  Research Laboratories Div., Detroit, Mich.
Gillette Safety Razor Co., Boston, Mass.
Gould-National Batteries, Inc., Depew, N. Y.
Graham, Crowley & Associates, Inc., Chicago, Ill.
Great Lakes Carbon Corp., New York, N. Y.
Hanson-Van Winkle-Munning Co., Matawan, N. J. (3 memberships)
Harshaw Chemical Co., Cleveland, Ohio (2 memberships)
Hercules Powder Co., Wilmington, Del.
Hooker Electrochemical Co., Niagara Falls, N. Y. (3 memberships)
Houdaille-Hershey Corp., Detroit, Mich.
International Minerals & Chemical Corp., Chicago, Ill.
Jones & Laughlin Steel Corp., Pittsburgh, Pa.
Kaiser Aluminum & Chemical Corp.
  Chemical Research Dept., Permanente, Calif.
  Div. of Metallurgical Research, Spokane, Wash.
P. R. Mallory & Co., Indianapolis, Ind.
McGean Chemical Co., Cleveland, Ohio
Merck & Co., Inc., Rahway, N. J.
Metal & Thermit Corp., Detroit, Mich.
Minnesota Mining & Mfg. Co., St. Paul, Minn.
Monsanto Chemical Co., St. Louis, Mo.
National Cash Register Co., Dayton, Ohio
National Lead Co., New York, N. Y.
National Research Corp., Cambridge, Mass.
Norton Co., Worcester, Mass.
Olin Mathieson Chemical Corp., Niagara Falls, N. Y.
  Aviation Div. (2 memberships)
  Industrial Chemicals Div. (2 memberships)
Pennsylvania Salt Manufacturing Co., Philadelphia, Pa.
Philips Laboratories, Inc., Irvington-on-Hudson, N. Y.
Poor & Co.
  Promat Div., Waukegan, Ill.
Potash Co. of America, Carlsbad, N. Mex.
Radio Corp. of America, Harrison, N. J.
Ray-O-Vac Co., Madison, Wis.
Reynolds Metals Co., Richmond, Va.
Shawinigan Chemicals Ltd., Montreal, Que., Canada
Speer Carbon Co.
  International Graphite & Electrode Div., St. Marys, Pa. (2 memberships)
Sprague Electric Co., North Adams, Mass.
Stackpole Carbon Co., St. Marys, Pa. (2 memberships)
Stauffer Chemical Co., Henderson, Nev., and New York, N. Y. (2 memberships)
Sylvania Electric Products Inc., Bayside, N. Y. (2 memberships)
Sarkes Tarzian, Inc., Bloomington, Ind.
Tennessee Products & Chemical Corp., Nashville, Tenn.
Texas Instruments, Inc., Dallas Texas
Titanium Metals Corp. of America, Henderson, Nev.
Udylite Corp., Detroit, Mich. (4 memberships)
Vanadium Corp. of America, New York, N. Y.
Victor Chemical Works, Chicago, Ill.
Wagner Brothers, Inc., Detroit, Mich.
Weirton Steel Co., Weirton, W. Va.
Western Electric Co., Inc., Chicago, Ill.
Wyandotte Chemicals Corp., Wyandotte, Mich.
Yardney Electric Corp., New York, N. Y.

For Removing RUST and SCALE

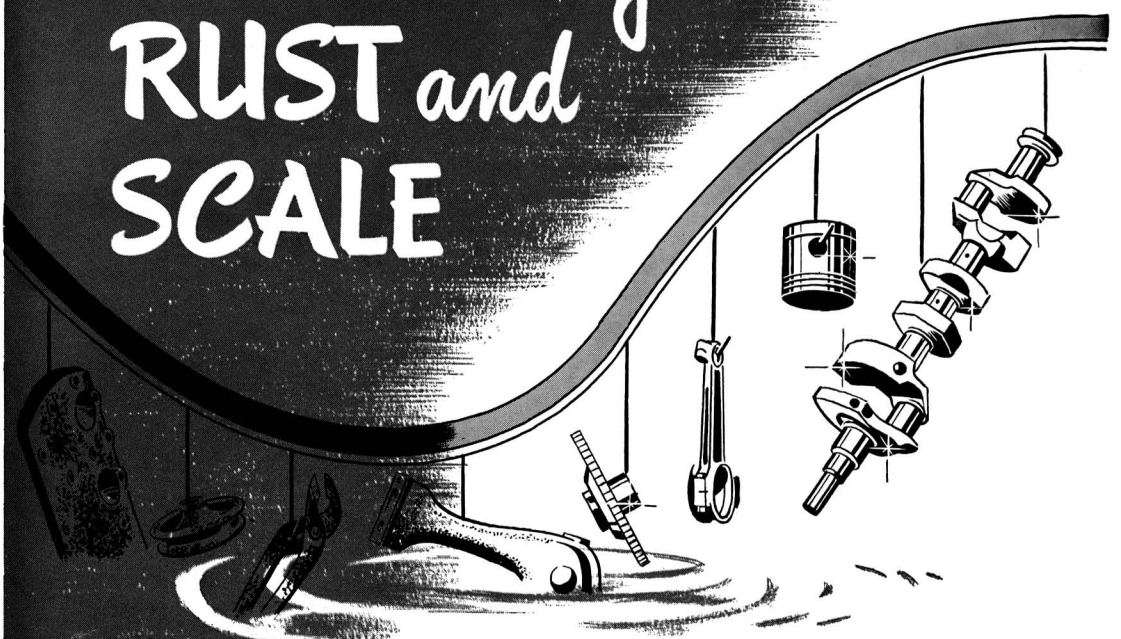

ALKA-DEOX® DERUSTING PROCESSES. Alkaline materials used both electrolytically and non-electrolytically for rapid removal of rust and scale from steel, cast iron and malleable iron. No attack on basis metal. Uses Enthone Alka-Deox 114 and Alka-Deox 134.

ENTHOL® — CLEANER AND RUST REMOVER FOR STEEL. A solvent acid cleaner for rapid removal of oil, rust and oxide from steel, zinc, aluminum and other metals to prepare them for painting or organic finishing.

DESCALER 2A — POWDERED ACID PICKLING COMPOUND. A powdered acidic compound added to water to make pickling solutions for iron and steel. Safer to handle than sulphuric acid. Gives controlled acidity to prevent overpickling.

ACTANE® 70 — POWDERED COMPOUND REPLACES HYDROFLUORIC ACID. A dispersing agent added to acid pickles to remove colloidal and siliceous films from metals. Also an additive for sulphuric and nitric acid pickles to promote faster pickling of stainless steel, aluminum and titanium.

INHIBITOR 8 — STOPS ACID ATTACK ON STEEL. An all-purpose inhibitor for acids including sulphuric and hydrochloric acids to stop attack on steel during pickling.

ACID ADDITION AGENT —STOPS ACID FUMES. A surface active material extensively used in acid pickles to reduce fuming, to give better wetting, and to promote better pickling.

Write for fully descriptive literature.

ENTHONE
INCORPORATED

442 ELM STREET, NEW HAVEN 11, CONNECTICUT
Metal Finishing Processes • Electroplating Chemicals